Physical and geochemical controls on oxygen dynamics at continental margins and shelf seas

Dissertation

Zur Erlangung des Doktorgrades

Dr. rer. nat.

Der Mathematisch-Naturwissenschaftlichen Fakultät

der Christian-Albrechts-Universität zu Kiel

vorgelegt von

Lorenzo Rovelli

Kiel, 2013

Referent:	Dr. Marcus Dengler
Korreferent:	Prof. Dr. Klaus Wallmann
Tag der Mündlichen Prüfung:	14. Februar 2014
Zum Druck genehmigt:	14. Februar 2014

Der Dekan

Hiermit erkläre ich, dass ich die vorliegende Doktorarbeit selbstständig und ohne Zuhilfenahme unerlaubter Hilfsmittel erstellt habe. Weder diese noch eine ähnliche Arbeit wurde an einer anderen Abteilung oder Hochschule im Rahmen eines Prüfungsverfahrens vorgelegt, veröffentlicht oder zur Veröffentlichung vorgelegt. Ferner versichere ich, dass die Arbeit unter Einhaltung der Regeln guter wissenschaftlicher Praxis der Deutschen Forschungsgemeinschaft entstanden ist.

Kiel, den 14. Februar 2014

Lorenzo Rovelli

Abstract

In light of increasing anthropogenic influences on natural waters and climate change, it is important to advance our understanding of the intricate interactions between biological, geochemical and physical processes that control constituent dynamics within aquatic systems. Among those constituents, dissolved oxygen (O_2) is a well-established indicator for biological activity and is also involved in most biogeochemical processes in both the water column as well as in the upper region of the sediment. While the different aspects of O_2 dynamics and their flux pathways are well investigated with the boundaries of each discipline, interdisciplinary studies are, at present, still relatively scarce. Within this multidisciplinary thesis, O_2 dynamics in the water column and at the sediment-water interface (SWI) were investigated using state-of-the-art high-resolution tools on seasonally stratified shelf seas (central North Sea) as well as on cold seep habitats at continental margins (off Chile). The aim of those studies is that of further investigating the role of the hydrodynamics in modulating costituent transport, with emphasis on O_2 transport.

The central North Sea process study on thermocline mixing and O_2 fluxes, which was performed with a turbulence profiler, fast O_2 microsensors and moored current measurements, revealed the occurrence of a second-mode, near-inertial internal wave. Zones of enhanced vertical shear of horizontal velocity and concomitant strong stratification were observed at the upper and lower limits of the interior layer where turbulence levels were also found to be a factor of ten higher than in the central interior region. High-resolution O_2 measurements further revealed a well-established O_2 maximum which occurred at the lower limit of the interior layer, from which a considerable, yet overlooked, O_2 flux towards the bottom boundary (BBL) was observed. It was hypothesized that due to this additional O_2 source, the carbon turnover between the thermocline and the BBL is much larger than previously regarded.

To overcome the shallow-depth rating limitations of fast O_2 sensor systems such as that used on the presented North Sea study, a newly designed fast O_2 system with deep sea ratings was developed based on pressure-compensated Clark-type microsensors. The system was embedded on a microstructure profiler and successfully tested at the Chilean continental margin. The O_2

gradients above the O_2 minimum were twice as high as reported by the standard O_2 sensor from the ship-operated CTD (Conductivity-Temperature-Depth). The fast O_2 system also proved to be accurate and fast enough to detected step-like structures in water-column O_2 profiles. Those were similar to the step-like structures observed in temperature and salinity that characterize a double-diffusive system (i.e., finger regime).

Controls on benthic O_2 and hydrogen sulfide (H_2S) fluxes were also investigated on two cold-seeps habitats at the Chilean continental margin using a state-of-the-art in-situ microprofiling transecting unit and corresponding flow measurements. The first habitat was characterized by recurrent bacterial mat coverage and the frequent occurrence of sulfide; conversely, the second habitat was less sulfidic with limited bacterial mat coverage. While H_2S fluxes were found to vary little between the habitats, the average diffusive O_2 uptake rate (*DOU*) was a factor of two higher in the more sulfidic habitat. The major contributions to the observed *DOUs* were seemingly dominated by sulfide oxidation and, to a lesser extent, by the particulate organic matter input from the overlaying water. Both habitats showed the occurrence of periods of transport limitation resulting from a flow-driven diffusive boundary layer (DBL) which modulated *DOU*. This limitation was more pronunced in the more sulfidic habitat, suggesting that increased geochemical activity might lead to increased physically-driven dampening of O_2 uptake. The implications of this transport limitation are therefore not only of importance for seep O_2 dynamics but also for organically enriched continental margins and shelfs characterized by enhanced O_2 uptake rates.

The results of this thesis also showed that the combination of high-resolution constituent measurements and accurate physical characterization is currently the best approach to further advance the knowledge on the O_2 dynamics.

Kurzzusammenfassung

In Anbetracht des zunehmenden anthropogenen Einflusses auf natürliche Gewässer und das Klima, ist es wichtig, unser Verständnis der komplexen Wechselwirkungen zwischen biologischen, geochemischen und physikalischen Prozessen, die die Dynamik der Bestandteile in aquatischen Systemen steuern, voranzutreiben. Zu den Bestandteilen zählt gelöster Sauerstoff (O_2) als ein gut etablierter Indikator für biologische Aktivität; O_2 ist an den meisten biogeochemischen Prozessen in der Wassersäule sowie im oberen Sedimentbereich beteiligt. Die verschiedenen Aspekte der Sauerstoffdynamik und ihres Flussverlaufs wurden zwar innerhalb der Grenzen der jeweiligen Disziplinen intensiv untersucht, jedoch sind komplexe interdisziplinäre Studien noch selten. Innerhalb der vorliegenden multidisziplinären Arbeit wurde die Sauerstoffdynamik in der Wassersäule als auch an der Sediment-Wasser Grenzschicht (SWI) untersucht. Das Ziel ist, der Einfluss der Hydrodynamik bei der Steuerung des Sauerstoffflüssen weiter zu untersuchen. Der Forschungsschwerpunkt lag hierbei auf saisonal geschichteten Schelfmeeren (zentrale Nordsee) sowie auf cold seeps Habitaten an Kontinentalrändern (offshore Chile); verwendet wurde hochauflösende Messtechnik entsprechend dem neuesten Stand der Technik.

Der Referenzstandort in der zentralen Nordsee wurde mit einer Mikrostruktursonde, schnellen Flachwasser-Sauerstoffsensoren und verankerten Strömungsmessgeräte bezüglich der Sprungschichtvermischung und Sauerstoffflüsse untersucht. Die Ergebnisse zeigen das Auftreten einer internen Trägheitswelle des zweiten Modus. An den oberen und unteren Grenzen der Sprungschicht wurden Zonen mit verstärkter vertikaler Scherung der horizontalen Geschwindigkeit und gleichzeitiger starker Schichtung beobachtet. Dazu wurde auch eine erhöhte Turbulenz nachgewiesen, die um einen Faktor zehn größer ist als im zentralen Bereich der Sprungschicht. Hochauflösende Sauerstoffmessungen ergaben das Vorkommen eines gut etablierten Sauerstoffmaximums an der unteren Grenze der Sprungschicht. Von dort aus entsteht ein beträchtlicher, aber bislang übersehener, Sauerstofffluss Richtung Bodengrenzschicht. Es wurde vermutet, dass aufgrund dieser zusätzlichen Sauerstoffquelle der Umsatz an organischem Kohlenstoff zwischen der Sprungschicht und der Bodengrenzschicht viel größer sein könnte als zuvor angenommen.

Um die Limitierungen des eingesetzten Sauerstoffsensors zu überwinden, wurde ein neu konzeptioniertes schnelles Tiefwasser-Sauerstoffsensoren-System entwickelt. Das System basiert auf druckausgleichenden Clark-Mikrosensoren, eingebettet in eine Mikrostruktur-CTD und es wurde erfolgreich auf dem chilenischen Kontinentalrand getestet. Die ermittelten Sauerstoffgradienten oberhalb der Oxykline waren mehr als doppelt so hoch wie die Messungen mit dem Standard Sauerstoffsensor des Schiff CTDs. Die kleinskalige Auflösung mit den schnell messenden O_2-Mikrosensoren ließ stufenähnliche Strukturen im Sauerstoffprofil erkennen. Diese ähneln den Stufen-Strukturen von Temperatur und Salzgehalt, die der Doppeldiffusion (Finger-Regime) zugeschrieben werden.

Kontrolle über benthische Sauerstoff- und Schwefelwasserstoffflüsse wurden ebensfalls an zwei cold seeps Habitaten auf dem chilenischen Kontinentalrand mittels der State-of-the- Art in situ Mikroprofil-Transektmessungen und Strömungsmessungen untersucht. Das erste Habitat wurde durch häufiges Auftreten von Bakterienmatten und Sulfid kennzeichnet. Das zweite Habitat war weniger sulfidhaltig und Bakterienmatten traten seltener auf. Während die Schwefelwasserstoffflüsse nur wenig zwischen den Habitaten variierten, war der durchschnittliche diffusive Sauerstofffluss (*DOU*) im sulfidhaltigerem Sediment um den Faktor zwei erhöht. Die wichtigsten Beiträge zu den beobachteten Sauerstoffflüssen wurden durch Sulfidoxidation und, in geringerem Maße, durch den Eintrag von partikulärer organischer Substanz aus der Wassersäule dominiert. Beide Habitate zeigten das Auftreten von Perioden mit Transportlimitierung und damit eine Steuerung der *DOUs* durch die strömungsgetriebene diffusive Grenzschicht. Die Transportlimitierung was stärker im sulfidhaltigerem Sediment, was darauf hindeutet, dass zunehmende geochemische Aktivitäten zu einer verstärkten physikalisch getriebene Dämpfung O_2 Aufnahme des Sediments führen könnten. Die Implikationen des Auftretens von Transportlimitierung ist deswegen nicht nur für die O_2 Dynamik in cold seeps, sondern auch für organisch angereicherte Kontinentalränder und Schelfe wichtig, da solche Habitatet auch durch erhöhte Sediment O_2 Aufnahme charakterisiert sind.

Die Ergebnisse dieser Studie zeigen darüber hinaus, dass die Kombination von hochauflösender Stoffmessungen und detaillierter physikalischer Charakterisierung der momentan beste Ansatz ist, die komplexe O2 Dynamik in den Ozeanen zu entschlüsseln.

Acknowledgements

First of all, I would like to thank, Dr. Marcus Dengler, Prof. Dr. Klaus Wallmann, Dr. Daniel McGinnis, Dr. Peter Linke, PD Dr. Mark Schmidt and Dr. Stefan Sommer for giving me the opportunity to carry out this PhD thesis.

Special thanks go to Dr. Claudia Lorrai, Dr. Daniel McGinnis and Prof. Dr. A. Wüest, who pulled me into aquatic research in the first place. Additional thanks go to Dr. Henrik Stahl, Prof. Dr. Ronnie N. Glud and Dr. Lee D. Bryant for their help and support during the last stages of this PhD thesis.

I am also grateful to the Sergiy Cherednichenko, Thomas Brandt, Ralf Schwarz, Uwe Koy, Asmus Petersen, Matthias Turk and all of the technicians of GEOMAR's Technology and Logistic center for their support in both cruise preparation and assistance at sea, as well as for their priceless, highly competent help in developing and troubleshooting several of the devices I used during my work.

For their every-day moral and scientific support, I would like to also thank my former and present colleagues: Elena, Jean-Philippe, Christian, Hauke, Jürgen, Markus; special thanks goes to Lee for her help in improving both the language and the style of this thesis.

I am also grateful to Kiel's Spanish-Catalan-Latin American-Italian-Swiss-German dream team for the friendly support in easing up stressful and difficult situations.

Although geographically far away, but always there when I need help, I would like to thank my closest friends Andrea, Ilan, Laura, Marco and Moira. A special thank goes to Katharina for her patience and support especially during the last phase of this PhD thesis.

Finally, I would like to thank my family and for their love and support and for making sure that I could realize my dreams.

Table of Contents

List of Figures

List of Tables

List of Symbols and Abbreviations

A	Amplitude
ADCP	Acoustic Doppler current profiler
AOM	Anaerobic oxidation of methane
BBL	Bottom (benthic) boundary layer
C_{org}	Organic carbon
c	Speed of sound
CH_4	Methane
CO_2	Carbon dioxide
cpd	Circles per day
cph	Cicles per hour
cpm	Circles per minute
CTD	Conductivity-temperature-depth
D	Molecular diffusion coefficient
DBL	Diffusive boundary layer
DCM	Deep Chlorophyll maximum
DOU	Diffusive O_2 uptake rate
F	Flux
Fe	Iron
g	Earth gravitational acceleration
H_2S	Hydrogen sulfide
ΣH_2S	Total sulfide
K_1	Diurnal declination tide
K_ρ	Diapycnal diffusivity
K_z	Vertical diffusivity
L_o	Ozmidov scale
M_2	Semi-diurnal tide
Mn	Manganese
N^2	Water column stability
NH_4^+	Ammonium
O_2	Dissolved oxygen
OM	Organic matter
R/V	Research vessel
Ri	Richardson number
S	Vertical shear of horizontal velocity
S^2	Shear variance
SBL	Surface boundary layer
SUR	Sediment O_2 uptake rate
SWI	Sediment-water interface
T	Temperature
z_{max}	Oxygen penetration depth

Γ, γ	Mixing efficiency
δ_{DBL}	Diffusive boundary layer thickness
ε	Dissipation rate of turbulent kinetic energy
η	Dynamic viscosity of seawater
μ, ν	Kinematic viscosity of seawater
ρ	Density
φ	Phase lag
ω	Frequency

I. Chapter

Introduction

I.1. Oxygen distribution and dynamics in the ocean and shelf seas

Global oxygen distribution on marine systems

In aquatic as well as in terrestrial environments, oxygen is a main constituent of the ecosystem as it is linked to the major nutrient cycles and biogeochemical processes. In aquatic systems, oxygen is primarily produced as a by-product of photosynthesis in the euphotic zone, which is the depth range of water in which enough sunlight penetrates to support photosynthesis, or it diffuses into the surface water from the atmosphere. Photosynthesis is performed by algae and other photosynthesis-capable organisms and requires light, nutrients and carbon dioxide (CO_2). Conversely, oxygen diffusion from the atmosphere to the surface water depends on physical forcing, e.g., from wind and waves, at the air-water interface.

The distribution of dissolved oxygen (O_2) in the ocean is not homogenous and depends on a balance between biological processes (producing and consuming oxygen) and physical processes (transporting and exporting oxygen) occurring within the water column as well as in the benthic compartment (*see* Glud 2008). For instance, the O_2 concentration at every ocean interior depth is the resulting balance of the O_2 supply from the surface waters through ventilation, transport and mixing, paired with O_2 consumption by biological processes. If the strength or extent of these processes changes, the O_2 distribution will shift, thus making O_2 a very sensitive indicator of variations in oceanic ecosystems (Joos et al. 2003). As shown in Fig. I.1, well-defined regions of high and low O_2 concentrations can be identified by looking at the global ocean interior oxygen distribution; these areas are defined by ventilated (i.e., oxygenated) regions and oxygen minimum zones (OMZs). The major ventilated regions, characterized by well-oxygenated waters, encompass the Labrador Sea, the Greenland Sea and the Antarctic Intermediate Zone. The major OMZs are located in the tropical region of the Pacific and Atlantic oceans, as well as in the Arabian Sea and the Bay of Bengal (*see* Paulmier and Ruiz-Pino 2009); these regions are characterized by strong depletion or even absence of O_2 in defined regions of the water column.

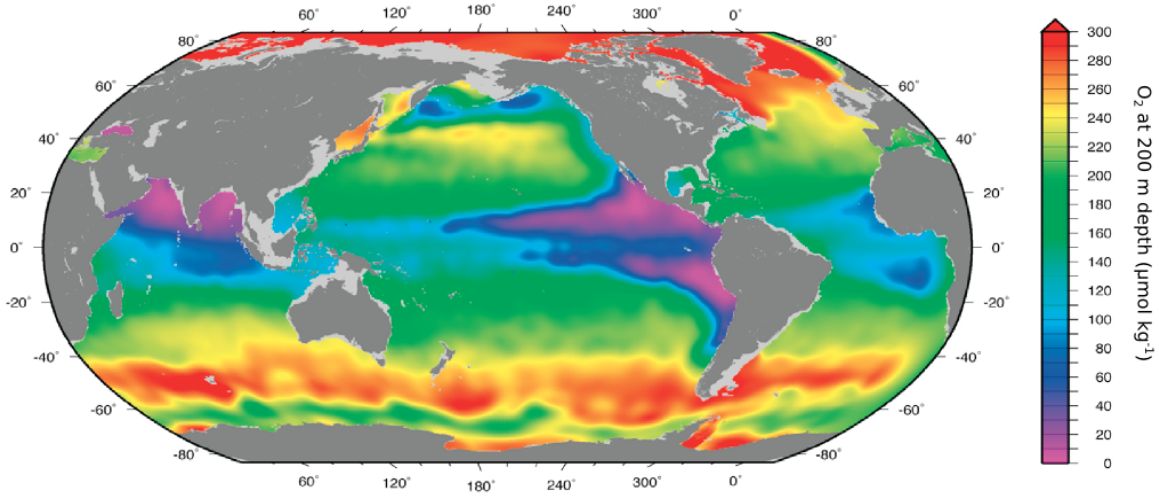

Fig. I.1. Mean global ocean oxygen concentrations at 200 meters below the surface. Adapted from Falkowski et al. 2011. Data from the World Ocean Circulation Experiment Global Hydrographic Climatology (Gouretski and Koltermann, 2004).

Importance of the degree of oxygenation

Because O_2 plays a major role in marine ecosystem dynamics, both in the water column and at the sea floor, changes in the degree of oxygenation have significant repercussions for ecosystem health and functioning, especially when O_2 is depleted. Studies have shown that O_2 concentrations below than 62.5 µmol L^{-1} (i.e., hypoxic regime; Vaquer-Sunyer and Duarte 2008) can produce significant stress on aquatic communities leading to increased mortality among fish communities and obvious repercussions on fisheries (Diaz 2001). Further decreases in O_2 concentrations to ≤ 10 µmol L^{-1} (i.e., suboxic regimes; Naqvi et al. 2010) can trigger the shift between aerobic and anaerobic reactions of several key biogeochemical processes. An example of that is the increased production of nitrogen oxide (N_2O) reported on OMZ, which is attributed to an increase in denitrification (e.g. Bianchi et al. 2012).

Changes in the degree of oxygenation in marine systems

The global spatial distribution of O_2 depleted zones is considerable (Fig. I.1) and, perhaps even more significantly, studies have revealed that the degree of oxygenation is decreasing in several marine systems. Most notable are the expansions of the OMZs of the Atlantic and Pacific Ocean (Stramma et al. 2008), as well as the emergence of hypoxia in several shelf seas and coastal

regions (Grantham et al. 2004; Chan et al. 2008; Crawford and Pena 2013). On a global scale, observations and modeling approaches also suggest a decline in the O_2 concentrations, both in the ocean interior (i.e., global deoxygenation; Keeling et al. 2010) as well as in coastal regions (Diaz and Rosenberg 2008). In order to understand why OMZs are increasing, how they are maintained and how they will react to local and global changes (ocean warming; Rabalais et al. 2010), emphasis has to be placed on advancing our knowledge of the processes controlling the O_2 distribution within marine systems.

Processes controlling O_2 distribution on marine systems

In the open ocean interior, the main factors controlling O_2 distribution are the surface water O_2 concentration, the rate of organic matter oxidation (referred to as the oxygen utilization rate; OUR), and the time required for a surface water parcel to reach the interior, which is often referred to as the ventilation time or ventilation age.

The surface water O_2 concentration depends on the amount of photosynthesis (primary production) and on the air-water exchange. Primary production rates are determined by the availability of light and macronutrients (e.g., carbon, nitrogen and phosphorus), as well as micronutrients (e.g., iron) and photosynthetic organisms. The air-water exchange, in contrast, depends mainly on the local near-surface wind dynamics (e.g., Wanninkof 1992) and the difference between the O_2 concentration at equilibrium with the atmosphere (i.e., saturation concentration) and the surface water O_2 concentration. While it is commonly accepted that open-ocean surface waters are typically at near-saturation O_2 concentrations due to rapid air-water gas exchange, at higher latitudes substantial winter under-saturation and summer over-saturation has been reported (Ito et al. 2004).

The OUR is mainly determined by the oxidation of organic particles sinking from the surface water, which is estimated from the fraction of primary production that is exported from the surface water into the ocean interior (i.e., particulate organic matter flux; Suess 1980; Martin et al. 1987; Dunne et al. 2007).

Ventilation facilitates O_2 replenishment from O_2-rich surface waters to the ocean interior. These processes can occur locally, where O_2 is transported from the surface water to the interior across density surfaces (diapycnal transport), or on a larger scale, where surface waters from higher

latitudes (outcrop areas) are transported with the main currents along regions of equal density to the ocean interior at lower latitudes (isopycnal transport). The ratio between ventilation time and OUR is therefore critical to the degree of oxygenation sustained in interior water.

As reviewed by Keeling et al. (2010), recent climate modeling approaches focusing on ocean warming suggest a reduction of oceanic O_2 concentrations of 1 – 7% in the next century. Factors contributing to this decrease include decreased O_2 saturation, increased strength of stratification, and subsequently reduced resupply to the interior (i.e., increased ventilation time). There is, however, an ongoing debate on whether a global oceanic deoxygenation process is already occurring and whether the global models can actually reproduce the processes regulating the O_2 budgets at a more localized scale, such as those defining OMZs. Based on half a century of O_2 time series, Stramma et al. (2008) showed a significant expansion of th OMZs in the tropical ocean, i.e., increased OMZ thickness, as well as a decrease in the lowest O_2 concentrations within the Atlantic OMZ. In the Pacific OMZs, no further reduction in the lowest O_2 concentrations was reported as the core of the OMZ is already anoxic.

As further expansion of OMZs is likely to threaten the habitat of economically valuable pelagic fishes (Stramma et al. 2012), emphasis was given to the processes governing O_2 dynamics within OMZs (e.g., Karstensen et al. 2008; Brandt al. 2010). OMZs are established due to high surface primary production, long ventilation times and limited circulation (*see* Helly and Levin 2004, Stramma et al. 2008). High surface productivity is often associated with wind-driven upwelling. Upwelling occurs at continental shelves due to surface-water movement from wind, which leads to sub-surface water rising up from beneath the surface to replace the water that was pushed away. In contrast to surface water, upwelled water tends to be colder, has decreased O_2 concentrations, and is rich in nutrients. Upwelling provides nutrients, which support high productivity; in facts, on the eastern boundary currents of both the Atlantic and Pacific oceans, upwelling-enhanced fish populations support up to 1/5 of the global fishery income (Pauly and Christensen 1995).

Limited ventilation of OMZs is mainly due to “shadow zones” created by their location, which is typically outside the main gyre or tropical current (e.g., Karstensen et al. 2008; Brandt al. 2010), and not ventilated at the basin-scale by wind-driven circulation (Luyten et al. 1983). A recent

study on O_2 replenishment to the tropical North Atlantic OMZ by Fischer et al. (2012) reported that the O_2 diapycnal flux contributes to a third of the OUR. The source of this O_2, however, was attributed to lateral replenishment by advective processes and eddies and, therefore, the overall O_2 supply to the OMZ was found to occur by remote pathways rather than by local processes. Similar conclusions were also found by Karstensen et al. (2008), who suggest a direct relationship between reduced outcrop ventilation and the occurrence of OMZs. They also argue that if the lower thermocline of the North Atlantic is not yet suboxic, it is because of the supply of O_2 from well-ventilated South Atlantic waters.

In contrast to the Atlantic and Pacific OMZs, the Arabian OMZ is not located within an upwelling system (Morrison et al. 1999) and the system dynamics, both in term of ventilation and biological activity, are strongly affected by seasonal monsoons. However, no significant changes in O_2 concentrations are observed at the annual and seasonal levels, thus suggesting a solid balance between O_2 sinks and sources (Morrison et al. 1999). A recent coupled biological-physical modeling study by Resplandy et al. (2012) showed that on an annual scale, biological O_2 consumption is counterbalanced by mesoscale structures such as eddies and filaments.

Upwelling, especially on the eastern boundary current system, can also strongly influence O_2 dynamics of shelf and coastal regions by fueling surface primary production with nutrient-rich bottom waters. This, together with reduced bottom water currents, can lead to shelf hypoxia. A well-known example of upwelling-induced hypoxia is the North-American Oregon shelf. Since 2000, basin-scale changes in the atmosphere-ocean dynamics in this region have lead to a decrease of the O_2 concentration in the upwelled waters. Paired with intensified upwelling, this resulted in an unprecedented occurrence of intense hypoxic conditions (Grantham et al. 2004). A similar situation was also reported on the British Columbia continental shelf by Crawford and Pena (2013). Upwelling is, however, not the only source of coastal and shelf hypoxia. Eutrophication, resulting from increased natural and anthropogenic nutrient-loading from land and riverine systems (e.g. Nixon 1995), also plays a significant role. In fact, the global distribution of costal O_2 depletion is very often associated with intense coastal urbanization and land farming (Diaz and Rosenberg 2008). Of course, other processes such as horizontal advection of O_2 depleted waters also play an important role in the occurrence of hypoxia; this is particularly evident within the Northern California current system (*see* Connolly et al. 2010).

In stratified shelf seas, hypoxia is generally the result of significant productivity and strong stratification. The productivity leads to large amounts of organic matter from eutrophication, algal blooms being exported to the bottom waters or deep chlorophyll maxima (DCM; Weston et al. 2005). In addition, seasonal stratification results in a strong and stable pycnocline, which limits mixing of O_2 to the bottom water, thus isolating the surface O_2-reach water from the nutrient-rich bottom water (e.g., Sharples et al. 2001). Due to the general semi-enclosed nature of shelf seas, the ventilation from isopycnal processes is also limited. This is particularly evident on the North Dogger and Oyster Ground sites in the British central North Sea, where the large banks prevents advection of more oxygenated waters from the shallower regions (Queste et al. 2013). O_2 replenishment may occur diapycnaly through the temporal disruption of the pycnocline during storms (Greenwood et al. 2010) or via diapycnal turbulent mixing across the pycnocline as the result of shear instability (Rippeth et al. 2009; Sharples et al. 2007). As detailed by Rippeth (2005), shear instability in shelf-sea stratified interiors results from internal tides, near-inertial oscillations, and breaking of internal waves over sloping boundaries. While, as mentioned above, hypoxia was reported in several shelf and coastal zones, there are still shelf seas such as the North Sea where hypoxia is not yet occurring, although low O_2 concentrations in the bottom water have been reported (Greenwood et al. 2010; Queste et al. 2013). However, model simulations on the O_2 dynamics in the bottom water of the Oyster Grounds, in the central North Sea, suggest an increased risk of hypoxia over the next century (Meire et al. 2013). A strengthening of stratification was identified to be the dominant factor (58%) leading to the simulated decrease of the bottom water O_2 levels followed by a decrease in O_2 solubility due to water warming (27%); an increase of the metabolic rates due to bottom-water warming was also found to contribute, although to a minor extent (15%). Because the North Sea ecosystem supports a large fish stock, the threat of hypoxia has highlighted the need for more extensive studies investigating the interaction between biological and physical processes modulating O_2 dynamics in the water column and at the sea floor.

Near-bottom and sediment O_2 dynamics

In order to obtain a complete overview of the O_2 dynamics in marine systems, e.g., for O_2 budgets estimations, not only water column processes but also near-bottom and sedimentary biological, geochemical and physical processes have to be taken into account. The main

processes influencing the amount of O_2 within the bottom waters of marine systems are carbon remineralisation (Suess 1980), benthic O_2 uptake (Glud 2008), and O_2 replenishment from, e.g., the surface waters or the interior. The bottom waters of marine systems are generally well mixed as the result of energy introduced to the system by tides (Wunsch and Ferrari 2004) and thus turbulence-driven transport is generally the dominant diapycnal transport process. However, when approaching the seafloor (cm-scale), flow first becomes laminar due to viscosity effects (i.e., the establishment of the viscous sublayer; VSL) and then becomes limited by molecular diffusion (mm-scale; diffusion boundary layer (DBL); Jørgensen and Revsbech 1985) immediately above the sediment-water-interface. The DBL thickness (δ_{DBL}) represents the bottleneck of benthic transport (Lorke et al. 2003) with benthic O_2 uptake being controlled by a balance between physical forcing, transport constraints, and sediment O_2 consumption processes (Jørgensen and Boudreau 2001). Physical forcing of benthic fluxes includes, e.g., near-bottom current (U) modulation and turbulence-induced variation in δ_{DBL} (Steinberger and Hondzo 1999; Lorke et al. 2003). O_2-consuming processes in the sediment include oxic diagnesis (aerobic organic matter degradation; *see* Froelich et al. 1979) as well as the reoxidation of reduced compounds (Canfield et al. 1993). Primary species involved with reoxidation reactions include ammonium (Kaplan 1983), hydrogen sulfide (Jørgensen and Nelson 2004), manganese (Mandernack et al. 1995), iron (Thamdrup 2000), iron sulfides (Aller 1980) and methane (Berner 1980). It is still however unknown whether O_2 uptake in marine sediments is more strongly controlled by water-side physical forcing or by sediment-side procesess (*see* Kelly-Gerreyn et al. 2005; Glud et al. 2007).

From the above, it is clear that the influence of O_2 dynamics in both the water column and sediment cannot be neglected. Characterization and quantification of O_2 transport is thus required for the understanding of the ecological functioning of aquatic systems. Several methods to estimate O_2 fluxes from the athmosphere, within the water column and at the sediment-water-interface have been developed to support this research.

I.2. Oxygen flux pathways and flux estimations

Various methods of O_2 flux estimation are used and each involve different assumptions of where the O_2 is measured or estimated as constant, e.g. water column, water-air or sediment-water interfaces, and the different processes involved in the flux pathway. The time scale taken into consideration also varies between methods, ranging from few seconds to years.

The O_2 gas exchange with the atmosphere at the air–water interface is inferred from the near-surface apparent oxygen utilization (AOU) and the local wind magnitude; this follows the parameterization initially provided by Wanninkhof (1992) for carbon dioxide (CO_2). More recently, other parameterizations for the wind-driven gas transfer velocity across the air-water interface have been suggested (Nightingale et al. 2000; Ho et al. 2006).

In the water column, diapycnal turbulent O_2 fluxes are estimated using the gradient method proposed by Osborn (1980), where concentration gradients are multiplied by the turbulent diapycnal eddy diffusivity (K_ρ) for mass. K_ρ can be inferred from microstructure profiles (Osborn 1980; Schafstall et al. 2010), deliberate tracer release experiments (Ledwell and Bratkovich 1995; Banyte et al. 2012), acoustic current measures and density profiles (Kunze et al. 2006; Fischer et al. 2012), as well as from temperature or density profiles alone (Thorpe 1997; Dillon 1982; Galbraith and Kelley 1996). The significance of flux estimations with the gradient method strongly depends on the accuracy of the concentration gradients, as well as on the number of observations, e.g., microstructure profiles (Davis 1996). Ideally, hundreds of microstructure profiles and high-resolution constituent profiles would be required to provide well-resolved gradients and samples of the natural variability of turbulence.

Diapycnal transport is, however, only one of several transport pathways contributing to the observed O_2 distribution; isopycnal transport and lateral transport processes are also major contributors (Marshall et al. 1993). Isopycnal transport, such as that from surface outcrop areas to the ocean interior, can be approximated assuming steady-state conditions where the O_2 net consumption equals O_2 transport to the study sites. Net consumption can be inferred from the AOU and the ventilation time (e.g. Karstensen et al. 2008) or from sediment traps and O_2 to carbon ratios (e.g. Suess 1980).

In the well-mixed bottom waters, turbulent diffusion represents the primary transport pathway; however, as there is no significant stratification, the Osborn (1980) method is not applicable. Here the turbulent fluxes can be estimated using the flux-ratio method (Holtappels et al. 2011b), which relies on the ratio between constituent gradients and their respective fluxes. The method can be coupled with momentum fluxes and velocity gradients from hydroacustic measurents, used directly with near-bottom turbulent diffusivity values (Holtappels et al. 2011a), or benthic constituent fluxes, estimated from other techniques, the eddy correlation (EC) technique.

While the EC technique is a well-known, non-invasive, method for measuring constitutes fluxes in the field of atmospheric science (Lee et al. 2004), its application for turbulent benthic O_2 flux estimations is also becoming rapidly established (Berg et al. 2003; Lorrai et al. 2010; McGinnis et al. 2011; Reimers et al. 2012; Rheuban and Berg 2013). The main advantage of the EC technique over more traditional flux measurement methods, e.g., microprofiling or benthic flux chambers, is that EC records undisturbed fluxes with high temporal resolution with no disruption of the local hydrodynamics.

Diffusive benthic fluxes can be estimated via ex-situ or in-situ acquisition of high-resolution concentration profiles across the sediment-water interface by using microsensors and applying Fick's first and second law of diffusion (Jørgensen and Des Marais 1990; Berg et al. 1998; Bryant et al. 2010). Benthic flux chambers are standard equipment for in-situ measurements of the total benthic flux for several constituents including O_2, methane and nutrients (Tengberg et al. 1996). The total flux obtained with this method encompasses diffusive fluxes, bioturbation and bioirrigation, as well as advective processes and is therefore often used for benthic constituent budgets, or for in-situ incubation and measurements under controlled conditions (Sommer et al. 2008). It is, however, an invasive method, that isolates a portion of the sediment surface from natural near-bottom hydrodynamics, which are an established control on sediment-water flux.

The main challenge marine researchers are currently facing when investigating dynamics is the integration and up-scaling of the interactions between the different processes and flux pathways from the process-level to the ecosystem level and from there to a more global perspective. In order to achieve such tasks, a comprehensive, multidisciplinary approach is required.

I.3 Thesis overview

Within the framework of this thesis on O_2 dynamics in marine system, benthic and water column O_2 flux pathways were investigated in seasonally stratified shelf seas (Central North Sea) as well as in the water column above and within the sediment at cold seep habitats along the central Chilean Subduction Zone, located at the boarder of the Tropical Pacific OMZ. The aim of these studies was to further investigate the role of the hydrodynamics and biogechemical processes in modulating O_2 dynamics, with emphasis on O_2 transport pathways, and to provide a better insight of the state-of-the-art methodological approch to advance the undestanding of the implication of processes for the studied ecosystems.

At the central North Sea site ("Tommeliten"; *see* Chapter II), emphasis was placed on thermocline mixing on seasonal stratified shelf seas considering the replenishment of O_2 depleted bottom waters in the summer time through vertical turbulent O_2 fluxes from the thermocline. In this process study, high-resolution hydroacoustic measurements were used to characterize the semidiurnal lunar tide (Otto et al. 1990) and near-inertial oscillations, which were often observed in the central North Sea during summer (e.g. van Haren et al. 1999). Turbulent mixing was investigated by coupling microstructure profiler data (*see* Lueck et al. 2002) with a state-of-the-art fast galvanic O_2 microsensor (0.2 s response time; AMT, Analysenmesstechnik GmbH, Rostock, Germany). This novel approach enabled the resolution of O_2 gradients at the cm scale, which was currently not possible with standard oceanographic tools, and is therefore well-suited to 1) resolve the sharp oxyclines observed during the summertime and 2) estimate the associated O_2 fluxes. At a later stage, a tentative bottom water O_2 budget was evaluated based on the estimated downward O_2 flux from the thermocline, benthic O_2 uptake rates from benthic flux chamber, and carbon remineralisation rates inferred from bottom water AOU. The findings were then discussed with respect to the bottom water carbon budget and its implication for ecosystem functioning.

The cold seep habitats at the continental margin within the central Chilean Subduction Zone were investigated to assess the role of the local hydrodynamics (i.e., DBL) and sediment processes on controlling benthic O_2 uptake rates (*see* Chapter III). It is known that benthic uptake

rates are controlled by physical forcing, enhancing or limiting molecular diffusion across the SWI, and by sediment aerobic oxydation of organic matter and reoxidation of reduced organic compounds (Jørgensen and Boudreau 2001). The extent of those contributions was subject to several modeling studies (Kelly-Gerreyn et al. 2005; Glud et al. 2007; Brand et al. 2009), but the controlling processes are still not defined. To add supporting data from actual field measurements to the knowledge base of this critical issue, a transecting in-situ microprofiler unit was deployed on two cold seeps habitats, where O_2 and hydrogen sulfide (H_2S) profiles were taken in close proximity to microbial mats, together with hydroacoustic measurements of the near-bottom current regime. The contribution to the estimated O_2 fluxes from measured changes in δ_{DBL} and sulfide oxidation (from total sulfide fluxes), in addition to effects of ammonium (NH_4^+) oxidation and organic matter degradation estimated from reference particulate organic matter export the seafloor, were subsequently evaluated and discussed with respect to transport-limiting conditions.

At the same location, the water column O_2 distribution was investigated in regard to the feasibility of high-resolution O_2 profiles for flux estimations (*see* Chapter IV). Commercially available fast O_2 systems are currently not well-suited to investigate the O_2 transport from oxygenated surface waters above the OMZs or from bottom waters to the depleted OMZs core, because they are either designed for shallow-water use (i.e., lacking oceanic depth rating) or do not have the required resolution for providing robust gradients. To fill the instrumental gap on oceanic high-resolution, water-column O_2 measurements, a prototype of a fast Clark-type O_2 microsensor system (<0.5 s response time) was mounted on a microstructure profiler and its performance in resolving O_2 gradient were evaluated and discussed.

I.4 References

Aller, R. C. 1980. Diagenetic processes near the sediment-water interface of Long Island Sound. II. Fe and Mn. *Adv. Geophys.* **22**: 351–415, doi:10.1016/S0065-2687(08)60068-0

Banyte, D., T. Tanhua, M. Visbeck, D. W. R. Wallace, J. Karstensen, G. Krahmann, A. Schneider, L. Stramma, and M. Dengler. 2012. Diapycnal diffusivity at the upper boundary of the tropical North Atlantic oxygen minimum zone. *J. Geophys. Res.* **117**: C09016, doi:10.1029/2011jc007762

Berg, P., N. Risgaard-Petersen, N., and S. Rysgaard. 1998. Interpretation of measured concentration profiles in sediment pore water. *Limnol. Oceanogr.* **43**: 1500–1510, doi:10.4319/lo.1998.43.7.1500

Berg, P., H. Roy, F. Janssen, V. Meyer, B. B. Jorgensen, M. Huettel, and D. de Beer. 2003. Oxygen uptake by aquatic sediments measured with a novel non-invasive eddy-correlation technique. *Mar. Ecol.: Prog. Ser.* **261**: 75–83, doi:10.3354/meps261075

Berner, R. A. 1980. Early diagenesis: A theoretical approach. Princeton University Press, Princeton, New Jersey, 241 p.

Bianchi, D., J. P. Dunne, J. L. Sarmiento, and E. D. Galbraith. 2012. Data-based estimates of suboxia, denitrification, and N_2O production in the ocean and their sensitivities to dissolved O_2. *Global Biogeochem. Cycles* **26**: Gb2009, doi:10.1029/2011gb004209

Brandt, P., V. Hormann, A. Kortzinger, M. Visbeck, G. Krahmann, L. Stramma, R. Lumpkin and C. Schmid. 2010. Changes in the Ventilation of the Oxygen Minimum Zone of the Tropical North Atlantic. *J. Phys. Oceanogr.* **40**: 1784–1801, doi:10.1175/2010jpo4301.1

Bryant, L. D., D. F. McGinnis, C. Lorrai, A. Brand, J. C. Little, and A. Wüest. 2010. Evaluating oxygen fluxes using microprofiles from both sides of the sediment-water interface. *Limnol. Oceanogr.: Methods* **8**: 610–627, doi:10.4319/lom.2010.8.0610

Canfield, D. E., B. B. Jørgensen, H. Fossing, R. Glud, J. Gundersen, N. B. Ramsing, B. Thamdrup, J. W. Hansen, L. P. Nielsen, and P.O. J. Hall. 1993b. Pathways of organic carbon oxidation in three continental margin sediments. *Mar. Geol.* **113**: 27–40, doi:10.1016/0025-3227(93)90147-N

Chan, F., J. A. Barth, J. Lubchenco, A. Kirincich, H. Weeks, W. T. Peterson, and B. A. Menge. 2008. Emergence of anoxia in the California current large marine ecosystem. *Science* **319**: 920–920, doi:10.1126/Science.1149016

Crawford, W. R., and M. A. Pena. 2013. Declining Oxygen on the British Columbia Continental Shelf. *Atmos. Ocean* **51**: 88–103, doi:10.1080/07055900.2012.753028

Connolly, T. P., B. M. Hickey, S. L. Geier, and W. P. Cochlan. 2010. Processes influencing seasonal hypoxia in the Northern California current system. *J. Geophys. Res.* **115**: C03021, doi:10.1029/2009jc005283

Davis, R. E. 1996. Sampling turbulent dissipation. *J. Phys. Oceanogr.* **26**: 341–358, doi:10.1175/1520-0485(1996)026<0341:Std>2.0.Co;2.

Diaz, R. J. 2001. Overview of hypoxia around the world. *J. Environ. Qual.* **30**: 275–281, doi:10.2134/jeq2001.302275x

Diaz, R. J., and R. Rosenberg. 2008. Spreading dead zones and consequences for marine ecosystems. *Science* **321**: 926–929, doi:10.1126/Science.1156401

Dillon, T. M. 1982. Vertical Overturns: A Comparison of Thorpe and Ozmidov Length Scales. *J. Geophys. Res.* **87**: 9601–9613, doi:10.1029/JC087iC12p09601

Dunne, J.P., J. L. Sarmiento, and A. Gnanadesikan. 2007. A synthesis of global particle export from the surface ocean and cycling through the ocean interior and on seafloor. *Global Biogeochem. Cycles* **21**: GB4006, doi: 10.1029/2006GB002907

Falkowski, P.G., T. Algeo, L. Codispoti, C. Deutsch, S. Emerson, B. Hales, R. B. Huey, W. J. Jenkins, L. R. Kump, L. A. Levin, T. W. Lyons, N. B. Nelson, O. S. Schofield, R. Summons, L. D. Talley, E. Thomas, F. Whitney, and C. B. Pilcher. 2011. Ocean Deoxygenation: Past, Present, and Future. *EOS Trans. AGU* **92**: 409–410

Fischer, T., D. Banyte, P. Brandt, M. Dengler, G. Krahmann, T. Tanhua, and M. Visbeck. 2012. Diapycnal oxygen supply to the tropical North Atlantic oxygen minimum zone. *Biogeosciences Discuss.* **9**: 1491–14325, doi:10.5194/bgd-9-14291-2012

Froelich, P. N., G. P. Klinkhammer, M. L. Bender, N. A. Luedtke, G. R. Heath, D. Cullen, and P. Dauphin. 1979. Early oxidation of organic matter in pelagic sediments of the eastern equatorial Atlantic: suboxic diagenesis. *Geochim. Cosmochim. Acta* **43**: 1075–1090, doi:10.1016/0016-7037(79)90095-4

Galbraith, P. S., and D. E. Kelley. 1996. Identifying overturns in CTD profiles. *J. Atmos. Ocean. Tech.* **13**: 688–702, doi:10.1175/1520-0426(1996)013<0688:IOICP>2.0.CO;2

Glud, R. N. 2008. Oxygen dynamics of marine sediments. *Mar. Biol. Res.* **4**: 243–289, doi:10.1080/17451000801888726

Glud, R. N., P. Berg, H. Fossing, B. B. Jørgensen. 2007. Effect of the diffusive boundary layer (DBL) on the benthic mineralization and O_2 distribution: a theoretical modelling exercise. *Limnol. Oceanogr.* **52**: 547–557, doi:10.4319/lo.2007.52.2.0547

Gouretski, V. V., and K. P. Koltermann. 2004. WOCE global hydrographic climatology, *Ber. Bundesamt Seeschiffahrt Hydrogr. Rep.* 35, Bundesamt Seeschiffahrt Hydrogr, Hamburg, Germany, 52 pp.

Grantham, B. A., F. Chan, K. J. Nielsen, D. S. Fox, J. A. Barth, A. Huyer, J. Lubchenco, and B. A. Menge. 2004. Upwelling-driven nearshore hypoxia signals ecosystem and oceanographic changes in the northeast Pacific. *Nature* **429**: 749–754, doi:10.1038/Nature02605

Greenwood, N., E. R. Parker, L. Fernand, D. B. Sivyer, K. Weston, S. J. Painting, S. Kroger, R. M. Forster, H. E. Lees, D. K. Mills, and R. W. P. M. Laane. 2010. Detection of low bottom water oxygen concentrations in the North Sea; implications for monitoring and assessment of ecosystem health. *Biogeosciences* **7**: 1357–1373, doi:10.5194/bg-7-1357-2010

Helly, J. J., and L. A. Levin. 2004. Global distribution of naturally occurring marine hypoxia on continental margins. *Deep-Sea Res.* **51**: 1159–1168, doi:10.1016/J.Dsr.2004.03.009

Ho, D. T., C. S. Law, M. J. Smith, P. Schlosser, M. Harvey, and P. Hill. 2006. Measurements of air-sea gas exchange at high wind speeds in the Southern Ocean: Implications for global parameterizations. *Geophys. Res. Lett.* **33:** L16611, doi:10.1029/2006gl026817.

Ito, T., M. J. Follows, and E. A. Boyle. 2004. Is AOU a good measure of respiration in the oceans? *Geophys. Res. Lett.* **31**: L17305, doi:10.1029/2004GL020900

Joos, F., G. K. Plattner, T. F. Stocker, A. Körtzinger, and D. W. R. Wallace. 2003. Trends in marine dissolved oxygen: Implications for ocean circulation changes and the carbon budget. *EOS Trans. AGU* **84**: 197–204.

Jørgensen, B. B., and B. P. Boudreau. 2001. Diagenesis and sediment-water exchange. p. 211–244. *In*: B. P. Boudreau and B. B. Jørgensen [eds.]. The benthic boundary layer: Transport processes and biogeochemistry. Oxford University Press, Oxford.

Jørgensen, B. B., and D. Des Marais. 1990. The diffusive boundary layer of sediments: oxygen microgradients over a microbial mat. *Limnol. Oceanogr.* **35**: 1343–1355, doi:10.4319/lo.1990.35.6.1343

Jørgensen, B. B., and D. C. Nelson. 2004. Sulfide oxidation in marine sediments: Geochemistry meets microbiology. *Spec. Pap. - Geol. Soc. Am.* **379**: 63–81, doi: 10.1130/0-8137-2379-5.63

Jørgensen, B. B., and N. P. Revsbech. 1985. Diffusive boundary layers and the oxygen uptake of sediments and detritus. *Limnol. Oceanogr.* **30**: 111–122, doi:10.4319/lo.1985.30.1.0111

Kaplan, W. A. 1983. Nitrification. p. 139–90. *In*: J. E. Carpenter and D. G. Capone [eds.]. Nitrogen in the Marine Environment, Academic Press, New York.

Karstensen, J., L. Stramma, and M. Visbeck. 2008. Oxygen minimum zones in the eastern tropical Atlantic and Pacific oceans. *Progr. Oceanogr.* **77**: 331–350, doi:10.1016/J.Pocean.2007.05.009.

Keeling, R. F., A. Kortzinger, and N. Gruber. 2010. Ocean Deoxygenation in a Warming World. *Annu. Rev. Mar. Sci.* **2**: 199–229, doi:10.1146/Annurev.Marine.010908.163855.

Kelly-Gerreyn, B. A., D. J. Hydes, and J. J. Waniek. 2005. Control of the diffusive boundary layer on benthic fluxes: a model study. *Mar. Ecol.: Prog. Ser.* **292**: 61–74, doi:10.3354/meps292061

Kemp, W. M., J. M. Testa, D. J. Conley, D. Gilbert, and J. D. Hagy. 2009. Temporal responses of coastal hypoxia to nutrient loading and physical controls. *Biogeosciences* **6**: 2985–3008, doi:10.5194/bg-6-2985-2009.

Kunze, E., E. Firing, J. M. Hummon, T. K. Chereskin, and A. M. Thurnherr. 2006. Global abyssal mixing inferred from lowered ADCP shear and CTD strain profiles. *J. Phys. Oceanogr.* **36**: 1553–1576, doi:10.1175/Jpo2926.1.

Ledwell, J. R., and A. Bratkovich. 1995. A tracer study of mixing in the Santa Cruz Basin. *J. Geophys. Res.* **100**: 20681–20704, doi:10.1029/95JC02164

Levin, L. A. 2003. Oxygen minimum zone benthos: Adaptation and community response to hypoxia. *Oceanogr. Mar. Biol.* **41**: 1–45.

Lorke, A., B. Müller, M. Maeki, and A. Wüest. 2003. Breathing sediments: The control of diffusive transport across the sediment–water interface by periodic boundary-layer turbulence. *Limnol. Oceanogr.* **48**: 2077–2085, doi:10.4319/lo.2003.48.6.2077

Lorrai, C., D. F. McGinnis, P. Berg, A. Brand and, A. Wuest. 2010. Application of Oxygen Eddy Correlation in Aquatic Systems. *J. Atmos. Oceanic Technol.* **27**: 1533–1546, doi:10.1175/2010JTECHO723.1

Lueck, R. G., F. Wolk, and H. Yamazaki. 2002. Oceanic velocity microstructure measurements in the 20th century. *J. Oceanogr.* **58**: 153–174, doi:10.1023/A:1015837020019.

Luyten, J. R., J. Pedlosky, and H. Stommel. 1983. The Ventilated Thermocline. *J. Phys. Oceanogr.* **13**: 292–309, doi:10.1175/1520-0485(1983)013<0292:Tvt>2.0.Co;2

Mandernack, K. W., M. L. Fogel, B. M. Tebo, and A. Usui. 1995. Oxygen isotope analyses of chemically and microbially produced manganese oxides and manganates. *Geochim. Cosmochim. Acta* **59**: 4409–4425, doi:10.1016/0016-7037(95)00299-F

Marshall, J. C., A. J. G. Nurser, and R. G. Williams. 1993. Inferring the Subduction Rate and Period over the North-Atlantic. *J. Phys. Oceanogr.* **23**: 1315–1329, doi:10.1175/1520-0485(1993)023<1315:Itsrap>2.0.Co;2

Martin, J. H., G. A. Knauer, D. M. Karl, and W. W. Broenkow. 1987. Vertex - Carbon Cycling in the Northeast Pacific. *Deep-Sea Res.* **34**: 267–285, doi:10.1016/0198-0149(87)90086-0

McGinnis, D. F., S. Cherednichenko, S. Sommer, P. Berg, L. Rovelli, R. Schwarz, R. N. Glud, and P. Linke. 2011. Simple, robust eddy correlation amplifier for aquatic dissolved oxygen and hydrogen sulfide flux measurements. *Limnol. Oceanogr.-Methods.* **9**: 340–347, doi:10.4319/lom.2011.9.340.

Meire, L., K. E. R. Soetaert, and F.J.R. Meysman. 2013. Impact of global change on coastal oxygen dynamics and risk of hypoxia. *Biogeosciences* **10**: 2633–2653, doi:10.5194/bg-10-2633-2013

Morrison, J. M., L. A. Codispoti, S. L. Smith, K. Wishner, C. Flagg, W. D. Gardner, S. Gaurin, S. W. A. Naqvi, V. Manghnani, L. Prosperie, and J. S. Gundersen. 1999. The oxygen minimum zone in the Arabian Sea during 1995 - overall seasonal and geographic patterns, and relationship to oxygen gradients. *Deep-Sea Res.* **46**: 1903–1931, doi:10.1016/S0967-0645(99)00048-X

Naqvi, S. W. A., H. W. Bange, L. Farias, P. M. S. Monteiro, M. I. Scranton, and J. Zhang. 2010. Marine hypoxia/anoxia as a source of CH_4 and N_2O. *Biogeosciences* **7**: 2159–2190, doi:10.5194/bg-7-2159-2010

Nightingale, P. D., G. Malin, C. S. Law, A. J. Watson, P. S. Liss, M. I. Liddicoat, J. Boutin, and R. C. Upstill-Goddard. 2000. In situ evaluation of air-sea gas exchange parameterizations using novel conservative and volatile tracers. *Global Biogeochem. Cycles* **14**: 373–387, doi:10.1029/1999gb900091.

Nixon, S.W., 1995. Coastal marine eutrophication - A definition, social causes, and future concerns. *Ophelia* **41**: 199–219.

Osborn, T. R. 1980. Estimates of the local rate of vertical diffusion from dissipation measurements. *J. Phys. Oceanogr.* **10**: 83–89, doi:10.1175/1520-0485(1980)010<0083: EOTLRO>2.0.CO;2

Otto, L., J. T. F. Zimmerman, G. K. Furnes, M. Mork, R. Saetre, and G. Becker. 1990. Review of the Physical Oceanography of the North-Sea. *Ned. J. Sea Res.* **26**: 161–238, doi:10.1016/0077-7579(90)90090-4

Paulmier, A., and D. Ruiz-Pino. 2009. Oxygen minimum zones (OMZs) in the modern ocean. *Prog. Oceanogr.* **80**:113–128, doi: 10.1016/J.Pocean.2008.08.001

Pauly, D., and V. Christensen. 1995. Primary production required to sustain global fisheries. *Nature* **374**: 255–257, doi:10.1038/374255a0

Queste, B. Y., L. Fernand, T. D. Jickells, and K. J. Heywood. 2013. Spatial extent and historical context of North Sea oxygen depletion in August 2010. *Biogeochemistry* **113**: 53–68, doi:10.1007/S10533-012-9729-9.

Rabalais, N. N., R. J. Diaz, L. A. Levin, R. E. Turner, D. Gilbert, and J. Zhang. 2010. Dynamics and distribution of natural and human-caused hypoxia. *Biogeosciences* **7**: 585–619, doi:10.5194/Bg-7-585-2010

Reimers, C. E., H. T. Ozkan-Haller, P. Berg, A. Devol, K. McCann-Grosvenor, and R. D. Sanders. 2012. Benthic oxygen consumption rates during hypoxic conditions on the Oregon continental shelf: Evaluation of the eddy correlation method. *J. Geophys. Res.* **117**: C02021, doi:10.1029/2011jc007564

Resplandy, L., M. Levy, L. Bopp, V. Echevin, S. Pous, V. V. S. S. Sarma, and D. Kumar. 2012. Controlling factors of the oxygen balance in the Arabian Sea's OMZ. *Biogeosciences* **9**: 5095–5109, doi:10.5194/Bg-9-5095-2012

Rheuban, J E., and P. Berg. 2013. The effects of spatial and temporal variability at the sediment surface on aquatic eddy correlation flux measurements. *Limnol. Oceanogr.: Methods* **11**: 351–359, doi:10.4319/lom.2013.11.351

Rippeth, T. P. 2005. Mixing in seasonally stratified shelf seas: A shifting paradigm. *Phil. Trans. R. Soc. A* **363**: 2837–2854, doi:10.1098/rsta.2005.1662

Rippeth, T. P., P. Wiles, M. R. Palmer, J. Sharples, and J. Tweddle. 2009. The diapcynal nutrient flux and shear-induced diapcynal mixing in the seasonally stratified western Irish Sea. *Cont. Shelf Res.* **29**: 1580–1587, doi:10.1016/j.csr.2009.04.009

Schafstall, J., M. Dengler, P. Brandt, and H. Bange. 2010. Tidal-induced mixing and diapycnal nutrient fluxes in the Mauritanian upwelling region. *J. Geophys. Res.* **115**: C10014, doi:10.1029/2009jc005940

Sharples, J., J. F. Tweddle, J. A. M.Green, M. R. Palmer, Y. N. Kim, A. E. Hickman, P. M. Holligan, C. M. Moore, T. P. Rippeth, J. H. Simpson, and V. Krivtsov. 2007. Spring-neap modulation of internal tide mixing and vertical nitrate fluxes at a shelf edge in summer. *Limnol. Oceanogr.* **52**: 1735–1747, doi:10.4319/lo.2007.52.5.1735

Sharples, J., C. M. Moore, T. P. Rippeth, P. M. Holligan, D. J. Hydes, N. R. Fisher, and J. H. Simpson. 2001. Phytoplankton distribution and survival in the thermocline. *Limnol. Oceanogr.* **46**: 486–496, doi:10.4319/lo.2001.46.3.0486

Sommer, S., M. Türk, S. Kriwanek, and O. Pfannkuche. 2008. Gas exchange system for extended in situ benthic chamber flux measurements under controlled oxygen conditions: First application - Sea bed methane emission measurements at Captain Arutyunov mud volcano. *Limnol. Oceanogr.: Methods* **6**: 23–33, doi:10.4319/lom.2008.6.23

Steinberger, N., and M. Hondzo. 1999. Diffusional mass transfer at sediment–water interface. *J. Environ. Eng.* **125**: 192–200, doi:10.1061/(ASCE)0733-9372(1999)125:2(192)

Stramma, L., G. C. Johnson, J. Sprintall, and V. Mohrholz. 2008. Expanding oxygen-minimum zones in the tropical oceans. *Science* **320**: 655–658, doi:10.1126/science.1153847

Stramma, L., S. Schmidtko, L. A. Levin, and G. C. Johnson. 2010. Ocean oxygen minima expansions and their biological impacts. *Deep-Sea Res.* **57**: 587–595, doi:10.1016/ J.Dsr.2010.01.005.

Stramma, L., E. D. Prince, S. Schmidtko, J. G. Luo, J. P. Hoolihan, M. Visbeck, D. W. R. Wallace, P. Brandt, and A. Kortzinger. 2012. Expansion of oxygen minimum zones may reduce available habitat for tropical pelagic fishes. *Nat. Clim. Change* **2**: 33–37, doi:10.1038/Nclimate1304.

Suess, E. 1980. Particulate Organic-Carbon Flux in the Oceans - Surface Productivity and Oxygen Utilization. *Nature* **288**: 260–263, doi:10.1038/288260a0

Tengberg, A., F. De Bovee, P. Hall, W. Berelson, B. Chadwick, G. Ciceri, P. Crassous, A. Devol, S. Emerson, J. Gage, R. Glud, F. Graziottin, J. Gundersen, D. Hammond, W. Helder, K. Hinga, O. Holby, R. Jahnke, A. Khripounoff, S. Lieberman, V. Nuppenau, O. Pfannkuche, C. Reimers, G. Rowe, A. Sahami, F. Sayles, M. Schurter, D. Smallman, B. Wehrli, and P. De Wilde. 1996. Benthic chamber and profile landers in oceanography- a review of design, technical solutions and functioning. *Prog. Oceanogr.* **35**: 253–294.

Thamdrup, B. 2000. Microbial manganese and iron reduction in aquatic sediments. *Advances in Microbial Ecology* **16**: 41–84.

Thorpe, S. A. 1977. Turbulence and mixing in a Scottish Loch. *Phil. Trans. R. Soc. A* **286**: 125–181, doi:10.1098/rsta.1977.0112

van Haren, H., L. Maas, J. T. F. Zimmerman, H. Ridderinkhof, and H. Malschaert. 1999. Strong inertial currents and marginal internal wave stability in the central North Sea. *Geophys. Res. Lett.* **26**: 2993–2996, doi:10.1029/1999gl002352

Vaquer-Sunyer, R., and C. M. Duarte. 2008. Thresholds of hypoxia for marine biodiversity. *P. Natl. Acad. Sci. USA.* **105**: 15452–15457, doi:10.1073/pnas.0803833105

Wanninkhof, R. 1992. Relationship between Wind-Speed and Gas-Exchange over the Ocean. *J. Geophys. Res.* **97**: 7373–7382, doi:10.1029/92jc00188

Weston, K., L. Fernand, D. K. Mills, R. Delahunty, and J. Brown. 2005. Primary production in the deep chlorophyll maximum of the central North Sea. *J. Plankton Res.* **27**: 909–922, doi:10.1093/plankt/fbi064

Wunsch, C., and R. Ferrari, 2004, Vertical mixing, energy and the general circulation of the ocean. *Annu. Rev. Fluid Mech.* **36**: 281–314, doi:10.1146/annurev.fluid.36.050802.122121

II. Chapter

Thermocline mixing and vertical oxygen fluxes in the stratified central North Sea

Lorenzo Rovelli, [a] Marcus Dengler, [a] Mark Schmidt, [a] Stefan Sommer, [a] Peter Linke, [a] and Daniel F. McGinnis [a,b]

[a] Helmholtz Centre for Ocean Research Kiel, GEOMAR, Kiel, Germany
[b] University of Southern Denmark, Institute of Biology, Nordic Center for Earth Evolution (NordCEE), 5320 Odense M, Denmark

To be submitted to *Continental Shelf Research*

Abstract

Vertical mixing processes during the summer stratification period are explored in the central North Sea. At the Tommeliten site, we performed moored fine-scale and microstructure observations of oxygen (O_2), currents, hydrography and turbulence. While current variability was dominated by the lunar semi-diurnal tide (M_2), a second vertical mode near-inertial internal wave was also present during the three-day observational period, with current amplitudes > 0.1 m s^{-1}. Regions of enhanced near-inertial vertical shear of horizontal current were situated in the upper and lower thermocline, coinciding with regions of strong stratification. Turbulent dissipation rates (ε) determined from microstructure shear profiles were moderate (~10^{-9} W kg^{-1}) in the thermocline but increased to 10^{-7} – 10^{-6} W kg^{-1} approaching the sea floor. In the regions of enhanced shear in the upper and lower thermocline values of ε were a factor of ten higher than within the thermocline. O_2 profiles measured with a fast galvanic O_2 sensor (0.2 s response time) mounted on the microstructure probe fully resolved the extent of the oxycline and revealed that the oxycline in the lower thermocline is a significant O_2 source to the otherwise seasonally isolated bottom waters, with a downward average flux of 54 mmol m^{-2} d^{-1} (9 – 134 mmol m^{-2} d^{-1}). This additional O_2 source suggests that there is a large carbon turnover between the central North Sea thermocline and bottom waters.

II.1. Introduction

North Sea

Cultural eutrophication, oil and gas production and climate change effects on the North Sea is a major concern. High nutrient inputs, increasing water temperature, and subsequent decreasing dissolved oxygen (O_2) concentrations threaten to alter the North Sea ecosystem (e.g., Greenwood et al. 2010; OSPAR 2010; Meyer et al. 2011). As shelf seas are directly adjacent to land, they are increasingly susceptible to eutrophication due to surface nutrient runoff and pollutants (OSPAR 2009). O_2 monitoring has been shown to be a robust indicator of these ocean changes (Joos et al. 2003).

Since 1984, surface water temperatures in the North Sea have increased by 1 – 2°C, greater than the global mean (OSPAR 2010; Meyer et al. 2011). On seasonal time scales, climate projections indicate an earlier start of stratification, longer duration, and stronger stratification of the thermocline (Lowe et al. 2009). Earlier onset and longer temperature stratification means increased periods of isolation of deep water, leading to potentially lower O_2 concentrations (Greenwood et al. 2010). Additionally, stronger density gradients will alter vertical transport rates of O_2 and nutrients during the stratification period.

O_2 is an indicator of eutrophication and ecosystem functioning, i.e., for aquatic organisms (Best et al. 2007). While the North Sea is not anoxic, low O_2 levels have been reported at several periods in the past (Anon 1993; Greenwood et al. 2010). Growing concerns of the occurrence of hypoxia in the North Sea (O_2 concentration less than 62.5 μmol L^{-1} or 2 mg L^{-1}; Vaquer-Sunyer and Duarte 2008) have highlighted the need for more specific studies on the O_2 dynamics and driving forces (Kemp et al. 2009).

The central North Sea typically stratifies in April around day 100 (e.g., Meyer et al. 2011). The extensive thermocline (around $1 – 5 \times 10^5$ km^2; Meyer et al. 2011) and the semi-enclosed nature of the North Sea leads to isolated bottom waters (Greenwood et al. 2010). The lower thermocline is an important zone for the establishment of primary production and the O_2 maximum layer (*see* Pingree et al. 1978). In fact, the North Sea deep chlorophyll maximum (DCM) is estimated to account for 58% of the water column primary production and 37% of the annual new production

for the summer stratified North Sea (Weston et al. 2005). The development of the associated O_2 maximum due to this production is thus important and so far not considered in the overall O_2 balance of the central North Sea.

Physical processes

Concentrations of dissolved constituents such as nutrients, O_2 and carbon dioxide (CO_2) within aquatic systems are largely dictated by physical transport processes. Among the different physical processes, turbulent mixing is frequently found to dominantly contribute to constituent balances (*see* Rippeth 2005). Mixing processes depend on the amount and sources of energy input to the system, e.g., wind and tidal motions (Wüest et al. 2000; Wunsch and Ferrari 2004), but also on the local water column stratification. In seasonally stratified shelf seas, for instance, the occurrence of sharp thermoclines acts as an important physical barrier separating surface layers from nutrient-rich deeper waters (Sharples et al. 2001). Investigating the processes that drive diapycnal (i.e., vertical) constituent fluxes across the thermocline throughout the stratification period is of major importance to advance understanding of the system biogeochemical dynamics (e.g., Sharples et al. 2001).

Measurements of shear and stratification have provided supporting evidence that the thermocline of seasonally stratified shelf seas, such as the North Sea, is in a state of marginal stability (van Haren et al. 1999; McKinnon and Gregg 2005). Additional sources of shear could thus trigger shear instability leading to local production of turbulence within the thermocline and thus enhanced vertical fluxes of constituents. Already Itsweire (1989) showed that layers of strong shear are likely to be found where strong stratification occurs. In general, internal tides and near-inertial oscillations are considered to be the major sources of shear in the thermocline (*see* Rippeth 2005).

The importance of internal tides for driving diapycnal nutrient fluxes, for the overall productivity in the thermocline as well as for the associated carbon export to the bottom water has clearly been demonstrated by Sharples et al. (2007) for the shelf edge of the Celtic Sea. There, the dissipation of the internal tidal waves, generated over the shelf edge, was found to be responsible for the observed elevated thermocline mixing.

The occurrence of near-inertial oscillations in shelf seas during the stratified season has been reported in several studies from the North Sea (van Haren et al. 1999; Knight et al. 2002) as well as in other shelf seas (e.g., Rippeth et al. 2002; McKinnon and Gregg 2005). In general, they are the oceans' response to sudden changes in wind forcing or are excited by a periodic wind forcing such as a sea breeze (Rippeth et al. 2002). In regions away from varying topography, like the central North Sea, they are often the dominant source of shear in the thermocline (van Haren et al. 1999; Knight et al. 2002). During the presences of baroclinic inertial waves in the water column, periods of enhanced shear taking the form of shear spikes that are separated by approximately one inertial period and occur in bursts lasting several days have been observed in the western Irish Sea (Rippeth et al. 2009), the Celtic Sea (Palmer et al. 2008) and the northern North Sea (Burchard and Rippeth 2009). A recent numerical study by Burchard and Rippeth (2009) provided an explanation for the dissipation of inertial oscillations and the associated mixing in the thermocline. The model results suggested that shear spikes arise from the alignment of the surface wind stress, bulk shear, and bed stress vectors due to tidal currents. Furthermore, the model results also highlighted the important role of the sense of rotation of the tide in determining the level of shear and diapycnal mixing, as previously suggested by Prandle (1982); and Simpson and Tinker (2009), as the alignment of wind stress is much more effective in generating thermocline shear spikes for anti-cyclonic tides than for cyclonic tides (Burchard and Rippeth 2009).

From the above it is clear that turbulence in the thermocline should often be enhanced. Thus, diapycnal fluxes of nutrients from the bottom boundary layer into the thermocline should play an important role in maintaining high primary production rates in seasonal stratified seas. On the other hand, diapycnal fluxes of O_2 and organic carbon from the thermocline (i.e., the O_2 maximum layer) into the O_2 depleted bottom boundary layer may also substantially contribute to the O_2 and carbon budgets. Adequate measurement programs to quantify the diapycnal O_2 flux contributions have not been performed, nor has this been considered in previous central North Sea O_2 budgets (e.g., Greenwood et al. 2010).

Present study

Our study focuses on the O_2 bottom boundary layer (BBL) balance and the hydrodynamics of the Tommeliten area in the central North Sea (Fig. II.1). The main goal is to advance the

understanding of the physical processes driving mixing in the stratified interior and its role in the ecological functioning of the central North Sea. In particular, the physical processes that are generating enhanced vertical mixing in the stratified water column (or cause shear in the water column) are analyzed. We present magnitude of dissipation rates of turbulent kinetic energy (ε) and diapycnal diffusivities (K_ρ) from the water column along with simultaneously measured high resolution O_2 data used to estimate vertical fluxes of O_2. Finally, we present our results in the prospective of ecological functioning by considering the implication of vertical O_2 transport in general and diapycnal O_2 fluxes specifically. Due to the location of the studied system, which is far away from the coast and from riverine inflows, the main constituent gradients are diapycnal and so a 1-dimensional approach will be used to quantify the O_2 transport; horizontal advective and diffusive transport processes will thus not be considered.

II.2. Methods

Study site

The data in this study were collected over a time period of three days (8 – 11 August 2009) during R/V *Celtic Explorer* cruise CE0913 (26 July to 14 August 2009) at the Tommeliten site (56°29'30" N, 2°59'00" E; Fig. II.1) in the Norwegian sector of the central North Sea (N. 1/9; Linke and Schmidt 2010). The site, which lays ~50 km northeast from the northern Dogger Bank (Greenwood et al. 2010), and its surrounding are characterized by shallow waters (~70 m) at a relatively long distance from coastal areas (on average 300 km) and is known since the 1980s for the presence of buried salt diapirs, methane (CH_4) seeps and bacterial mats (Hovland and Judd 1988). Bathymetric surveys from Schneider von Deimling et al. (2010) in the area revealed a rather flat sandy seabed with almost no features. The currents of the North Sea are predominantly controlled by the semi-diurnal lunar (M_2) tide (12.42 hrs period; Otto et al. 1990), which is also apparent in the data presented in Schneider von Deimling et al. (2010).

Equipment

We investigated the 'Tommeliten' site using a microstructure profiler with a fast O_2 sensor, a lander equipped with an acoustic Doppler current profiler (ADCP) and conductivity-temperature-

depth (CTD) logger, optode O_2 sensors as well as with a ship operated CTD profiler and on-board chemical analyses.

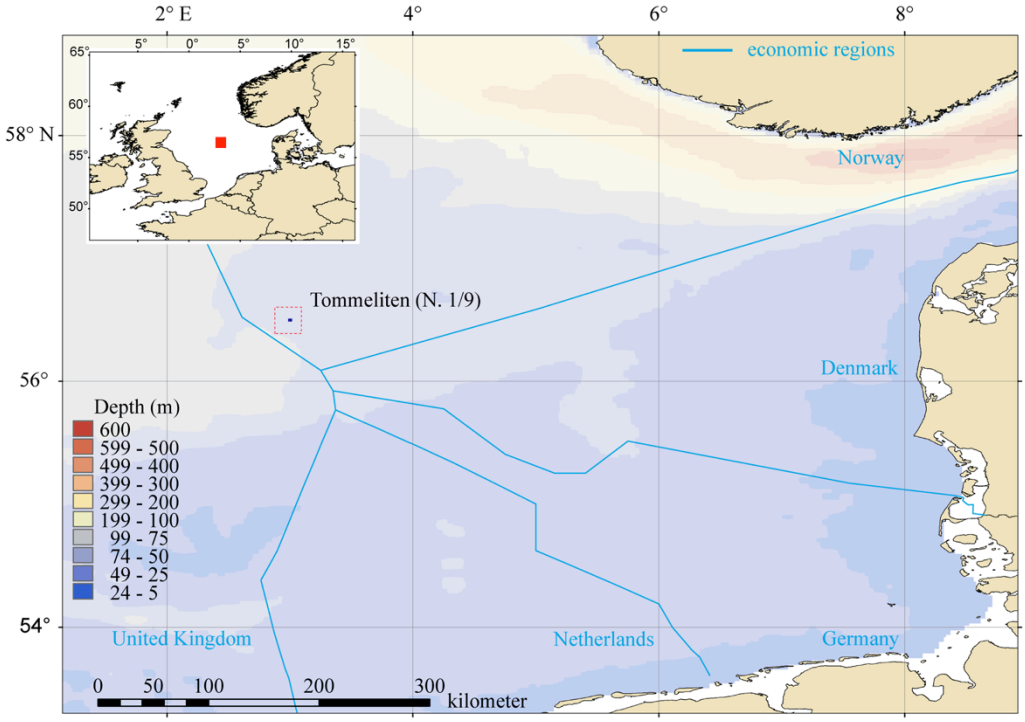

Fig. II.1. Map of the North Sea indicating the water depths and location of the Tommeliten site as well as the borders of the economical regions of the surrounding European countries.

Turbulence and microstructure profiler: Microstructure turbulence profilers are well-established oceanographic instruments (*see* Lueck et al. 2002) capable of profiling the water column with a very high resolution (mm scale) and collect turbulent shear and temperature fluctuation data. We deployed a MSS90-L profiler (ISW Wassermesstechnik, and Sea and Sun Technology, Trappenkamp, Germany).

The MSS90-L is a free-falling, loosely-tethered probe in which the cable is used for data transfer and probe recovery. The probe samples at 1024 Hz with 16 channels and is designed for an optimal sink rate of 0.5 – 0.6 m s^{-1}. During the field survey, the probe was equipped with two air-foil shear probes, an accelerometer (to correct for probe pitch, roll, and vibration), a fast temperature sensor (FP07, 7–12 ms response time) and standard CTD sensors (temperature, pressure, conductivity, Oxyguard® membrane O_2). In addition, we tested a fast (0.2 s response time) galvanic O_2 sensor (AMT, Analysenmesstechnik GmbH, Rostock, Germany). The absolute

O_2 concentrations were computed based on the measured O_2 saturation levels and the in-situ high resolution temperature measurements following the saturation equation of Garcìa and Gordon (1992).

POZ-lander: For current characterization, we deployed the Paleoceanography (POZ) lander; a relatively compact benthic lander equipped with an upward-looking ADCP and a CTD. The lander was deployed using a video guided launcher (Pfannkuche and Linke 2003). The 300 kHz ADCP was deployed and recorded 3-dimensional current velocity profiles and acoustic backscatter information up to 80 m from the bottom (Workhorse Sentinel, Teledyne RD Instruments) and sampled every 15 s with a bin size of 0.5 m (first bin at 2.75 m from the bottom). The logging CTD (XR-420 CT logger, RBR, Kanata, Canada) measured temperature, conductivity and pressure with 2 s resolution and was equipped with a high-precision pressure sensor (Digiquarz, Paroscientific, Redmond, United States).

Profiling CTD: CTD profiles were routinely taken to provide background information on water column stratification with depth, and other scalar parameters. We deployed the shipboard Seabird SBE9plus CTD system, which samples at 24 Hz and was equipped with standard temperature, conductivity and pressure as well as O_2 and light transmission. The SBE9 was equipped with a 12 10L-Niskin-bottles Rosette for discrete water sampling that was used to calibrate the fast O_2 profiles via Winkler titrations.

Benthic chamber: For this study, a benthic chamber was also deployed, with the remotely-operated-vehicle (ROV Kiel 6000, Schilling Robotics, Davis, United States; *see* http://www.geomar.de/en/institute/central-facilities/technology-logistics-centre/rovkiel6000/).
The chamber mainly consists of a 5 L Plexiglas canister with an internal diameter of 19 cm that is inserted up to ~15 cm in the sediment, thus isolating the water inside that chamber from the surroundings. The chamber is equipped with 2 Optodes (Aanderaa, Bergen, Norway) that are located inside and outside the chamber, respectively. Once the system is deployed on the seafloor, the chamber is firstly flushed for 30 min using a pump to ensure that the initial concentration within the chamber is equal to the one of the surrounding water. After the flushing, the pumped is switched off and changes in the O_2 concentration within the chamber are measured at 1 min intervals until the chamber recovery. To prevent the occurrence of

stratification, the enclosed water is lightly agitated by a chamber-mounted slow rotating plastic stirrer. The sediment O_2 uptake rate (SUR) is then estimated by dividing the apparent O_2 loss during the deployment time over the enclosed sediment area. In contrast to the other much larger and complex GEOMAR benthic chambers (Sommer et al. 2008, 2010) the deployed chamber system is small enough to be ROV operated. The main advantage is that the system can be deployed with precision in the designated spot.

Wind measurements: The true wind directions and magnitudes were obtained from the onboard BATOS weather station (Meteo-France). The station features a static ultrasonic anemometer (Windsonic, Gill Instruments)

Physical analyses

The collected physical data were analyzed with regard to wind, tidal and near-inertial forcing, water column stratification as well as turbulence and diapycnal (vertical) fluxes.

Current characterization: To understand the contribution and implication of tidal and non-tidal forcing on water column measurements, the tidal regime was characterized by considering changes in the hydrostatic pressure, determining barotropic (approximated as depth-average) and baroclinic (variable with depth) velocity contributions, computing theoretical particle displacement tracks and performing spectral analysis to identify the tidal components and to quantify non-tidal contributions.

The variance analysis is determined by rotating the coordinate system of the current velocities u and v over a stepwise increasing rotation angle (r) as $u_{rot} = u \cdot \cos(-r) - v \cdot \sin(-r)$ respectively $v_{rot} = u \cdot \sin(-r) - v \cdot \cos(-r)$, and by computing the current velocity variance at each step. It is thus possible to identify the major and minor axis of the tidal ellipsoid.

Barotropic and baroclinic flow contributions of tides were separated by least-square fitting the detrended velocity time series to harmonics $u = A \cdot \cos(\omega \cdot t + \varphi)$ with A, ω, φ being the amplitude, frequency, and the phase lag, respectively. In the analysis below, barotropic semi-diurnal principle lunar tide (M_2) and diurnal declination tide (K_1) contributions having frequencies of 1.93227 cycles per day (cpd) and 1.00274 cpd, respectively were subtracted from the time series to analyze residual flow. For barotropic contributions, the fit was applied to the

depth average of the time series, while baroclinic contributions were obtained by fitting the harmonics to the velocities time series from each 0.5m ADCP bin.

To investigate the occurrence of enhanced shear in the stratified water column, vertical shear of horizontal velocity was calculated from the ADCP data by computing the vertical gradients between adjacent bins of East and North velocity (0.5 m resolution).

Spectral analysis: Frequency spectra of the time series of horizontal velocity and vertical shear of horizontal velocity were calculated using fast-Fourier transforms combined with a ½-cosine tapper (Hanning window) that was applied to the first and last 10% of the time series data.

Water column stability: The water column stability N^2 is the buoyancy frequency N squared. N is the oscillatory motion experienced by a perturbed, i.e., upward or downward adiabatically displaced, water parcel as it tends to return to is equilibrium position. N^2 is also used to describe the degree of stratification in fluids, (water column stability) and is defined as $N^2 = -g(\rho^{-1}\partial\rho/\partial z - g/c^2)$, where ρ is density, g the earth's gravitational acceleration and c speed of sound. High values of N^2 are found in the thermocline. If the water column is well mixed, the N^2 values will approach $0\ s^{-2}$ while N^2 will turn negative in case of unstable stratification, i.e., in overturns. Throughout this study, N^2 is calculated from temperature, salinity and pressure data using the adiabatic method (Fofonoff, 1985).

Temperature gradient: Unstable stratified regions (i.e., overturns) having $N^2<0$ within the stratified water column are due to turbulent eddies. If density is predominately determined by temperature, a graphical representation of the temperature gradient (dT/dz) can be used to visualize, on a qualitative scale, overturns. At the boundaries, however, as temperature is homogenous, intermittent positive and negative values on small scales just represent measurement inaccuracies.

Dissipation rates of turbulent kinetic energy: Turbulent kinetic energy dissipation rate (ε) can be quantified from the airfoil shear readings by integrating shear wavenumber spectra assuming isotropic turbulence (Batchelor 1953):

$$\varepsilon = 7.5\mu \int_{k_{\min}}^{k_{\max}} E_{du'/dz}(k)\,dk \qquad \text{(II.1)}$$

where μ is the dynamic viscosity of seawater. Shear spectra $E_{du'/dz}(k)$ were calculated from one-second ensembles (1024 values) and integrated between a lower k_{min} = 3 cycles per minute (cpm) and an upper wavenumber k_{min} that varied between 14 cpm and 30 cpm depending on the Kolmogorov wavenumber. Here, a Bartlett window was applied to the whole ensemble prior to spectral decomposition. Loss of variance due to the limited wavenumber band was taken into account by fitting the observed shear spectra to the universal Nasmyth spectrum. Similarly, corrections for the loss of variance due to finite sensor tip of the airfoil probes were applied (*see* Schafstall et al. 2010). The detection limit, or noise level, for ε is inferred to be 1×10^{-9} W kg^{-1} for the used profiler (Schafstall et al. 2010); the upper detection limit, however, is a function of the shear sensor geometry (up to 10^{-4} W kg^{-1}; Prandke and Stips 1998).

Microstructure measurements were performed from the stern while steaming with about 1 knot into the wind. Unfortunately, it was found that the bow thruster of R/V *Celtic Explorer* circulated surface water up to 25 m deep. R/V *Celtic Explorer* is equipped with an omnidirectional 700kW Gill Jet at the bow that is used to accelerate and maneuver the vessel by pumping water through a rotatable vended discharge defector. The water jet from this propulsion was occasionally captured by our microstructure probe while sampling at the vessels stern at several depths within the surface layer. The water jet was associated with very high turbulence (above 1×10^{-5} W kg^{-1}), strong intermittent temperature gradients and strong echo amplitude signals in the vessel-mounted ADCP data presumable caused by small entrained air bubbles

The data from the microstructure profiler collected within the water jet from the thrusters was carefully flagged on the basis of the three parameters above. Additionally, a consistency check in which the Thorpe scales (Thorpe 1977) calculated from the microstructure temperature data were compared with the Ozmidov scales, $L_O = \left(\varepsilon / N^3\right)^{1/2}$ determined from microstructure shear data, was performed within turbulent patches. In turbulent patches arising from the thrusters, Thorpe scales were strongly elevated relative to Ozmidov scales as surface waters having the respective surface temperature characteristic were advected into the deeper water column. In a final editing step, all data sampled from the surface to 5m below the deepest jet flagged data point were additionally flagged to ensure that no contaminated data are used in this study. Additional editing of the data was performed to account for collisions of the shear sensors with small particles and

rarely occurring cable spooling problems during the descent of the profiler (e.g., cast 7). It should be noted that cast 36 was not successful and casts 16 to 23 were not performed down to the sea floor providing a gap in the BBL dissipation rate data.

Although mixing events are often of low magnitude and short duration, rarely occurring energetic events will cause substantial irreversible changes in the water column. Here, average quantities for ε and related parameters are determined by arithmetical averages (Davis 1996) and not by maximum likelihood estimate of a log-normal distribution (Baker and Gibson 1987) as departures of log-normal distributions of these quantities have been reported (Davis 1996).

Vertical fluxes

There are several well-established methods for estimations of the turbulent eddy diffusivities (K_ρ). Some rely on temporal and spatial gradients (Budget-gradient methods; Powell and Jassby 1974) other on direct measurements of the vertical concentration changes with time during deliberate tracers release experiments (Ledwell and Bratkovich 1995). The method used in this study depends on measurements of dissipation rates of turbulent kinetic energy, ε, and water column stability, N^2, and is based on the assumption of a local equilibrium of production and dissipation of turbulent kinetic energy (Osborn 1980).

Flux gradient method: As suggested by Osborn (1980), the turbulent eddy diffusivity of mass K_ρ can be approximated as $K_\rho = \gamma\varepsilon / N^2$ where γ is the mixing efficiency. As horizontal density gradients at the study site are small compared to vertical gradients, we equate diapycnal eddy diffusivities with vertical diffusivities (i.e., $K_\rho = K_z$). The vertical constituent fluxes are then obtained from K_z and the concentration gradient for the measured solute (θ) as $F_\theta = K_z \frac{\partial \theta}{\partial z}$. In order to provide robust K_z values, time and depth variability as well as the methods limitations, have to be considered. The Osborn (1980) approximation and thus the gradient method are not applicable for N^2 values approaching 0, as K_z would be undefined. In stratified waters the mixing efficiency γ is 0.15 ± 0.05 (Ivey and Imberger 1991) and decreases in weakly stratified waters such as the BBL (Lorke et al. 2008). To account for this decrease, Shih et al. (2005) provided a parameterization for γ and hence K_z based on turbulence activity parameter $\varepsilon / \nu N^2$, with ν being

the kinematic viscosity. In energetic regimes, that were defined for $\varepsilon / \nu N^2 > 100$, they found that the eddy diffusivity is better estimated as $K_p = 2\nu(\varepsilon / \nu N^2)^{1/2}$.

The water column stability, N^2, as well as ε are the main variables affecting K_z values in the stratified ocean. To obtain representative mean turbulent eddy diffusivities, both variables have to be averaged in depth and time to reduce uncertainties due to the patchiness of turbulence and temporal fluctuation of N^2. Additionally, the mixing efficiency is not constant for a given environment but varies over time (*see* Smyth et al. 2001). To provide more robust results, the microstructure data will be evaluated in ensembles of three to four consecutive profiles. As proposed by Ferrari and Polzin (2005), the level of uncertainty of the averaged K_z can be quantified as:

$$\Delta K_z = K_z \left[\left(\frac{\Delta \Gamma}{\Gamma} \right)^2 + \left(\frac{\Delta \varepsilon}{\varepsilon} \right)^2 + \left(\frac{\Delta N^2}{N^2} \right)^2 \right]^{1/2} \tag{II.2}$$

with Δ being the absolute uncertainty of the various average terms. Here, the uncertainties are evaluated in the region of strong vertical O_2 gradients (*see* below) and in 2 m depth bins. The absolute uncertainty from the mixing efficiency ($\Delta\Gamma$) was assumed to be 0.04 (*see* St. Laurent and Schmitt 1999). The absolute uncertainty on N^2 (ΔN^2) was determined by the standard error of the 2 m averaged N^2. The standard error here refers to the standard deviation divided by the square root of the number of estimates. Finally, the statistical uncertainty of ε for each bin is calculated using a bootstrap method (10^4 resamples; Efron 1979). Accordingly, the uncertainty on the estimates of averaged turbulent O_2 fluxes is given by:

$$\Delta Flux_{O_2} = Flux_{O_2} \left[\left(\frac{\Delta K_z}{K_z} \right)^2 + \left(\frac{\Delta \partial_z [O_2]}{\partial_z [O_2]} \right)^2 \right]^{1/2} \tag{II.3}$$

where $\Delta \partial_z [O_2]$ denotes the standard error of mean vertical gradients of O_2 concentrations. It should be noted that the analysis does not include biases or uncertainties due to measurement error. The total error of the flux calculation may thus be larger than the statistical error presented above.

II.3. Results

Water column characteristics: CTD casts were collected to obtain background information on the water column structure (Fig. II.2).

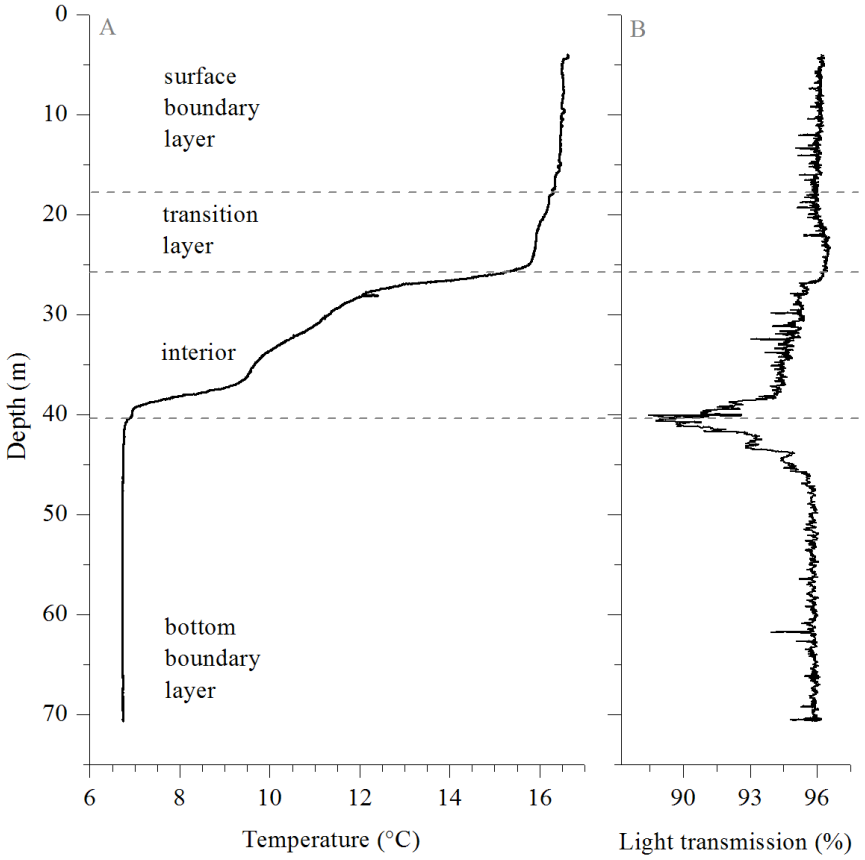

Fig. II.2. Water column physical and chemical background information. (A) potential temperature and (B) light transmission profiles obtained during CTD cast 18. The temperature profile was used to identify the water column layers assuming a 0.2°C and 1.5°C decrease from a 3–6 m average for the lower end of the surface boundary layer and transition layer respectively; a 0.2°C increase from the 50–60 m average was also used to identify the upper end of the bottom boundary layer. The average salinity was 35.08 with little variation throughout the water column (35.04 to 35.1).

At the time of the cruise the ~70 m deep water column displayed four well-defined vertical layers (Fig. II.2A); a well-mixed surface boundary layer (SBL) and BBL, 15 m and 30 m thick respectively, separated by a weakly-stratified transition layer (~15–25 m depth) and a strongly stratified interior layer (~25–40 m depth,). The layers were identified by changes of temperature

over defined depth intervals. The bottom depth of the SBL and the transition layer were taken as the depth where surface temperature (3–6 m average) had decreased by 0.2°C and 1.5°C, respectively. The upper depth of the BBL was defined as the depth where temperature had increase by 0.2°C relative to the BBL average determined from temperature between 50–60 m depth. The interior layer was characterized by two very sharp thermoclines situated in the upper (27–30 m depth) and lower (36–39 m depth) region of the layer and exhibiting vertical temperature gradients of up to 2°C m^{-1}. These two layers were found to persist during the whole measurement campaign.

The light transmission ranged from 89% to 96%, thus indicating low water turbidity. The most turbid layer was observed at the lower limit of the interior layer (at 40 m depth) suggesting the presence of phytoplankton, zooplankton and suspended particles.

Current characterization: The POZ-Lander was deployed for three days in which both velocity data and CTD data were collected (Fig. II.3A). Changes in the water level as the result of the tide were found to range from 0.6 to 0.9 m. Although the velocity data (Fig. II.3B, C) clearly showed a dominance of the barotropic semi-diurnal tide at all depths, there was an indication of the presence of baroclinic velocity contributions superimposed on the tidal currents. A variance analysis on the velocity data identified the major and minor axis of the tidal ellipsoid components to occur at 45° and 135° from true north respectively. Along those axis, the current amplitudes where 0.21 m s^{-1} and 0.04 m s^{-1}, indicating a narrow tidal current ellipse. These amplitudes agree well with previous measurements and model results from the central North Sea (e.g., Otto et al. 1990). From least-square fitting of the depth-averaged velocity time series to the tidal harmonic, east (zonal) and north (meridional) barotropic M_2-current amplitudes of 0.12 m s^{-1} and 0.17 m s^{-1}, and K_1-current amplitudes of 0.005 m s^{-1} and 0.03 m s^{-1} were obtained, respectively. The site is characterized by a negative (clockwise) tide polarity for the semi-diurnal tides. As shown by Simpson and Tinker (2009) for Celtic Sea sites, tide polarity is related to the strength of mixing in the BBL and thus its vertical extension (*see* discussion below).

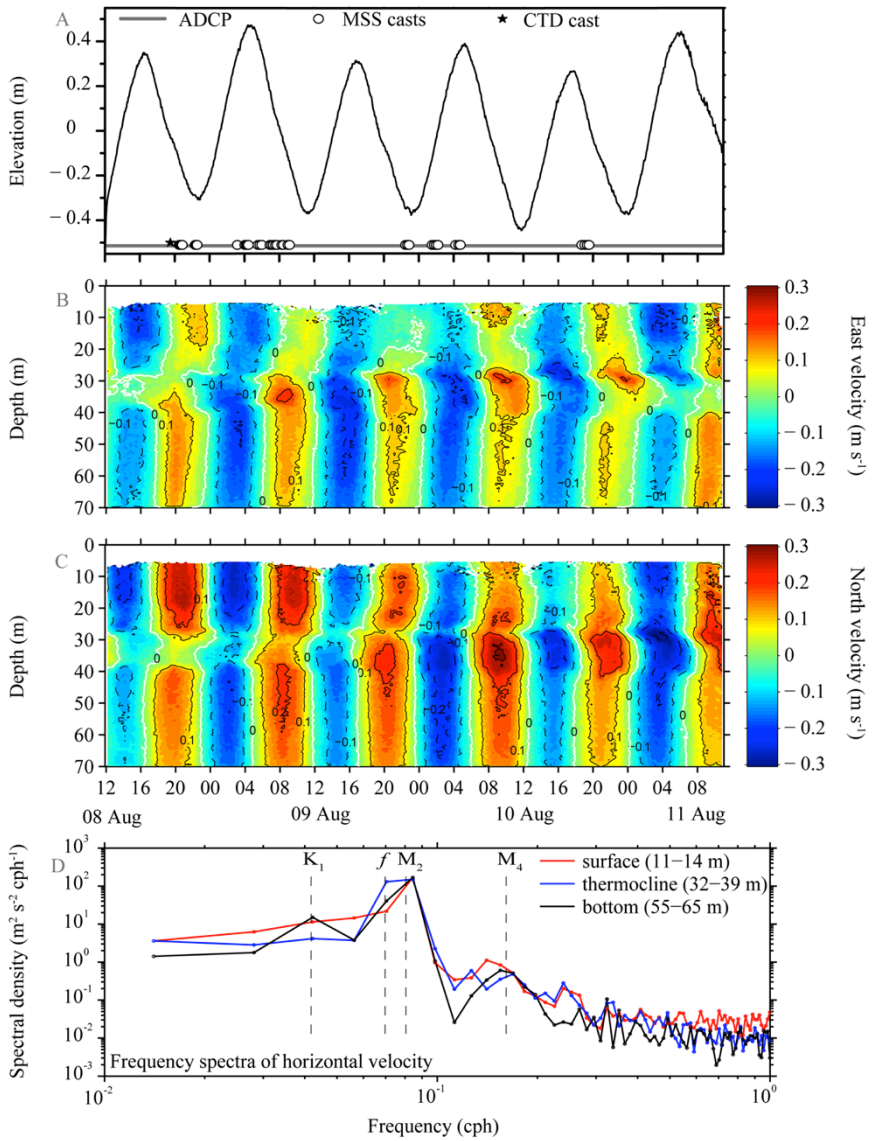

Fig. II.3. (A) Sea surface elevation relative to average level during the observational period (elevation = 0 m) and schedule of different instrument deployments. Tidal induced oscillations in the water level were 0.6 to 0.9 m. (B,C) Horizontal velocities, showing 20 min averaged east (B) and north (C) velocities. Note that although the velocities field is dominated by barotropic M_2 variability, there is a clear presence of a baroclinic oscillation having lower frequencies. Note that panels A to C have the same time axis. (D) Frequency spectra of horizontal velocity calculated from the ADCP data for selected depth ranges for the SBL (red line), interior (blue line), and BBL (black line). The inertial *f* as well as the K_1, M_2 and M_4 frequencies are marked. Note that near-inertial currents *f* are evident in the thermocline.

To elucidate velocity contributions from other velocity driving components, spectra of horizontal velocity, i.e., east and north currents, were calculated for different layers (Fig. II.3D). Although

the limited length of the ADCP velocity time series did not allow for full separation of the semi-diurnal and inertial frequencies, the spectral density functions indicate maximum energy at frequencies of about the semi-diurnal tide. This maximum varies little with depth indicating barotropic M_2 motions. Additionally, the spectra show the presence of near-inertial motions having lower frequencies that are most pronounced in the thermocline (32 – 39 m). Lower but still elevated energy densities at the near-inertial band were also found in the SBL and BBL, suggesting a baroclinic nature of these fluctuations. Average amplitudes of the near-inertial fluctuations in the thermocline obtained from least-square fitting were 0.11 m s^{-1}. In the BBL and SBL, average amplitudes were 0.06 m s^{-1} and 0.04 m s^{-1}, respectively. Somewhat elevated energy is also visible at higher frequency in the range of 0.11 cph to 0.25 cph that may originate from wave-wave interaction of the dominant fluctuations (e.g., van Haren 1999).

In stratified shelf seas, near-inertial oscillations are often reported to exhibit a baroclinic structure having one or more 180°-phase shifts between the upper and lower layers, which in turn results in elevated velocity shear in the interfaces (*see* Knight et al. 2002, van Haren et al. 1999). To better visualize the characteristics of the near-inertial feature, the dominant barotropic M_2 and K_1 tidal contributions were subtracted from the measured currents using the harmonic fit parameters. Fig. II.4A and B show the residual current for both east (u') and north (v') velocities. It is quite evident that the residual flow in the upper layer (8–30m depth) and in the thermocline (30–40m depth) is of opposite phase. Similarly although less pronounced, the flow in the thermocline exhibits a 180° phase shift compared to the flow in the BBL (40–70m depth) during the latter part of the time series. However, a thermocline – BBL phase shift is not so evident during the first 1.5 days. In fact, the phase difference between the residual thermocline and BBL flow gradually approaches 180° between mid-day of August 9 and morning of August 10 (not shown). Nevertheless, the dominant vertical structure of the near-inertial oscillation in the velocity data is best described as a second vertical mode feature. The lack of a clear 180°-phase shift in the lower water column may be due to superimposed oscillations or the fact that the mode was being set up during the observational period. It should be noted that the inertial oscillation in the data set here contrasts earlier observations of near-inertial waves in the northern

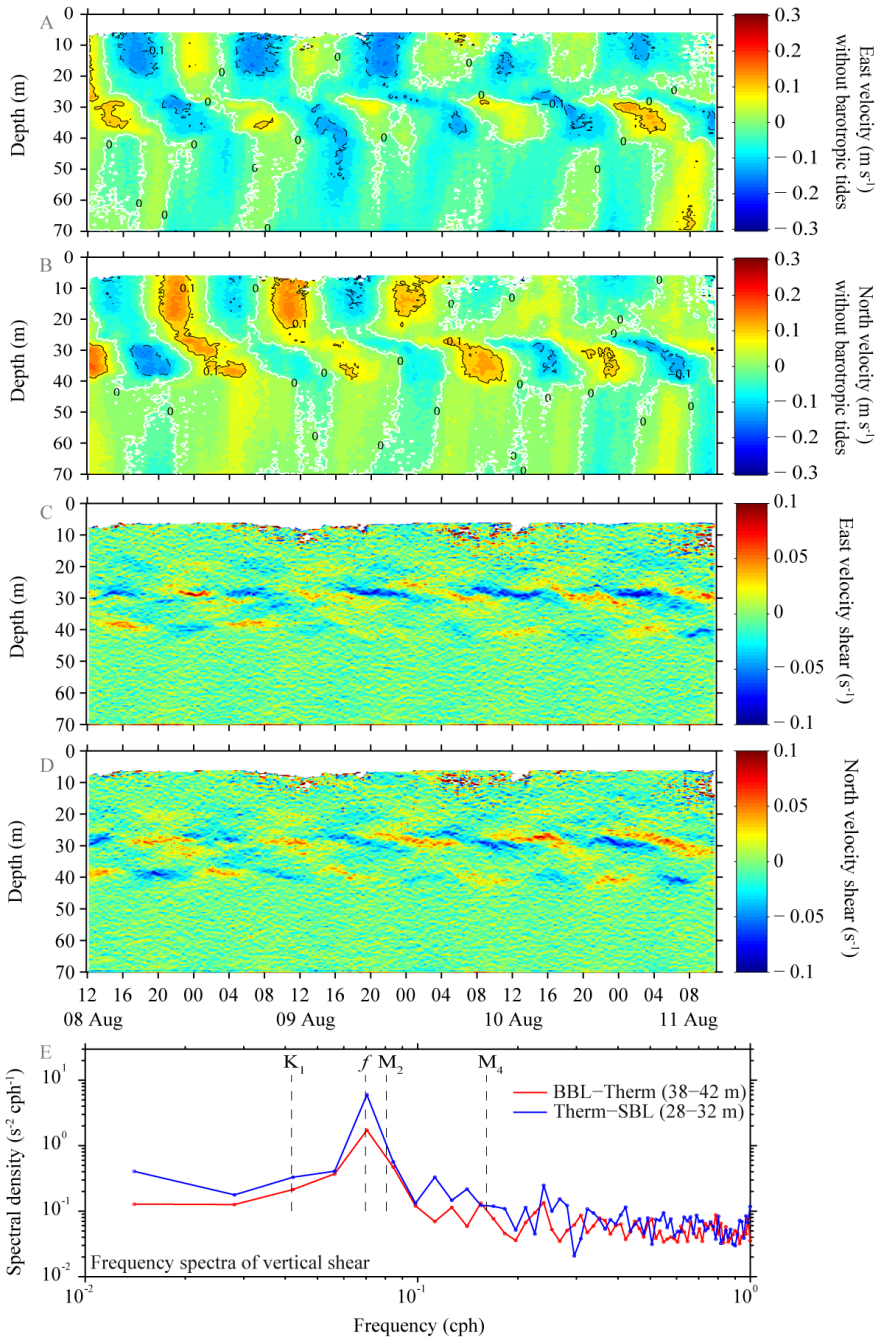

Fig. II.4. Non barotropic current velocities and vertical shear of horizontal velocity. (A, B) Current velocities as in Fig. II.3B and C, but without barotropic contributions for east (A) and north (B) velocities, respectively. (C, D) Vertical shear of horizontal velocity, S, for east (C) and north (D) velocity calculated from the ADCP data (*see* Fig. II.3B and C) indicating enhanced shear within the interior that is proposed to be the source of mixing in an otherwise well-stratified layer. Note that panels A to C have the same time axis. (E) Frequency spectra of vertical shear of horizontal velocity, S, calculated from the ADCP data for the maximum shear layers detected in (C, D). Note that the spectra clearly indicate near-inertial oscillation (*f*) to be the main contributor to the detected enhanced shear.

North Sea by Knight et al. (2002) who found a 1st vertical mode wave to be dominant from data collected in September and October 1998.

As already suggested by the vertical distribution of velocity (Fig. II.4) and by the phase shift analysis above, enhanced vertical shear of horizontal velocity (S) is found in the interfacial regions: between the interior layer and the transition layer as well as between the interior layer and the BBL (Fig. II.4C, D). The high vertical resolution (0.5 m) of the velocity data allows resolution of the interfacial shear layers, which are typically 2 to 3 m thick and exhibit elevated values of up to 0.05 s^{-1}. Comparisons with CTD data showed that they are collocated with the two enhanced temperature gradients layers in the thermocline (between 27 to 30 m and 36 to 39 m depth, respectively). It should be emphasized that in between these interfacial shear layers, vertical shear is strongly reduced, while additional shear was also detected at the SBL-transition layer interface (18 – 20 m depth). As indicated by the spectral density function of the shear time series from the interior interfacial layers (Fig. II.4D), the shear is due to the inertial velocity fluctuations that were present during the measurement campaign. However, particularly the amplitude of shear in the upper thermocline is subjected to temporal variability as will be discussed below.

Microstructure temperature and O_2 profiles: A total of 39 profiles were obtained at the same location within the Tommeliten site, but during different tidal phases (Fig. II.3A). As the profiler falls freely through the water column, high resolution temperature, O_2, and shear measurements are not affected by cable drag from the vessels movement due to surface waves, thus allowing for a detailed high vertical resolution characterization of those properties. In addition, the galvanic O_2 sensor was fast enough (0.2 s time constant) to resolve O_2 fine-structure at the cm scale (10 cm resolution) even at the fast profiling speed (0.5 – 0.6 m s^{-1}) of the probe.

Fig. II.5 shows four selected MSS90 profiles. These profiles belong to the longest measurement cluster and were chosen as they cover a period of about half of the tidal and inertial cycle; the time interval between those profiles is 1.5 h. Most striking are the sharp vertical temperature gradients (dT/dz) in the two thermocline boundaries of the interior layer that exhibit temperature gradients of up to 4°C m^{-1} and little vertical displacement variability during the course of the tidal cycle. Stratification (N^2) in those layers calculated over 2 m intervals exceeds 10^{-3} s^{-2}. As

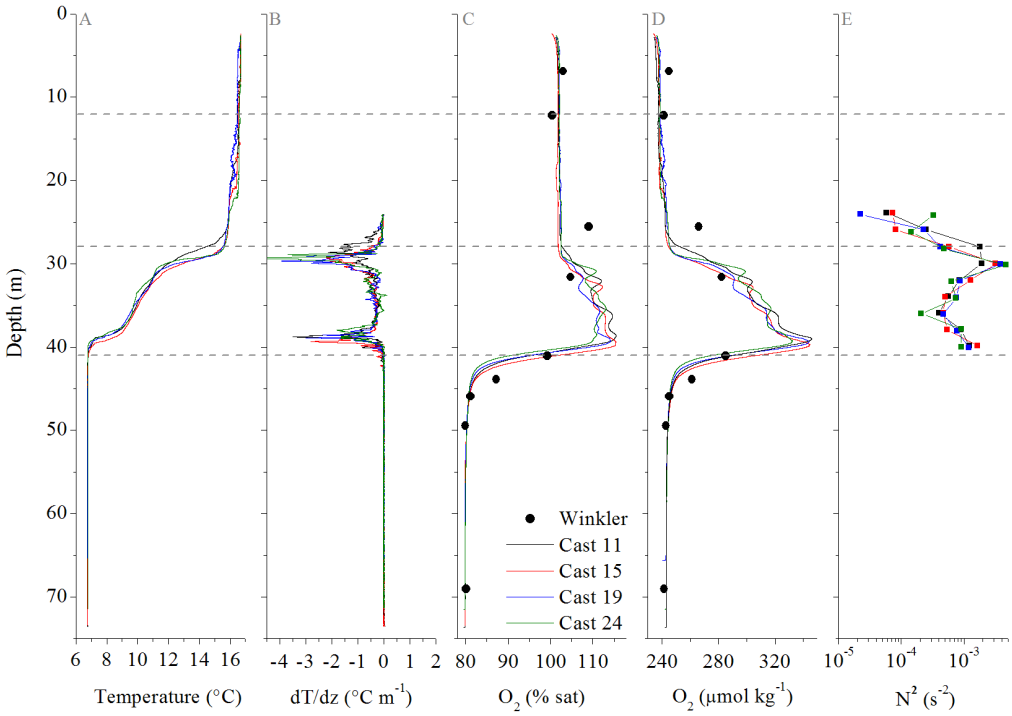

Fig. II.5. Selected profiles from the MSS casts showing temperature (A), temperature gradient (dT/dz; B), O_2 in % saturation (% sat; C) and absolute concentration (D) as well as water column stability (N^2) profiles (D). The dashed lines represent the temperature layers as in Fig. II.2A. N^2 profiles display averaged data; below the thermocline N^2 values are ~ 0. Please note that the data in the upper 25m of the water column are contaminated by the vessels thrusters and thus disregarded from further analysis. Panel C also provides the Winkler derived saturation percentages that were used to correct the fast O_2 sensor readings

noted above, the sharp thermoclines are also the regions of elevated velocity shear. In contrast, the O_2 profiles from the fast-responding galvanic sensor indicate that the lower thermocline was associated with an O_2 maximum that sharply decayed towards the BBL while somewhat reduced O_2 values were measured in the interior layer above. The oxycline at the interior-BBL interface was 2 – 3 m thick and displayed a highly enhanced O_2 vertical gradient on the order of 34 µmol kg^{-1} m^{-1}. Here, the temperature dependence of solubility resulting from the associated temperature gradient increases the vertical O_2 gradient by 3 – 4 µmol kg^{-1} m^{-1}. The temperature dependency of the O_2 sensor is accounted for during data acquisition using a sensor-specific factory correction, which is embedded in the microstructure profiler data collection algorithms (Dr. Andreas Schmuhl, AMT, pers. comm.). It should be noted that the interior O_2 values were persistently oversaturated reaching up to 114% at the O_2 maximum while in the SBL and BBL,

O_2 was near-saturation and 80% saturation, respectively (Fig. II.5). The fast O_2 sensor readings correction was performed based on O_2 saturations percentage obtained from Winkler titrations on discrete water sampling. As the O_2 maxima, which existed over 1 m, could not be properly sampled with the large 10 L bottles, SBL and BBL readings were considered for the correction. With the exception of the BBL, the fast thermistor data from the MSS90 profiles revealed slight temporal changes in temperature stratification in the upper region of the interior layer, which is probably related to the near-inertial oscillation. The water column stability N^2 (Fig. II.5) peaks (10^{-3} s^{-2}) in the interior layer are concomitant with the stable thermocline. In the well-mixed BBL, $N^2 \sim 0$ as there are no detectable density gradients.

Turbulent dissipation: Turbulent dissipation rates (ε) determined from microstructure shear profiles (Prandke and Stips 1998) were particularly low ($2 - 5 \times 10^{-9}$ W kg^{-1}) in the center of the interior layer and strongly elevated (up to 10^{-6} W kg^{-1}) near the sea floor (Fig. II.6). In the interior layer, however, elevated dissipation rates were frequently observed at the upper and lower limits. These coincide with the depth range of the interfacial shear layers (Fig. II.4A) and the water column stability maxima (Fig. II.5).

To determine system representative dissipation rates during the observational period, all non-flagged ε profiles were used to calculate a mean profile (Fig. II.6). 95%-confidence intervals were obtained from bootstrapping (Efron 1979). At the upper and lower interior layer limits, the dissipation rates were increased (5×10^{-9} W kg^{-1} and 2×10^{-8} W kg^{-1}, respectively). Those regions are separated by a region having strongly reduced ε values of on average 2×10^{-9} W kg^{-1}. In the BBL, the averaged profile showed a near-exponential increase with depth, and elevated values occurring during maximum tidal flow near the ocean floor.

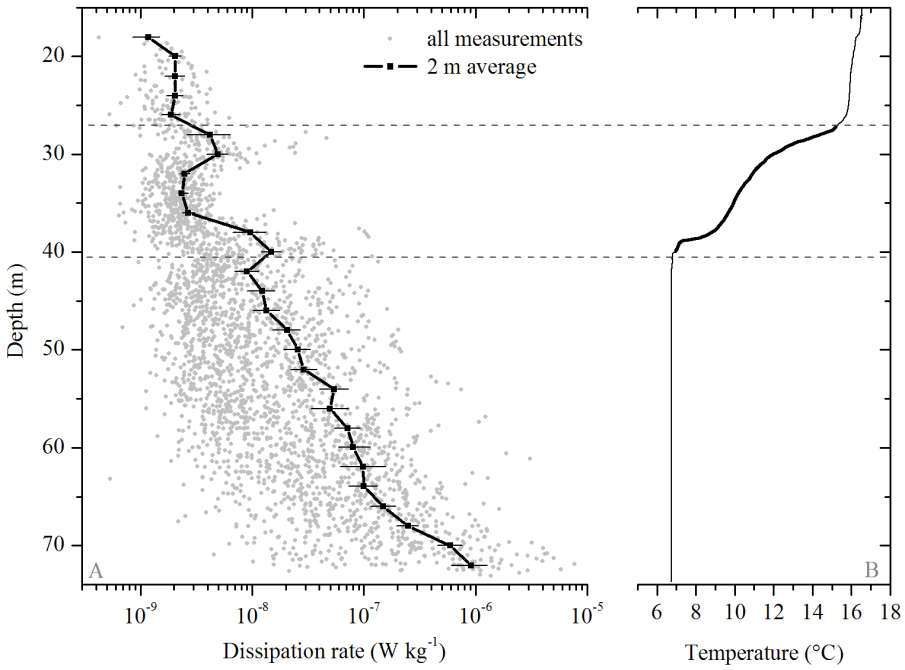

Fig. II.6. Profiles overview and averaged turbulence profile. (A) Dissipation from all profiles (dots) together with the arithmetic mean (solid line). Note the dissipation peaks at the stratified upper and lower end of the interior (~ 30 and 40 m, respectively). The water level varied by ± 0.4 m due to the tide (Fig. II.3A). Note that values below the profiler noise level (1 x 10^{-9} W kg^{-1}) were not considered in the averaged profile. (B) Representative temperature profile showing the different temperature layers (thin and thick lines) as shown in Fig. II.2A.

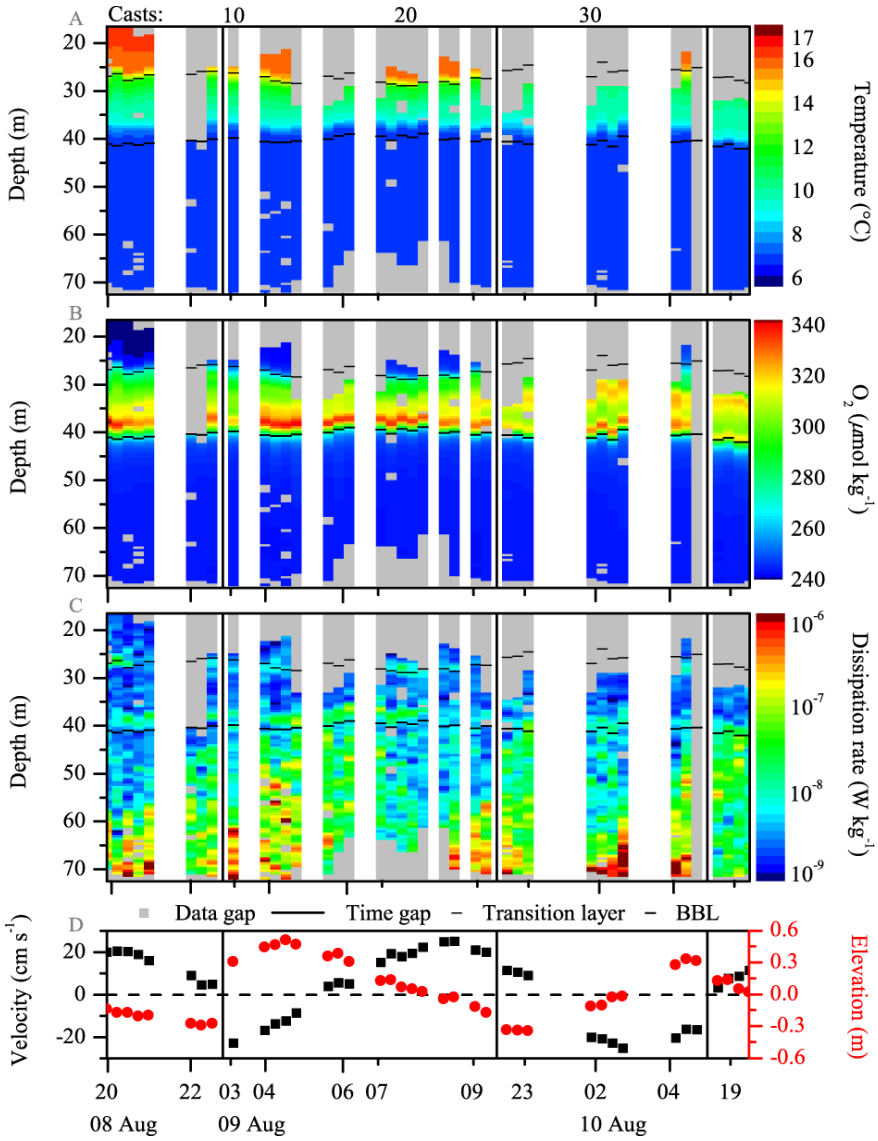

Fig. II.7. Tidal referenced temperature, O_2, and turbulence contour plots. (A) temperature, (B) O_2, and (C) turbulence contour plot of all MSS90 casts together with the temperature layers (thin and thick dashes for transition layer and BBL, respectively) defined from the temperature profiles as explained on Fig. II.2. Note that in the interior increased dissipation rates were detected at its upper and lower end, which is where the strongest stratification was also detected (*see* Fig. II.5). The empty gray spots in the ε contour plot are due to data that were flagged as possible ship thrusters contamination (SBL and transition layer) or collisions (interior and BBL), casts not reaching the bottom (casts 16 – 23) or unsuccessful casts (profile 36); to enable direct comparisons the same temperature and O_2 data were omitted as well. The vertical black lines indicate the transition (time gaps) between consecutive profile ensembles. (D) Background information on bottom current and sea surface elevation (*see* Fig. II.3) during the casts as collected by the deployed POZ lander. Note that as a result of the time gaps between the consecutive MSS90 casts (*see* Fig. II.3A) the time scale, which is the same for all panels, is not linear.

From the temporal evolution of the turbulent dissipation rates (Fig. II.7) the following can be elucidated:

- Turbulence patterns in the BBL suggest a phase lag between maximum bottom dissipation rates, which are in phase with maximum tidal flow and result from bottom friction, and the occurrence of the associated dissipation rate maxima further up in the BBL. This can be explained by upward-propagating shear stress that generates turbulence away from the bottom boundary and results in the phase lag between maximum dissipation rates near the bottom and in the interior BBL (*see* Simpson et al. 2000; Burchard et al. 2008).
- Temporal variability of the dissipation rates in the upper and lower boundary of the interior layer correlates with temporal variability of the magnitude of interfacial shear due to the inertial oscillations.
- Dissipation rates in the region of the elevated O_2 gradients in the lower interior layer are elevated due to the interfacial shear layers (e.g., profiles 4 – 22) but also due to upward-propagating shear stress from the bottom boundary (e.g., profiles 12 – 18 and 38 – 40).

Also evident are apparent displacements of the interior-BBL interface even between consecutive profiles that are likely due to issues with the pressure sensor. For determining eddy diffusivities and diapycnal O_2 fluxes, the pressure of individual profiles was offset such that elevated oxygen gradient zones between the interior layer and the BBL were located at the same depth.

Eddy diffusivities: K_z values were found to range from 6×10^{-7} m^2 s^{-1} below the upper oxycline to 3×10^{-6} m^2 s^{-1} in the lower region of the transition layer (Fig. II.8A). At the interior-BBL interface where the vertical O_2 gradient was the strongest, K_z reached 2×10^{-5} m^2 s^{-1}. The error bars shown in the figure refers the uncertainty level in K_z resulting from the changes in the dissipation rates (Fig. II.6), N^2 fluctuations (Fig. II.4) as well as reductions of the mixing efficiency based on the Shih et al. (2005) parameterization (*see* Methods). In the lower interfacial layer (BBL - thermocline) increased turbulence (Fig. II.6) and weaker stratification (Fig. II.7) are responsible for the increased eddy diffusivities. In contrast, in the upper interface (thermocline - transition layer) where ε is elevated with respect to the central interior but reduced compared to the lower interfacial layer (Fig. II.6), larger N^2 values (Fig. II.5) reduce the eddy diffusivities. However, as most of the data above 25 m were flagged due to thruster contamination, these

estimates are too heavily biased to be comparable to the remainder of the dataset; the result will be shown but disregarded from further analysis. Larger mixing events during the presence of the inertial wave may have been completely missed.

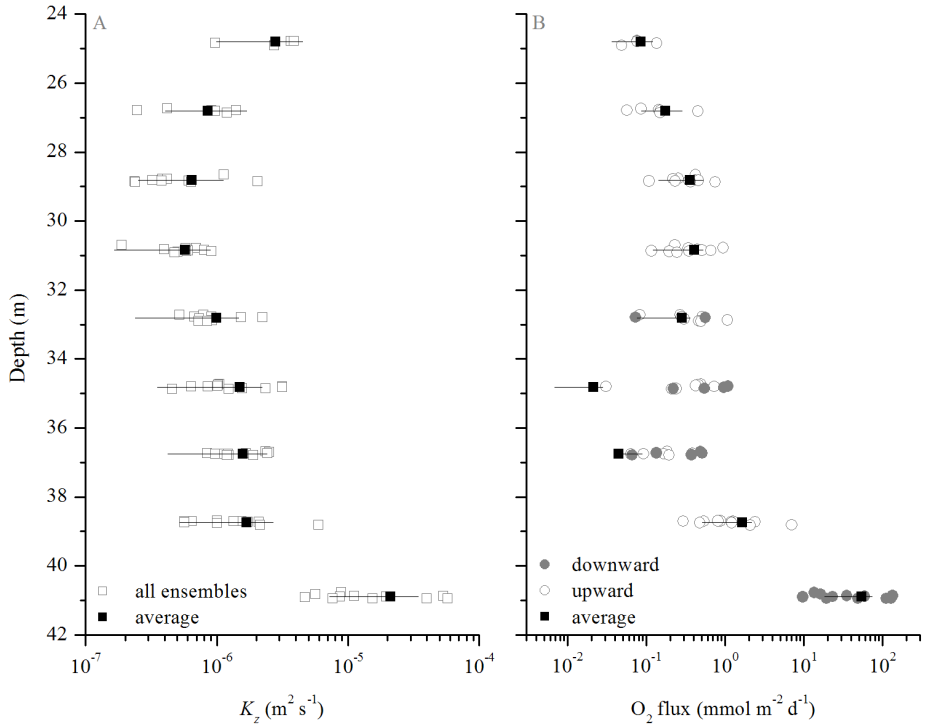

Fig. II.8. Vertical eddy diffusion coefficient and O_2 fluxes. (A) Average vertical eddy diffusion coefficient K_z with uncertainties bars as well as the K_z values for every ensemble (open squares), which represent the average over 3 to 4 consecutive profiles. Note that at the lower end of the interior (at the dissipation rate peaks, Fig. II.6) K_z values are up to a factor 10 higher than in the central interior. (B) Average O_2 flux over 2 m bins with the respective uncertainties intervals (solid square and black line). The values for each profile cluster are shown both downward and upward fluxes (solid and open squares, respectively).

Oxygen fluxes: Fig. II.8B shows the 2 m bin average for the lower transition layer (until about 25 m depth) and the interior (below about 25 m) O_2 fluxes based on the AMT sensor together with the averages from each ensemble. A substantial O_2 flux divergence of 54 mmol m^{-2} d^{-1} (ranging from 9 to 134 mmol m^{-2} d^{-1}) was identified from the lower thermocline to the nutrient rich BBL. Considering the flux uncertainties (*see* Methods) the confidence interval associated with the average O_2 flux was 18 – 74 mmol m^{-2} d^{-1}. On the contrary, small O_2 fluxes (~1 mmol m^{-2} d^{-1}) were estimated for the other regions in the thermocline. This suggests that little oxygen is

transported upward from the oxygen maximum to the rest of the interior. How much of that O_2 is then transported from the interior to the transition layer remains unknown as on this study K_z could not be estimated robustly enough due to the data flagging.

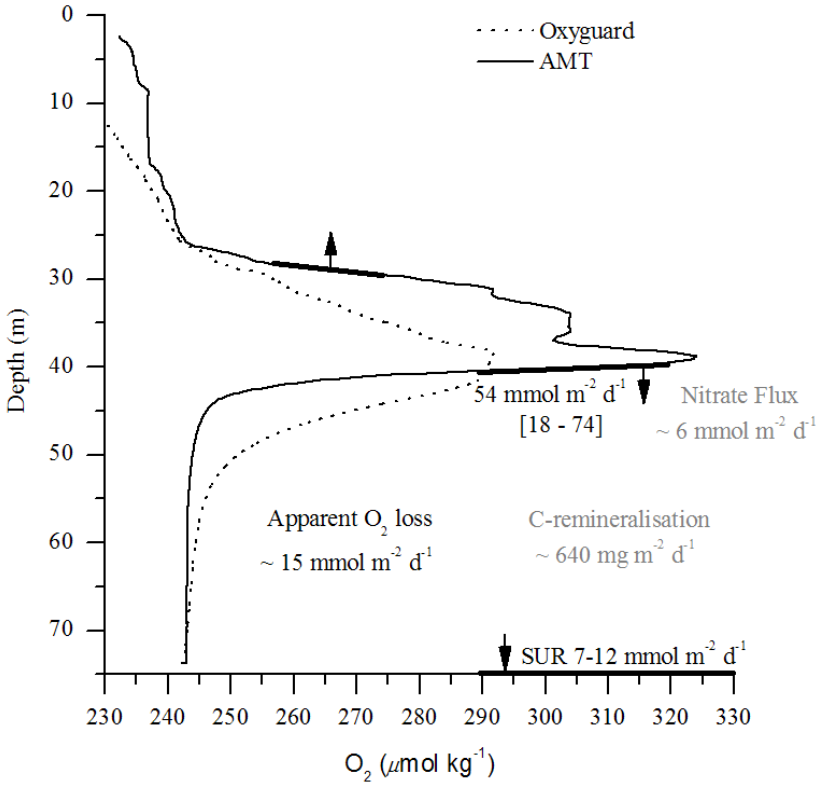

Fig. II.9. Main turbulent O_2 fluxes determined in this study. The ranges shown for the interior O_2 fluxes refer to the associated uncertainty and intermittency levels. The sediment uptake rate (SUR) was estimated from benthic chamber deployments (this study) or reported from parallel studies in the same working area (McGinnis et al., *in prep.*). In addition, based on a simple O_2 budget, the apparent BBL O_2 loss rates as well as the corresponding organic C export (and subsequent remineralization) were also estimated. Furthermore we provide a nitrate flux that would be required to reach the thermocline to support the steady-state new primary production to replace that which is exported.

The total benthic O_2 flux was inferred from one benthic chamber deployment; the chamber was deployed for 23 hrs and showed an average O_2 loss rate of 1.7 µmol L^{-1} per hour from which a SUR of 7 mmol m^{-2} L^{-1} was derived.

II.4. Discussion

The importance of determining the turbulent processes and accurately resolving the O_2 gradient is immediately apparent for the O_2 interior dynamics and budget within this region of the North Sea. The formation of the O_2 maximum zone due to primary production at the base of the thermocline and the turbulence interactions have significant implications for the O_2 flux to the BBL and lead to some important insights regarding the carbon turnover within the system. Within these contexts, we will: 1) Discuss the turbulent mechanisms leading to these O_2 fluxes and those promoting the formation of the O_2 maximum zone in terms of primary productivity; 2) present an estimate of the BBL O_2 budget for our period of measurement; 3) discuss the implications for nitrate and organic carbon turnover.

Sources of mixing in the seasonal thermocline

As noted previously, the thermocline of the Central North Sea is often in a state of marginal stability (van Haren et al. 1999), i.e., Richardson number ($Ri = N^2/S^2$) ~ 1, and additional sources of shear could lead to local production of turbulence and thus to enhanced mixing – in affect apparent in our high values for O_2 fluxes. During the observational period, it was found that near-inertial oscillations in the interior were the main contributors to the detected enhanced shear (Fig. II.4). As recently shown in a model study by Burchard and Rippeth (2009) based on a two layer system, short-lived elevated shear maxima during the presence of baroclinic inertial oscillations and barotropic tidal currents (as were the conditions during our observational campaign) originate from an interaction of the surface wind stress with the shear vector of the baroclinic inertial oscillation and the bottom stress vector of the barotropic tide. In the model, the maximum shear production will occur when those vectors are aligned, while the actual shear maxima will occur at the turning point, so when the shear production will stop (i.e., $dS^2/dt = 0$). The authors report that the shear maxima usually occurs ~¼ of an inertial period after the initial vectors alignment and that their interfacial shear maxima were sensitive to both the direction and phase of the wind stress.

Although the state of the North Sea during the time of our measurements would need to be described by a more complex three (SBL, Interior, BBL) or four layer model and not a two layer

one, the data presented here indicate several of the ingredients that were required in their model. Changes in wind directions were frequently observed (Fig. II.10A) leading to the wind vector showing both clockwise and anticlockwise rotations (Fig. II.10B). An alignment with the clockwise rotating shear vector in the upper interfacial layer (Fig. II.10D) is indeed happening several times during the observational period. Furthermore, several shear spikes were detected in the upper interfacial layer and found to occur at perhaps the local inertial period (Fig. II.10C). Although variable in magnitude, those shear maxima provide some support for the mechanism described by Burchard and Rippeth (2009). Some of those shear spikes, however, were not associated with the vectors alignment and may arise from other processes associated with changes in the wind forcing. In terms of turbulence measurements and shear instability it is worth noting that most of the measurements where performed before or after those events (Fig. II.10C). Measurements during a shear spike (cast 10 to 23 on the 9 August) revealed that the upper interfacial layers moved from an initial state of marginal stability to shear instability ($Ri <$ 0.25) during the shear maxima, thus supporting a possible local production of turbulence.

With this regard the lower interfacial layer, with the exception of a shear maxima occurring in the late afternoon of the 8th of August and lasting several hours, there was no clear evidence of shear spikes production as result of a Burchard and Rippeth (2009) mechanism actually occurring. Nevertheless, some of the increased O_2 fluxes detected, especially in the first half of the observational period, might still be a result of local turbulence production due to the occurrence of shear maxima. As a matter of fact, the enhanced turbulence in the lower interior during the first MSS90 ensembles (casts 2 – 9, first two MSS clusters) was associated with a shear maximum (late night of the 8th of August). In the later profile ensembles, however, BBL turbulence reached into the lower thermocline (Fig. II.7) and contributed to elevated mixing and increased O_2 fluxes. It should thus be stated that the turbulence dynamics and resulting fluxes reported here may not be representative for the general summer time period of the central North Sea as it is still unclear how often these shear maxima occur and how distinctive is the observed phenomenon.

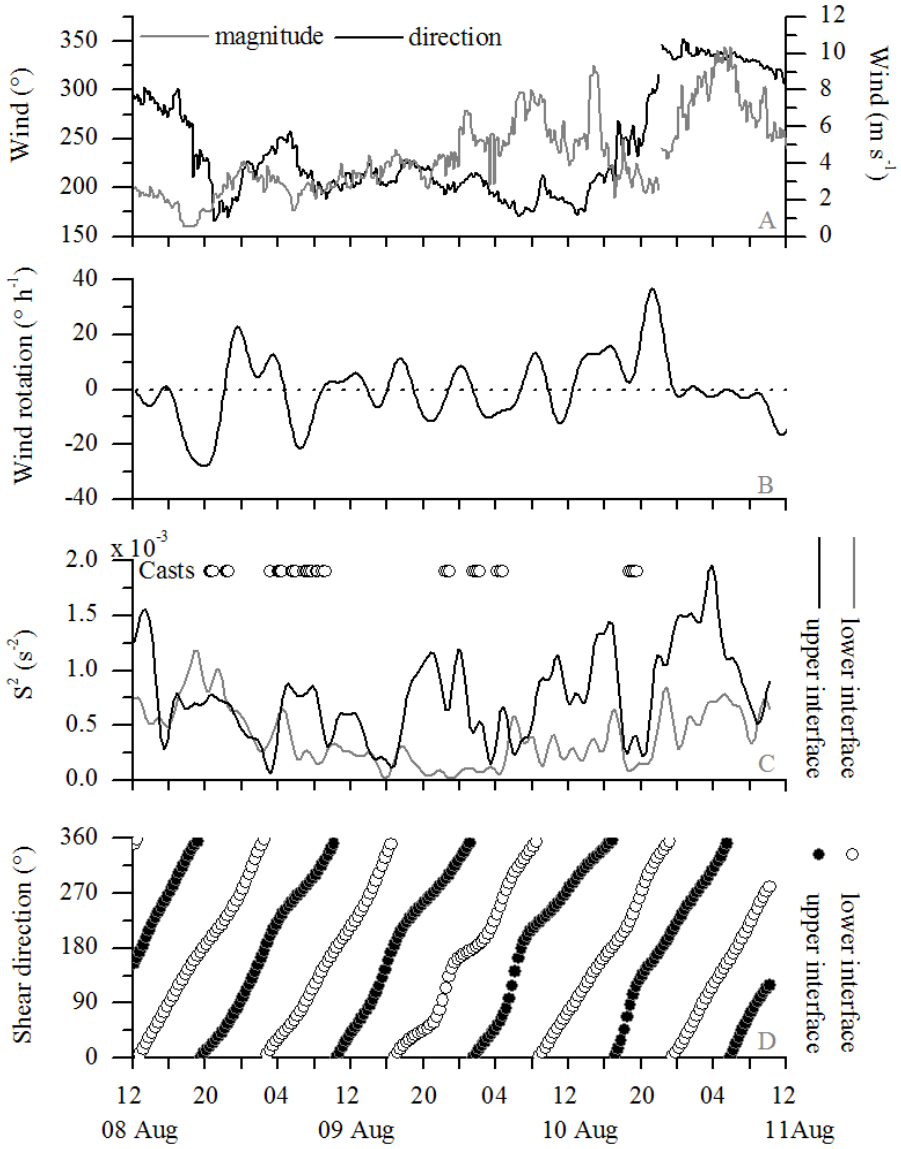

Fig. II.10. Wind and shear spikes. (A) Wind data provided by the ship meteorological station showing wind direction (black line) and magnitude (gray line); the gap in the dataset was due to a malfunction. (B) Temporal changes in the wind direction between two consecutive measurements (10 min) with positive values defined as clockwise rotations; to remove the dataset noise and to enhance the readability a 60 min low-pass filter was applied to reduce the noise and the values are up-scaled to degrees per hour. (C) Shear variance (S^2) indicating the occurrence of several short-lived shear maxima that are more are more frequent and of larger magnitude in the upper interfacial layer (black line) than in the lower one (gray line). Note that also the MSS profiles are listed on the figure (filled circles) to provide a better identification of the measurements ensembles. (C) Direction of the clockwise rotating shear vector for both the upper and lower interfacial layer (filled and unfilled circles, respectively); the displayed data were filtered with a 120 min low-pass filter. Note that the time axis is the same for all three panels.

BBL O_2 budget

While it is too speculative to upscale the O_2 fluxes to the whole summer period, a simple BBL O_2 budget can be performed for the conditions encountered during the observational period. This requires, besides the average O_2 flux into the BBL and the SUR, also the apparent seasonal O_2 loss in the bottom water.

With the fast responding AMT galvanic O_2 sensor we were able to resolve the O_2 gradient with the highest resolution that is currently technically possible on a microstructure profiler. These measurements revealed higher O_2 concentrations at the maximum and much sharper gradients than those measured by the slow (5 s response time) Oxyguard sensor O_2 sensors (Fig. II.9). The Oxyguard sensor also showed a substantial disagreement in the SBL and transition layer (up to 25 m), by largely underestimating the O_2 concentrations. The disagreement was attributed to the increasing hydrostatic pressure acting on the Oxyguard sensor membrane and thus reducing the spacing between the membrane and the cathode until the membrane properly fits to the cathode. The AMT revealed a substantial O_2 flux divergence from the base of the thermocline into the BBL, with an average of -54 mmol m^{-2} d^{-1}.

The SUR based on the benthic chamber was 7 mmol m^{-2} d^{-1}. A parallel study based on eddy correlation and in-situ O_2 microprofiling during the same observational period reported an average SUR of up to 12 mmol m^{-2} d^{-1} (McGinnis et al., *in prep.*). Based on both studies, a SUR of 10 mmol m^{-2} d^{-1} was chosen for further analysis.

The apparent O_2 loss in the BBL can be estimated considering the time elapsed from the onset of seasonal stratification (April, around day 100; Meyer et al. 2011) when the O_2 was ~100% saturated to the time of this survey where the BBL O_2 was at 80% saturation. Assuming a constant BBL temperature (6.8°C; Fig. II.5), the 35 m thick BBL was then characterized by an apparent O_2 loss of 15 mmol m^{-2} d^{-1} (Fig. II.9) leading to a O_2 concentration difference of about -50 µmol L^{-1} over ~120 days (-0.42 mmol m^{-3} d^{-1}), which is in good agreement with the study of Greenwood et al. (2010), conducted on the nearby North Dogger.

Performing a simple 1-d model of a slice of the BBL with a 1 m^2 area and 35 m height, and neglecting advective transport (a reasonable assumption given the large distance to the boundaries in the North Sea, the presumed homogeneous conditions, and thus the relative

isolation of the bottom water in this location), the 1 m^2 section of the North Sea BBL can be represented as a simple continuously mixed tank reactor. We further assume that the observed long-term water column loss rate remains constant over the studied period. The mass balance equation is then given as:

$$\frac{\partial C}{\partial t}\frac{V}{A} = F_{in} - F_{out} + R \quad (\text{mmol m}^{-2}\ \text{d}^{-1}) \tag{II.5}$$

where C is the O_2 concentration, t is time, V/A is the volume-to-area ratio of our model (35 m), F_{in} is the flux from the thermocline (54 mmol m^{-2} d^{-1}), F_{out} is the SUR (10 mmol m^{-2} d^{-1}), and thus R should represent our water column gain or loss flux. Rearranging and solving for R yields a water column flux loss rate of -60 mmol m^{-2} d^{-1}. Therefore, the total actual O_2 loss rate in the BBL is -70 mmol m^2 d^{-1}. While there is considerable uncertainty in this estimate, the results suggest several factors higher than the value reported by Greenwood at al. (2010). This implies that the concentration loss is about 2 µmol L^{-1} d^{-1}, which, without the thermocline as an O_2 source (in addition to a carbon source), would result in a depletion of 240 µmol L^{-1}, and thus a BBL showing ~20% O_2 saturation instead of the observed 80% saturation.

Implications for nutrient fueling and carbon cycle

Summer O_2 dynamics in the thermocline of the central North Sea were also investigated by Weston at al. (2005) based on chlorophyll and primary production measurements. The authors reported the occurrence of a clear thermocline chlorophyll maximum (deep chlorophyll maximum) that, partly due to nutrient fluxes from the BBL, was responsible for a substantial and continuous primary production over the whole summer. Rippeth et al. (2009) went further and based their analysis on nitrate flux estimations from which the thermocline new production was inferred. They report a significant BBL-nitrate fuelled new production, comparable with that of spring blooms.

Nitrate: In the present study, nitrate distributions were not measured and thus fluxes and gradients cannot be calculated. An order-of-magnitude estimation, however, can still be performed assuming that primary production in the lower thermocline during the observational period is mainly BBL-nitrate fuelled. Therefore the turbulent O_2 flux into the BBL needs to be balance by an upward turbulent nitrate flux sustaining primary production in the lower thermocline. With an O_2 to nitrogen (N) ratio of 138:16 (Redfield et al. 1963) the average nitrate

flux would amounts to ~6 mmol N m^{-2} d^{-1}, which is higher than reported by Rippeth et al. (2009) but comparable with the fluxes reported by e.g., Sharples et al. (2007) for the Celtic Sea. The authors reported average nitrate fluxes of 1.3 and 3.5 mmol m^{-2} d^{-1} for neap and spring tide but also enhanced fluxes up to 9 mmol m^{-2} d^{-1} as a result of short-lived mixing events associated with the passage of internal solitons. The nitracline is inferred, from the nitrate flux and the measured eddy diffusivities across the BBL-lower thermocline interface (Fig. II.8), to be up to 3 µmol L^{-1} m^{-1}. Assuming a summer BBL nitrate concentration of up to 7 µmol L^{-1} and interior concentrations below 1 µmol L^{-1} (Weston et al 2005), the nitracline would be ~2 m thick, and thus thinner and sharper than in other shelf seas (e.g., Hickman et al. 2009), but not out of the question as the thickness of the observed oxycline below the O_2 maximum is of similar vertical extent.

Organic carbon: The large O_2 demand in the BBL may also be the consequence of a 'turbulent' carbon flux occurring by the same mechanisms and route as the turbulent O_2 flux – a process that essentially results from the ejection of biomass, which thrives within the base of the thermocline and also produces the O_2 maximum. Thus, the organic matter exported to the BBL from the base of the thermocline is accompanied by the necessary O_2 to deal with its mineralization.

Assuming a 1:1 O_2 utilization for carbon re-mineralization (Canfield 1993), we can infer the carbon fluxes and remineralization based on our O_2 balance. With an average of 54 mmol m^{-2} d^{-1} O_2 flux from the thermocline to the BBL, and thus the same amount of carbon, we estimate that 640 mg m^{-2} d^{-1} of organic carbon accompanies the transported O_2. Expressing the total O_2 loss flux (R) as carbon yields around 850 mg m^{-2} d^{-1} with about 120 mg m^{-2} d^{-1} (15%) to the sediment and the remaining 85% in the water column. These amounts are well in agreement with the common assumption that only 15% – 50% of pelagic primary production reaches the sediment (Canfield 1993; Wollast 1998; Glud 2008). The calculated export of carbon is high, exceeding those values modeled by Sharples (2008) for a typical NW European shelf sea that were from ~35 to ~200 mg m^{-2} d^{-1} for neap and spring tide, respectively. However, these modeled values did not include the daily tidal variation, and thus could be much higher on shorter timescales.

We acknowledge that extrapolating our results to carbon budgets is somewhat speculative within the context of this study. However, we believe that our estimates of the O_2 balance and carbon

budget emphasize that the exchange of organic carbon and rates of primary productivity may be significantly underestimated within the central North Sea BBL and thermocline. Of course a validation of these results would require a more extensive investigation of the upper water column processes with emphasis on the air-sea CO_2 flux and O_2 contributions from the DCM (unfortunately not quantifiable on this study) and the atmosphere. As net community production was found to be a major process controlling the distribution of dissolved inorganic carbon and CO_2 in the central and northern regions of the North Sea (*see* Bozec et al. 2006), the CO_2 contributions from the atmosphere needs to be taken into account to build up more robust O_2 and C budgets.

The results of this study suggest that the O_2 maximum zone resulting from primary production at the base of the thermocline is a significant source of O_2 (and by extension, organic carbon) to the bottom boundary layer. The occurrence of short-lived shear maxima and enhanced turbulence at the base of the thermocline resulting from upward shear stress propagation were determined to substantially enhance these fluxes over short time scales. Our results show an interesting interaction between the interior layer and the bottom boundary layer due to turbulence and hydrodynamics, and – due to the presence of algae (*see* Weston et al. 2005) in the bottom of the thermocline – the subsequent impact on the O_2 and carbon turnover. This has further implications for the nitrogen turnover rates, as nitrate fluxes into the O_2 maximum zone would likely be high during these periods of enhance turbulence at the base of the thermocline, to further sustain primary production. Resolving the nutrient concentration gradient over the small depth ranges reported here, will however pose a new challenge for future studies in the central North Sea region. Obviously, a more detailed, interdisciplinary and fine-scale study would be necessary to further explore these interesting interactions.

II.5. Acknowledgements

We are thankful to the captain and crewmembers of the R/V *Celtic Explorer* for their outstanding collaboration and support during the survey, Uwe Koy and Rudolf Link for their logistic support, and Jens Schafstall, Tim Fischer and Markus Faulhaber for their help in data collection and processing. We are grateful for the technical development and support in deployment of the benthic chamber by Ralf Schwarz, Sergiy Cherednichenko and the ROV Kiel 6000 team. Financial support was provided by the Sonderforschungsbereich 754 “Climate – Biogeochemisty in the tropical Ocean” (LR) and by the Excellence Cluster “Future Ocean” (project 2009/1 CP 0915, LR, both supported by the Deutsche Forschungsgemeinschaft (DFG). The cruise was financed by Wintershall within the Fluid and Gas Seepage in the Southern German North Sea (SDNS) project.

II.6. References

Anon. 1993. North Sea Quality Status Report. Oslo and Paris Commissions.

Baker, M. A., and C. H. Gibson. 1987. Sampling turbulence in the stratified ocean: Statistical consequences of strong intermittency. *J. Phys. Oceanogr.* **17**: 1817–1836, doi:10.1175/1520-0485(1987)017<1817:STITSO>2.0.CO;2

Batchelor, G. K. 1953. The theory of homogeneous turbulence. Cambridge University Press, Cambridge, 212 p.

Best, M. A., A. W. Wither, and S. Coates. 2005. Dissolved oxygen as a physico-chemical supporting element in the Water Framework Directive. *Mar. Pollut. Bull.* **55**: 53–64, doi:10.1016/j.marpolbul.2006.08.037

Bozec, Y., H. Thomas, L. Schiettecatte, A. V. Borges, K. Elkalay, H. J. W. de Baar. 2006. Assessment of the processes controlling the seasonal variations of dissolved inorganic carbon in the North Sea. *Limnol. Oceanogr.* **51**: 2746–2762, doi:10.4319/lo.2006.51.6.2746

Burchard, H., P. D. Craig, J. R. Gemmrich, H. Van Haren, P. P. Mathieu, H. E. M. Meier, W. A. M. N. Smith, H. Prandke, T. P. Rippeth, E. D. Skyllingstad, W. D. Smyth, D. J. S. Welsh, and H. W. Wijesekera. 2008. Observational and numerical modeling methods for quantifying coastal ocean turbulence and mixing. *Progr. Oceanogr.* **76**: 399–442, doi:10.1016/j.pocean.2007.09.005

Burchard, H., and T .P. Rippeth. 2009. Generation of bulk shear spikes in shallow stratified tidal seas. *J. Phys. Oceanogr.* **39**: 969–985, doi:10.1175/2008JPO4074.1

Canfield, D. E. 1993. Organic matter oxidation in marine sediments, p. 333–363. *In*: R. Wollast, F. T. Mackenzie, and L. Chou [eds.]. Interactions of C, N, P and S biogeochemical cycles and global change. Springer, Berlin.

Davis, R. E. 1996. Sampling turbulent dissipation. *J. Phys. Oceanogr.* **26**: 341-358, doi:10.1175/1520-0485(1996)026<0341:STD>2.0.CO;2

Efron, B. 1979. 1977 Rietz lecture - bootstrap methods - another look at the jackknife. *Ann. Stat.* **7**: 1–26.

Ferrari, R., and K. L. Polzin. 2005. Finescale structure of the T-S relation in the eastern North Atlantic. *J. Phys. Oceanogr.* **35**: 1437–1454, doi:10.1175/JPO2763.1

Fofonoff, N. P. 1985. Physical properties of seawater: A new salinity scale and equation of state for seawater. *J. Geophys. Res.* **90**: 3332–3342, doi:10.1029/Jc090ic02p03332

Glud, R. N. 2008. Oxygen dynamics of marine sediments. *Mar. Biol. Res.* **4**: 243–289, doi:10.1080/17451000801888726

Garcìa, H. E., and L. I. Gordon. 1992. Oxygen solubility in seawater: Better fitting equations. *Limnol. Oceanogr.* **37**: 1307–1312, doi:10.4319/lo.1992.37.6.1307

Greenwood, N., E. R. Parker, L. Fernand, D. B. Sivyer, K. Weston, S. J. Painting, S. Kroger, R. M. Forster, H. E. Lees, D. K. Mills, and R. W. P. M. Laane. 2010. Detection of low

bottom water oxygen concentrations in the North Sea; implications for monitoring and assessment of ecosystem health. *Biogeosciences* **7**: 1357–1373, doi:10.5194/bg-7-1357-2010

Hickman, A. E., P. M. Holligan, C. M. Moore, J. Sharples, V. Krivtsov, and M. R. Palmer. 2009. Distribution and chromatic adaptation of phytoplankton within a shelf sea thermocline. *Limnol. Oceanogr.* **54**: 525–536, doi:10.4319/lo.2009.54.2.0525

Hovland, M., and A. Judd. 1988. Seabed pockmarks and seepage: Impact on geology, biology and the marine environment. Graham and Trotman, London, 293 p.

Itsweire, E. C., T. R. Osborn, and T. P. Stanton. 1989. Horizontal distribution and characteristics of shear layers in the seasonal thermocline. *J. Phys. Oceanogr.* **19**: 302–320, doi:10.1175/1520-0485(1989)019<0301:HDACOS>2.0.CO;2

Ivey, G. N., and J. Imberger. 1991. On the nature of turbulence in a stratified fluid. Part I: The energetics of mixing. *J. Phys. Oceanogr.* **21**: 650–658, doi:10.1175/1520-0485(1991)021<0650:OTNOTI>2.0.CO;2

Joos, F., G.-K. Plattner, T. F. Stocker, A. Körtzinger, and D. W. R. Wallace. 2003. Trends in marine dissolved oxygen: Implications for ocean circulation changes and the carbon budget. EOS Trans. AGU **84**: 197–204

Kemp, W. M., J. M. Testa, D. J. Conley, D. Gilbert, and J. D. Hagy. 2009. Temporal responses of coastal hypoxia to nutrient loading and physical controls. *Biogeosciences* **6**: 2985–3008, doi:10.5194/bg-6-2985-2009

Knight, P. J., M. J. Howarth, and T. P. Rippeth. 2002: Inertial currents in the northern North Sea. *J. Sea Research* **47**: 269–284, doi:10.1016/S1385-1101(02)00122-3

Ledwell, J. R., and A. Bratkovich. 1995. A tracer study of mixing in the Santa Cruz Basin. *J. Geophys. Res.* **100**: 20681–20704, doi:10.1029/95JC02164

Linke, P., and M. Schmidt. 2010. Fluid and gas seepage in the North Sea. R/V *Celtic Explorer* Cruise Report CE0913. IFM-GEOMAR Report 36. doi:10.3289/ifm-geomar_rep_36_2010

Lorke, A., L. Umlauf, and V. Mohrholz. 2008. Stratification and mixing on sloping boundaries. *Geophys. Res. Lett.* **35:** L14610, doi:10.1029/2008GL034607

Lowe, J. A., T. P. Howard, A. Pardaens,J. Tinker, J. Holt, S. Wakelin, G. Milne, J . Leake, J. Wolf, K. Horsburgh, T. Reeder, G. Jenkins, J. Ridley, S. Dye, and S. Bradley. 2009. UK Climate Projections science report: Marine and coastal projections. Met Office Hadley Centre.

Lueck, R. G., F. Wolk, and H. Yamazaki. 2002. Oceanic velocity microstructure measurements in the 20th century. *J. Oceanogr.* **58**: 153–174, doi:10.1023/A:1015837020019

MacKinnon, J. A., and M. C. Gregg. 2005. Near-inertial waves on the New England Shelf: The role of evolving stratification, turbulent dissipation, and bottom drag. *J. Phys. Oceanogr.* **35**: 2408–2424, doi:10.1175/JPO2822.1

Meyer, E. M. I., T. Pohlmann, and R. Wiesse. 2011. Thermodynamic variability and change in the North Sea (1948-2007) derived from a multidecadal hindcast. *J. Mar. Syst.* **86**: 35–44, doi:10.1016/j.jmarsys.2011.02.001

Osborn, T. R. 1980. Estimates of the local rate of vertical diffusion from dissipation measurements. *J. Phys. Oceanogr.* **10**: 83–89, doi:10.1175/1520-0485(1980)010<0083: EOTLRO>2.0.CO;2

OSPAR (Oslo-Paris convention for the protection of the marine environment of the North-East Atlantic). 2009. EcoQO Handbook—Handbook for the application of ecological quality objectives in the North Sea, 2nd edn. OSPAR Biodiversity Series 2009/307. Available from http://ww.wospar.org/v_publications/browse.asp

OSPAR. 2010. Quality Status Report 2010. OSPAR Commission. London. Available from http://qsr2010.ospar.org/en/index.html

Otto, L., J. T. F. Zimmerman, G. K. Furnes, M. Mork, R. Saetre, and G. Becker. 1990. Review of the physical oceanography of the North Sea. *Ned. J. Sea Res.* **26**: 161–238, doi:10.1016/ 0077-7579(90)90091-4

Palmer, M. R., T. P. Rippeth, and J. H. Simpson. 2008. An investigation of internal mixing in a seasonally stratified shelf sea. J. Geophys. Res. **113**: C12005, doi:10.1029/2007JC004531

Pfannkuche, O., and P. Linke. 2003. GEOMAR landers as long-term deep-sea observatories. *Sea Technol.* **44**: 50–55.

Pingree, R. D., P. M. Holligan, and G. T. Mardell. 1978. The effect of vertical stability on phytoplankton distributions in the summer on the Northwest European Shelf. *Deep Sea Res.* **25**: 1011–1028, doi:10.1016/0146-6291(78)90584-2

Powell, T., and A. Jassby. 1974. The estimation of vertical eddy diffusivities below the thermocline in lakes. *Water Resour. Res.* **10**: 191-198, doi:10.1029/WR010i002p00191

Prandle, D. 1982. The vertical structure of tidal currents. *Geophys. Astrophys. Fluid Dyn.* **22**: 385–398, doi:10.1080/03091928208221735

Prandke, H., and A. Stips. 1998. Test measurements with an operational microstructure-turbulence profiler: Detection limit of dissipation rates. *Aquat. Sci.* **60**: 191–209, doi:10.1007/s000270050036

Redfield A. C., B. H. Ketchum, and F. A. Richards. 1963. The influence of organisms on the composition of sea water. p. 26–77. *In*: M. N. Hill [ed.]. The sea. Vol II, Interscience Publishers, New York.

Rippeth, T. P. 2005. Mixing in seasonally stratified shelf seas: A shifting paradigm. *Phil. Trans. R. Soc. A* **363**: 2837–2854, doi:10.1098/rsta.2005.1662

Rippeth, T. P., P. Wiles, M. R. Palmer, J. Sharples and J. Tweddle. 2009. The diapcynal nutrient flux and shear-induced diapcynal mixing in the seasonally stratified western Irish Sea. *Cont. Shelf Res.* **29**: 1580–1587, doi:10.1016/j.csr.2009.04.009

Rippeth, T. P., J. H. Simpson, R. Player, and M. C. Garcia. 2002. Current oscillations in the diurnal-inertial band on the Catalonian Shelf in spring. *Cont. Shelf Res.* **22:** 247–265, doi:10.1016/S0278-4343(01)00056-5.

Schafstall, J., M. Dengler, P. Brandt, and H. Bange. 2010. Tidal-induced mixing and diapycnal nutrient fluxes in the Mauritanian upwelling region. *J. Geophys. Res. Oceans* **115**: C10014, doi:10.1029/2009jc005940

Schneider von Deimling, J., J. Greinert, N. R. Chapman, W. Rabbel, and P. Linke. 2010. Acoustic imaging of natural gas bubble ebullition in the North Sea: Sensing the temporal, spatial and activity variability. *Limnol. Oceanogr.: Meth*ods **8**: 155–171, doi:10.4319/lom.2010.8.155

Sharples, J. 2008. Potential impacts of the spring-neap tidal cycle on shelf sea primary production. *J. Plankton Res.* **30**: 183–197, doi:10.1093/plankt/fbm088

Sharples, J., J. F. Tweddle, J. A. M.Green, M. R. Palmer, Y. N. Kim, A. E. Hickman, P. M. Holligan, C. M. Moore, T. P. Rippeth, J. H. Simpson, and V. Krivtsov. 2007. Spring-neap modulation of internal tide mixing and vertical nitrate fluxes at a shelf edge in summer. *Limnol. Oceanogr.* **52**: 1735–1747, doi:10.4319/lo.2007.52.5.1735

Sharples, J., C. M. Moore, T. P. Rippeth, P. M. Holligan, D. J. Hydes, N. R. Fisher, and J. H. Simpson. 2001. Phytoplankton distribution and survival in the thermocline. *Limnol. Oceanogr.* **46**: 486–496, doi:10.4319/lo.2001.46.3.0486

Shih, L. H., J. R. Koseff, G. N. Ivey, and J. H. Ferziger. 2005. Parameterization of turbulent fluxes and scales using homogeneous sheared stably stratified turbulence simulations. *J. Fluid Mech.* **525**: 193–214, doi:10.1017/S0022112004002587

Simpson, J. H., T. P. Rippeth, and A. R. Campbell. 2000. The phase lag of turbulent dissipation in tidal flow. p. 57–67. *In*: T. Yanagi [ed.]. Interactions between Estuaries, Coastal Seas and Shelf Seas. Terra Scientific Publishing, Tokyo.

Simpson, J. H., and J. P. Tinker. 2009. A test of the influence of tidal stream polarity on the structure of turbulent dissipation. *Cont. Shelf Res.* **29**: 320–332, doi:10.1016/j.csr.2007.05.013

Smyth, W.D., J.N. Moum, and D.R. Caldwell. 2001. The efficiency of mixing in turbulent patches: inferences from direct simulations and microstructure observations. *J. Phys. Oceanogr.* **31**: 1969–1992, doi:10.1175/1520-0485(2001)031<1969:TEOMIT>2.0.CO;2

Sommer, S., M. Turk, S. Kriwanek, and O. Pfannkuche. 2008. Gas exchange system for extended in situ benthic chamber flux measurements under controlled oxygen conditions: First application - sea bed methane emission measurements at Captain Arutyunov mud volcano. *Limnol. Oceanogr.: Methods* **6**: 23–33, doi:10.3354/meps07956

Sommer, S., P. Linke, O. Pfannkuche, H. Niemann, and T. Treude. 2010. Benthic respiration in a seep habitat dominated by dense beds of ampharetid polychaetes at the Hikurangi Margin (New Zealand). *Mar. Geol.* **272**: 223–232, doi:10.1016/j.margeo.2009.06.003

St. Laurent, L., and R. W. Schmitt. 1999. The contribution of salt fingers to vertical mixing in the North Atlantic Tracer Release Experiment. *J. Phys. Oceanogr.* **29**: 1404–1424.

Thorpe, S. A. 1977. Turbulence and mixing in a Scottish Loch. Philosophical Transactions of the Royal Society of London Series A **286**: 125–181, doi:10.1098/rsta.1977.0112

van Haren, H., L. Mass, J. T. R. Zimmerman, H. Ridderinkhof, and H. Malschaert. 1999. Strong inertial currents and marginal internal wave stability in the central North Sea. *Geophys. Res. Lett.* **26**: 2993–2996, doi:10.1029/1999GL002352

Vaquer-Sunyer, R., and C. M. Duarte. 2008. Thresholds of hypoxia for marine biodiversity. *P. Natl. Acad. Sci. USA*. **105**: 15452–15457, doi:10.1073/pnas.0803833105

Weston, K., L. Fernand, D. K. Mills, R. Delahunty, and J. Brown. 2005. Primary production in the deep chlorophyll maximum of the central North Sea. *J. Plankton Res.* **27**: 909–922, doi:10.1093/plankt/fbi064

Wollast, R., 1998. Evaluation and comparison of the global carbon cycle in the coastal zone and in the open ocean. p. 213–252. *In*: The Sea, The Global coastal ocean, processes and methods, K.H. Brink, and A.R. Robinson, eds. Wiley and Sons, New York.

Wüest, A., G. Piepke, and D. C. Van Senden. 2000. Turbulent kinetic energy balance as a tool for estimating vertical diffusivity in wind-forced stratified waters. *Limnol. Oceanogr.* **45**: 1388–1400, doi:10.4319/lo.2000.45.6.1388

Wunsch, C., and R. Ferrari, 2004, Vertical mixing, energy and the general circulation of the ocean. *Annu. Rev. Fluid Mech.* **36**: 281–314, doi:10.1146/annurev.fluid.36.050802.122121

III. Chapter

Influence of variable seep sediments and bottom-water hydrodynamics on oxygen fluxes at the sediment-water interface

Lorenzo Rovelli, [a] Stefan Sommer, [a] Lee D. Bryant, [a] Sonja Kriwanek, [a] and Peter Linke [a]

[a] Helmholtz Centre for Ocean Research Kiel, GEOMAR, Kiel, Germany

Submitted to *Deep-Sea Research*

Abstract

The effects of hydrodynamics in controlling benthic diffusive oxygen (O_2) consumption in two cold-seep habitats on the Chilean continental margin were investigated in-situ using a state-of-the-art lander-based transecting profiler. A total of up to 54 O_2 and 27 hydrogen sulfides (H_2S) profiles were collected over each of the two 45-cm-length transects, in parallel with concurrent near-bottom current measurements and seafloor imaging. The first deployment (transect on seep habitat P1) revealed moderate coverage with sulfur-bacterial mats on the sediment surface, generally more sulfidic sediments, and an average diffusive O_2 uptake (*DOU*) rate of 7.9 ± 4.5 mmol m^{-2} d^{-1}. The transect on the second deployment (seep habitat P2) was less sulfidic, with an average *DOU* of 4.0 ± 2.3 mmol m^{-2} d^{-1}, and had only sporadic bacterial mat coverage. O_2 fluxes scaled with DBL thickness (δ_{DBL}) variability, which indicates transport limitation for deep-sea sediments.

Sediment reactivity, defined here as the potential sediment metabolic O_2 requirements, was estimated considering sulfide oxidation rates based on observed total sulfide fluxes and estimates of organic matter (OM) degradation. While at seep P2 the *DOU* could account for the sulfide oxidation and organic matter degradation, at seep P1 other processes such as small-scale topography and aerobic methane oxidation were estimated to account for up to 35% of the observed *DOU*. This study highlights that at reactive sedimentary environments, such as seeps or organic rich continental margin and shelf sediments where O_2 demand is very high, hydrodynamics can impede O_2 transport into the sediment. Consequently, in these environments, *DOU* is significantly less than the potential O_2 demand as dictated by O_2 consumption processes in the sediment.

III. 1. Introduction

The availability and dynamics of dissolved oxygen (O_2) are of major importance to benthic ecosystems. O_2 is not only an indicator of biological activity via respiration (Glud 2008) but also plays a major role in the degradation of organic matter (Emerson and Hedges 2004) as well as in the reoxidation of reduced compounds (Canfield et al. 1993). In order to understand and quantify sediment O_2 uptake, it is crucial to comprehensively understand controlling processes which include physical forcing as well as sediment O_2 consumption (Jørgensen and Boudreau 2001).

One of the primary controls on solute transport across the sediment-water-interface (SWI) is a thin, mm-scale layer immediately above the sediment, which is referred to as the diffusive boundary layer (DBL). In the DBL, transport occurs via molecular diffusion (Jørgensen and Revsbech 1985); thus, depending on its thickness (δ_{DBL}) the DBL is regarded as an important barrier that can limit benthic O_2 transport across the SWI (e.g., Jørgensen and Revsbech 1985; Lorke et al. 2003). The δ_{DBL} is modulated by the local hydrodynamic regime. Several studies on DBL dynamics have reported both strong correlations between current velocity in the bottom boundary layer (BBL) and δ_{DBL} (Steinberger and Honzo 1999; Jørgensen and Des Marais 1990) as well as with the BBL turbulence regime (Higashino et al. 2003; Lorke et al. 2003; Bryant et al. 2010a; Wang et al. 2013). Depending on the bottom water current velocity, δ_{DBL} varies on the scale of sub-millimetres under relatively high current velocities (e.g., > 2 cm s^{-1}) but becomes thicker as current velocity decreases. Under such conditions, thicker DBLs impede solute exchange between the sediment and the water column and biogeochemical processes in the sediment may become transport limited as a result. It is, however, still not fully understood to what extent hydrodynamic-induced changes in δ_{DBL} effectively control the uptake or release of solutes at the SWI.

Studies on mesotrophic lakes have shown that these systems can become transport-limited during periods of reduced flow and consequently reduced BBL turbulence (Lorke et al. 2003; Brandt et al. 2009; Bryant et al. 2010a). The sediments of these lakes are characterized by high amounts of reactive organic matter (OM) with a high demand for O_2.

Significant work has been done to assess the role of δ_{DBL} on benthic O_2 fluxes, although the majority of these studies have been limited to modeling approaches showing that in systems characterized by reactive OM, the DBL plays a modulating role over the O_2 uptake (Kelly-Gerreyn et al. 2005; Brand et al. 2009). Conversely, in marine environments, where benthic O_2 consumption primarily results from reoxidation of reduced compounds, modeling studies inferred that the DBL had only a marginal role (Glud et al. 2007). Despite the fact that much work has been done on this topic, field assessments are extremely rare (Gundersen and Jørgensen 1990; Glud et al 2003, 2009) and quantitative in-situ data are much needed.

The primary goals of this study were to use data obtained in-situ to evaluate the significance of hydrodynamics and corresponding variability in δ_{DBL} on diffusive O_2 uptake (*DOU*) rates and to constrain the main biogeochemical processes sustaining the observed *DOU*. These goals were achieved with a comprehensive in-situ O_2 and hydrogen sulfide (H_2S) microprofiling survey which characterized both δ_{DBL} and sediment geochemistry, including organic matter degradation and the reoxidation of H_2S. H_2S was utilized as a primary indicator of redox activity as in methane seep habitats H_2S represents a key species which is liberated into the porewater during the microbial anaerobic methane oxidation (AOM), representing an important sink for methane in these environments (Judd and Hovland 2007 and reference therein). To the authors' knowledge, this is the first time controls on *DOU* have been assessed in highly heterogeneous marine sediment using in-situ data.

III. 2. Methods

Study site

O_2 and H_2S flux measurements were performed along two ~ 40-cm-long transects within a cold-seep habitat at the Chilean continental margin. The site was selected due to the heterogeneity of the habitat characterized by localized occurrences of bacterial mats and reduced sediments. This allowed for flux measurements to be obtained over a "gradient" of mat-free sediment and bacterial mats of different coverage and thus over a range of sediment reactivities and hence O_2 demand. The O_2 and H_2S microprofiles presented in this study were collected at the central Chilean subduction zone (35°S to 37°S; Klaucke et al. 2012) during the R/V *Sonne* SO210 cruise

from 23 September to 1 November 2010. The sampling site (36°28.25' S / 73°40.75' W) is within a ~ 4 km^2 region referred to as the Concepción Methane Seep Area (CMSA) Box 2 within which bathymetric surveys and acoustic imaging from sidescan sonars and sub-bottom profilers have revealed active seepage (Klaucke et al. 2012). The sea floor displayed typical cold-seep features such as sediments covered with sulfide-oxidizing bacterial mats, reduced and sulfidic sediments, live tubeworms, and authigenic carbonates (Linke et al. 2011).

Profiler Lander

The Profiler lander (Fig. III.1) used for this study consists of a transecting microsensor-equipped profiling unit mounted on a standard GEOMAR lander (Pfannkuche and Linke 2003). A TV-guided launching system allowed smooth placement of the lander at selected sites on the sea floor.

The profiling unit in the lander consists of lower and upper glass-fiber frames, which are connected by four glass-fiber poles. The upper frame extends ~ 50 cm towards the front defining an area of ~ 0.15 m^2 across which the sensor array can be moved in mm increments along the x- and the y-axes, which are 450 mm and 330 mm long, respectively. Along the vertical z-axis, the sensor array can be moved in self-designated increments ranging from 100 µm to several mm, over a total vertical distance of 190 mm. The rear section of the profiling unit contains pressure housings for data logging, the control unit (i.e., for sensor array movement), and batteries. A total of four microsensors can be deployed simultaneously. Microsensors used for this study were Clark-type O_2 microelectrodes (Revsbech 1989) with a tip diameter of ~ 50-µm, as well H_2S microsensors (Jeroschewski 1996) and pH microsensors (Unisense, Aarhus, Denmark). The lateral distance between each of the microsensors on the profiling unit was 25 mm. Two optodes (Aanderaa; Bergen, Norway) were also mounted on the profiling unit to record time series of O_2 and temperature in the bottom water at ~ 1 m and ~ 18 cm above the seafloor.

The Profiler lander was further equipped with an upward-looking acoustic Doppler current profiler (300 KHz Workhorse Sentinel; RD Instruments, California, United States) and a Conductivity-Temperature-Depth logger (CTD; RBR, Ottawa, Canada). A camera system (Ocean Imaging System; Massachusetts, United States) was used to obtain images of the sediment surface.

Profile acquisition

Vertical microsensor-profile acquisition consisted of two steps: (1) a fast-search profile was performed in mm steps until the SWI was detected, then the sensor array was retracted and moved 3 mm forward along the x-axis where (2) the actual high resolution profile was performed. High-resolution profiling was performed in 100-µm steps from a programmable safety distance (19 mm for this study) above the depth of the previously detected SWI to a pre-selected profile length into the sediment (24 mm for this study). During each deployment, the sensor array was moved 16 mm along the x-axis between each successive profile. If the fast-search profile failed to detect the SWI, the array was set to again move 16 mm forward and perform another search profile. For each of the two deployments, profiling was programmed to last slightly less than 48 h.

Two deployments of the profiler were performed in relatively similar seep habitats. The first Profiler deployment, a transect across seep habitat P1, was carried out on 14th October 2012, while the second deployment, a transect across seep habitat P2, was conducted on 18th October 2012 approximately 100 m away from the P1 location. The P1 transect was performed using two O_2 sensors, an H_2S sensor and a pH sensor over a transect length of 45.0 cm. 37 O_2 and 27 H_2S profiles were obtained; however, the pH sensor failed. The P2 transect was conducted with the same H_2S and O_2 sensors used for P1 and collected 40 O_2 and 27 H_2S profiles over a length of 41.6 cm. Due to technical malfunctions, the sensor array performed shorter steps along the x-axis between profiles 6 – 7 and 13 – 14 as well as a larger step between profiles 26 – 27 on P2. The time period between the profiles, however, remained constant.

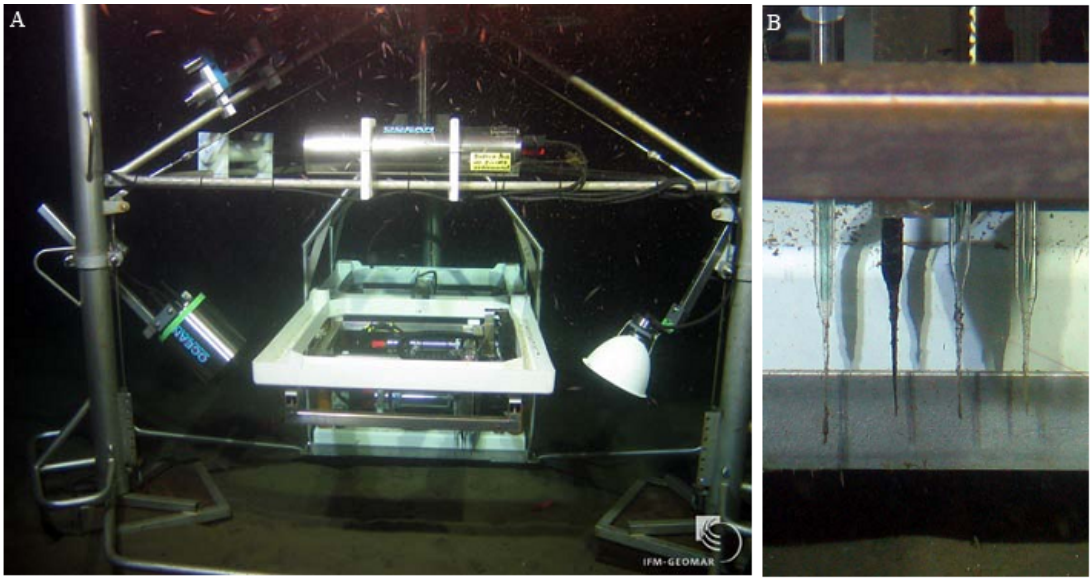

Fig. III.1. In-situ transecting profiler system (A) mounted on the GEOMAR lander frame. (B) Close-up of the profiler sensor array showing, from left to right, one pH microsensor, one H_2S microsensor, and then two O_2 microsensors (pictures courtesy of GEOMAR ROV Kiel 6000).

O_2 profile processing

Each O_2 profile was calibrated individually using O_2 concentrations in the well-mixed water overlaying the sediment based on Winkler-corrected optode measurements at the beginning of each profile and the anoxic sediment at the end of each profile (0 μmol L^{-1}). *DOU* rates were calculated from the calibrated profiles based on Fick's first law of diffusion (Jørgensen and Des Marais 1990) as:

$$DOU = -\varphi D_{O_2} \frac{\Delta O_2}{\delta_{DBL}} \quad \text{(III.1)}$$

with φ being sediment porosity, D_{O_2} the molecular diffusion coefficient of O_2 in seawater and $\Delta O_2 = C_{bulk} - C_{SWI}$ being the O_2 concentration difference between the SWI (C_{SWI}) and the upper DBL boundary (C_{bulk}), respectively (*see* Jorgensen and Revsbech 1985; Bryant et al. 2010a,b). The upper DBL boundary was defined as the intersection of the linearly extrapolated concentration gradient within the DBL and C_{bulk} in the overlying water. The SWI was determined by considering distinct slope changes in the O_2 concentration profiles as the result of the change between D_{O_2} in water and the O_2 diffusion coefficient in porous media (Jørgensen and Des Marais 1990; Bryant et al. 2010b). The O_2 diffusion coefficient D_0 (1.57 x 10^{-9} m^2 s^{-1} at 10°C;

Broeker and Peng 1974) was corrected for in-situ temperature and salinity following the Einstein-Stokes relationship (Li and Gregory 1974). As the O_2 flux was estimated from the water-side, a porosity value of $\varphi = 1$ was used.

The measured δ_{DBL} was also compared to the theoretical thickness estimated assuming Law-of-the-Wall (LOW; Imboden and Wüest 1995) as:

$$\delta_{DBL} \approx \delta_\nu \left(D_{O_2}/\nu\right)^{1/3} \quad \text{(III.2)}$$

where $\delta_\nu \approx 10\,\nu/u^*$ is viscous sublayer thickness, ν is molecular viscosity at in-situ conditions, and u* is friction velocity.

H_2S profile calibration and processing

The H_2S sensors were calibrated in the lab using a dilution of sodium sulfide – sodium hydroxide stock solution (total sulfide concentrations of 60 mmol L^{-1} and 58.17 mmol L^{-1} for P1 and P2, respectively) with phosphate buffer solution (pH 7). A linear relationship between the sensor reading and the H_2S concentration was assumed (Jeroschewski et al. 1996). By adding a specific amount of stock solution to 100-ml buffer solutions, four-point calibrations were performed prior to each deployment using four different solutions with known total sulfide concentrations (ΣH_2S). The concentration of H_2S in each of the pH 7 solutions was calculated following Jeroschewski et al. (1996) as:

$$H_2S = \Sigma H_2S/(1 + 10^{-pK1}/10^{-pH}) \quad \text{(III.3)}$$

with pK1 being the H_2S dissociation constant based on lab conditions (21°C; *see* Millero et al. 1988). The H_2S sensor calibration range for P1 was 3 – 31 µmol L^{-1} H_2S. For the P2 calibration, the range was broadened to 3 – 123 µmol L^{-1} to ensure increased accuracy at high concentrations. The hydrogen sulfide H_2S flux was then estimated for each calibrated profile as:

$$F_{H_2S} = \varphi D_{(s)H_2S} \frac{\Delta H_2S}{\Delta z} \quad \text{(III.4)}$$

with $D_{(s)H_2S}$ being the in-situ H_2S diffusion coefficient in the sediment, and $\Delta H_2S/\Delta z$ the concentration gradient estimated based on the region of the concentration profile between the depth where H_2S was detected and the end of the profile. The concentration gradient within this depth interval of interest was approximated to be linear. If the "linear" concentration profile displayed appreciable slope changes, the segment close to the H_2S detection depth was

considered for flux estimations; otherwise, the entire length of the measured H_2S profile was considered. $D_{(s)H_2S}$ was defined as $D_{(s)H_2S} = \varphi D_{H_2S}$ with the H_2S diffusion coefficient in water, D_{H_2S}, estimated based on in-situ salinity and temperature from the reference value of 2.1 x 10^{-9} m^2 s^{-1} at 25°C (Boudreau 1997). Tortuosity was accounted for by multiplying D_{H_2S} with φ (*see* Berg et al. 2003). An average sediment ϕ of 0.75 was also determined using the same core and following the method of Haeckel et al. (2001). Due to the failure of the pH microsensor, pH values were taken from ex-situ microsensor measurements of a sediment core collected in the study area.

Total sulfide concentrations were obtained using the sulfide dissolution equation (Eq. 3) for in-situ conditions. Total sulfide flux ($F_{\Sigma H_2S}$) was approximated based on the estimated H_2S fluxes as:

$$F_{\Sigma H_2S} = F_{H_2S} \frac{\Sigma H_2S}{H_2S} \frac{D_{\Sigma H_2S}}{D_{(s)H_2S}} \quad \text{(III.5)}$$

with $\Sigma H_2S/H_2S$ being the total sulfide to hydrogen sulfide ratio. $D_{\Sigma H_2S}$ is defined here as the weighted average of $D_{(s)H_2S}$ and the sediment molecular diffusion coefficient of sulfide, D_{HS^-} (1.73 x 10^{-9} m^2 s^{-1} at 25°C; Li and Gregory 1974), accounting for both H_2S and HS^- ratios to ΣH_2S for the in-situ conditions. S^{2-} concentration was assumed to be negligible at the in-situ conditions and thus not considered in Eq. 6:

$$D_{\Sigma H_2S} = \frac{H_2S}{\Sigma H_2S} D_{(s)H_2S} + \frac{HS^-}{\Sigma H_2S} D_{HS^-} \quad \text{(III.6)}$$

III. 3. Results

Deployment overview

The deployments were performed at similar water depths (~700 m) and in similar physical settings (i.e., temperature, salinity). ADCP-based current measurements, performed 5.8 m above the seafloor, also revealed comparable current velocities with average magnitudes of 8.5 and 9.3 cm s^{-1} for P1 and P2, respectively. On P2, the range was slightly broader (2.5 – 18.3 cm s^{-1}) than that of P1 (2.5 – 15.7 cm s^{-1}). Current direction ranged from 40 to 140° for P1 and 150 to 240° for P2 with an apparent periodicity of ~12 h.

The P1 transect was characterized by the frequent occurrence of sulfide oxidizing bacterial mats of varying spatial extents (Fig. III.2A). Microscale topography revealed a maximum difference in elevation of 23 mm (Fig. III.2B). Due to a technical malfunction, the sensor array made an increased step along the x-axis between profiles 10 and 11, thus leaving a 130-mm gap where no profiles were performed. Time elapsed between profiles 10 and 11, however, was the same as between other profiles. Due to this inconsistency in horizontal spacing, profiles will be plotted versus deployment time throughout this study. In contrast to P1, during the P2 transect bacterial mats were only present towards the end of the transect in a region where sulfidic sediments occurred (Fig. III.2C). A 21-mm-deep depression was also detected in this region (Fig. III.2D). No inconsistencies in spacing occurred during P2.

O_2 profiles

Characteristic profiles for both transects are shown in Fig. III.3. The near-bottom O_2 concentration measured at ~18 cm distance from the seafloor showed little variability on both transects (131 ± 3 µmol L^{-1} during P1 and 165 ± 5 µmol L^{-1} during P2; Fig III.4A, C). The O_2 concentration offset between the deployments was attributed to calibration error in one of the sensors and was accounted for during analysis.

The O_2 profiles typically displayed well-defined DBLs with δ_{DBL} ranging from 0.1 to 1.6 mm (average 0.5 ± 0.4 mm) and from 0.2 to 1.3 mm (average 0.5 ± 0.5 mm) for P1 and P2, respectively. For a few profiles (eight on P1, four on P2), the location of the SWI and corresponding δ_{DBL} could not be clearly determined although the presence of a DBL was evident.

For such cases where multiple estimates of δ_{DBL} were possible for a single profile (due to, e.g., unclear determination of the SWI or scatter in near-sediment O_2 concentration data), an average δ_{DBL} based on up to three estimates of δ_{DBL} were considered for *DOU* quantification as well as for deployment averages; the range of these δ_{DBL} estimates was also reported (Fig. III.5).

There were periods were trends in δ_{DBL} followed an inverse relationship to trends in near-bottom current (Fig. III.5; shaded areas), as expected theoretically. Similarities were observed on P1 during the period 12 – 21 h and 24 – 35 h and on P2 for the periods 7 – 15 h and 20 – 28 h. On P1, average δ_{DBL} during high flow (~11 cm s^{-1} on average; period 16 – 20 h and 28 – 32 h after deployment) was 0.3 mm; during low flow (~5 cm s^{-1} on average; period 20 – 24 h after deployment) δ_{DBL} increased to 0.8 mm. Conversely, during P2, average δ_{DBL} was 0.2 mm during high flow (~13 cm s^{-1} on average; period 8 – 10 h and 44 – 48 h after deployment) and increased only slightly to 0.4 mm during low flow (~6 cm s^{-1} on average; period 14 – 18 h and 38 – 44 h post-deployment).

On P1, where the sediment was more widely covered with bacterial mats, the depth of O_2 penetration into the sediment (z_{max}) displayed limited variability along the transect and was generally much shallower than that observed on P2 (1.7 mm as compared to 5.8 mm on average; Fig. III.4B). On P2, z_{max} strongly decreased in close proximity to reduced, anoxic sediments covered with bacterial mats (Fig. III.4D). A clear suboxic zone, defined as the zone between z_{max} and the depth of H_2S detection, was observed in all profiles where H_2S was present (*see* Fig. III.3). Suboxic-zone thickness ranged from 2.9 to 20.2 mm (average 14.3 ± 4.6 mm) for P1 and from 2.1 to 18.8 mm (average 10.6 ± 4.6 mm) for P2.

DOUs on P1 ranged from 2.0 to 21.6 mmol m^{-2} d^{-1} (Fig. III.6A) with an average *DOU* of 7.9 ± 4.5 mmol m^{-2} d^{-1}. In contrast, on P2 a narrower *DOU* range (1.0 to 13.1 mmol m^{-2} d^{-1}; Fig. III.7A) was observed with an average *DOU* of 4.0 ± 2.3 mmol m^{-2} d^{-1} during the final section of the transect with bacterial-mat coverage (Fig. III.2C).

H_2S profiles

The occurrence of H_2S was detected in 71% of the P1 profiles (15 of 21) and in 22% of the P2 profiles (6 of 27). H_2S concentrations reached up to 132 µmmol L^{-1} (profile 23 at P2). H_2S fluxes

ranged from 0.3 to 1.5 mmol m^{-2} d^{-1} for P1 and from 0.1 to 1.2 mmol m^{-2} d^{-1} for P2 with average H_2S fluxes of ~0.4 mmol m^2 d^{-1} for habitats. The corresponding total-sulfide-based $F_{\Sigma H2S}$ fluxes (Eq. III.5 for the in-situ conditions shown in Table 1) were a factor of 4.08 higher than those of hydrogen-sulfide-based F_{H2S} for P1 and 4.09 higher for P2 (Fig III.6B and Fig. III.7B).

Larger H_2S gradients (and thus higher fluxes) corresponded to both decreased O_2 penetration and reduced variability in z_{max} (Fig. III.6C and III.7C). This was most evident on P2, where the average z_{max} in sediment with H_2S was ~ 52% lower than sediment in which H_2S was not detected. On P1 the same trend is also present, although less distinct (16%). In both transects, *DOUs* were on average ~ 27% higher in the presence of H_2S (Table III.1) and similar trends in O_2 and H_2S flux variability were observed. This correlation was stronger on P1 for profiles 1 – 4 and 14 – 18 (Fig. III.6) and on P2 for profiles 19 – 27 (Fig. III.7). However, an offset between the occurrence of the *DOU* and H_2S flux maxima was identified during both transects. On P1, the maximum *DOU* was detected during profile 9 while the highest H_2S flux peak occurred on profile 12. On P2, *DOU* and H_2S flux maxima occurred during profiles 25 and 23, respectively. This offset was attributed primarily to the arrangement of the sensor array, i.e., the lateral spatial separation between the O_2 and H_2S sensors (*see* section III.4).

Due to (1) the relatively few profiles in which H_2S was not observed on P1 and (2) in which H_2S was observed on P2, the P1 transect was characterized as a more reactive, sulfidic habitat while the P2 transect was considered less reactive. This characterization was also evident when considering average *DOU* for each of the habitats (7.9 and 4.0 mmol m^{-2} d^{-1}, for P1 and P2, respectively).

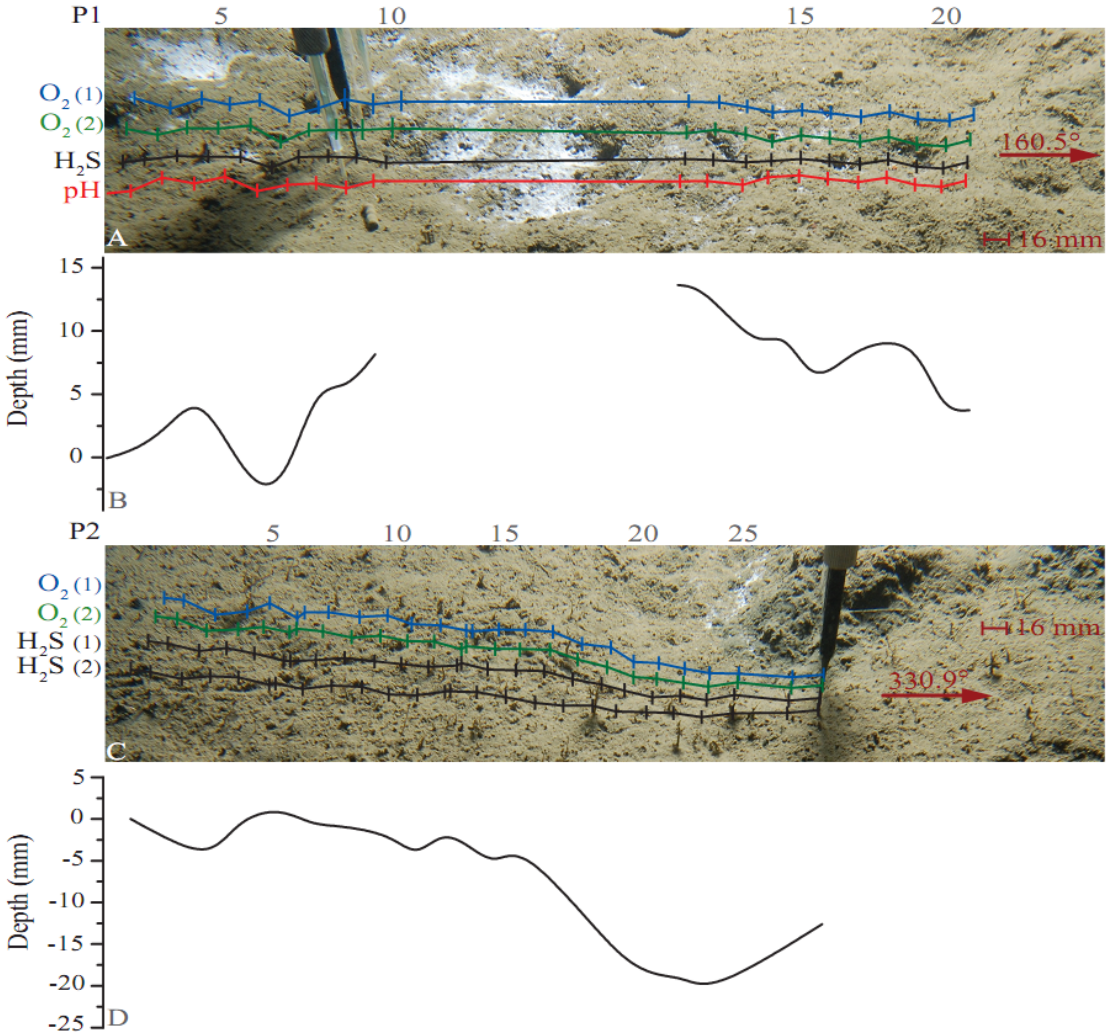

Fig. III.2. Profiling transect area and elevation profile from P1 (upper panels A, B) and P2 (lower panels C, D) deployments. The vertical thick lines indicate the location of each profile along the transect length. (A) P1 transect area image overlaid with the location of the measured O_2, H_2S and pH profiles. The arrow indicates the direction of the x-axis. The elevation profile was derived from the depth of the SWI as detected from sensor 1 and 2 for P1 and P2, respectively. Note that due to technical malfunctions, the system performed a step larger than the programmed 16 mm between P1 profiles 10 and 11, thus leaving a 130-mm section of the transect unsampled; also, shorter steps in the x direction were performed between P2 profiles 6 – 7 and 13 – 14, while a longer step was detected between P2 profiles 26 – 27.

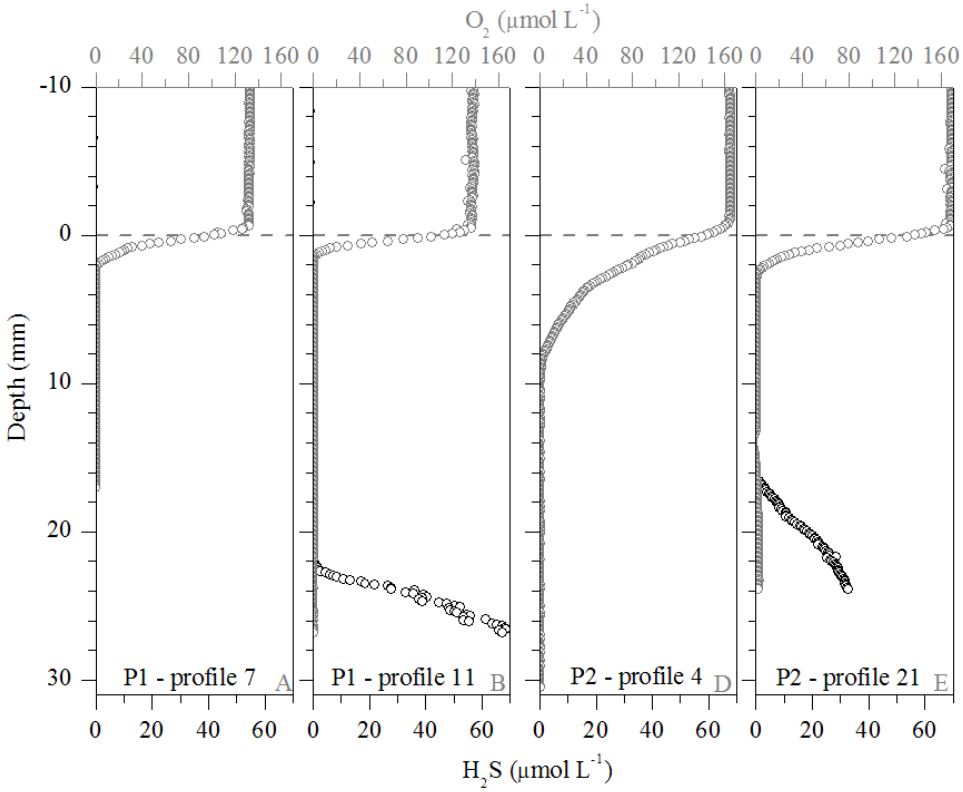

Fig. III.3. Typical O_2 and H_2S profiles from P1 (panels A, B) and P2 (panels C, D) deployments. The dashed lines indicate the sediment water interface (SWI; depth=0). Well-resolved diffusive boundary layers (DBL) were typically observed with an average δ_{DBL} of 0.5 ± 0.4 mm for P1 and 0.5 ± 0.5 for P2.

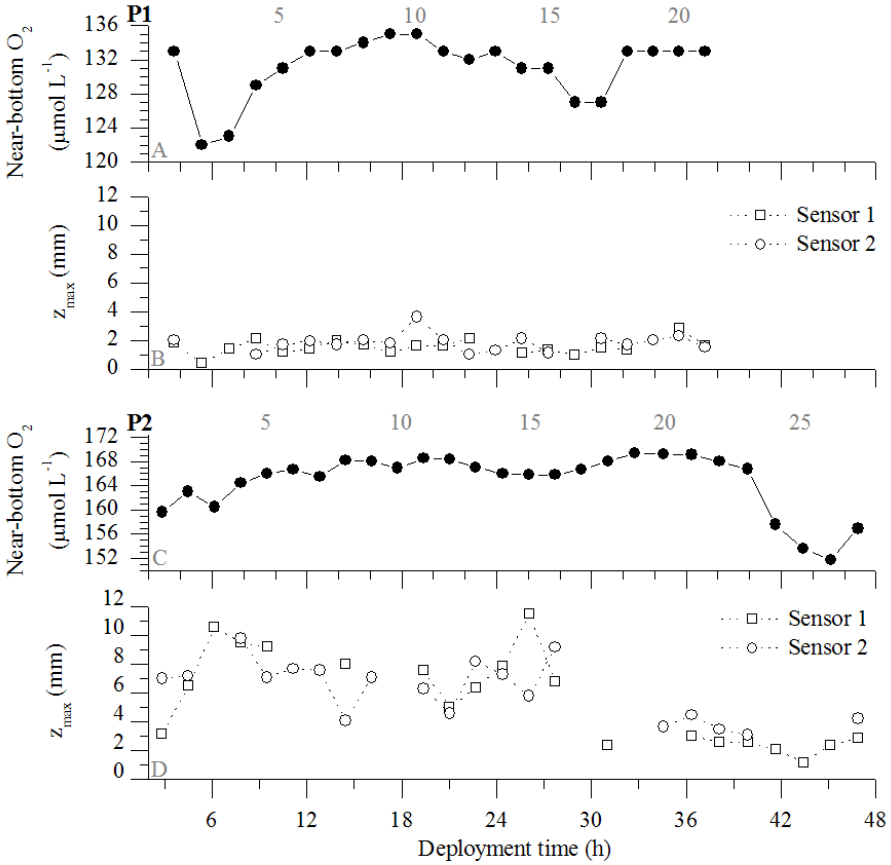

Fig. III.4. O_2 bottom water concentrations measured about 18 cm above the sea floor and maximum O_2 penetration depth (z_{max}) during deployments on P1 (A, B) and P2 (C, D). Numbers indicate profile number.

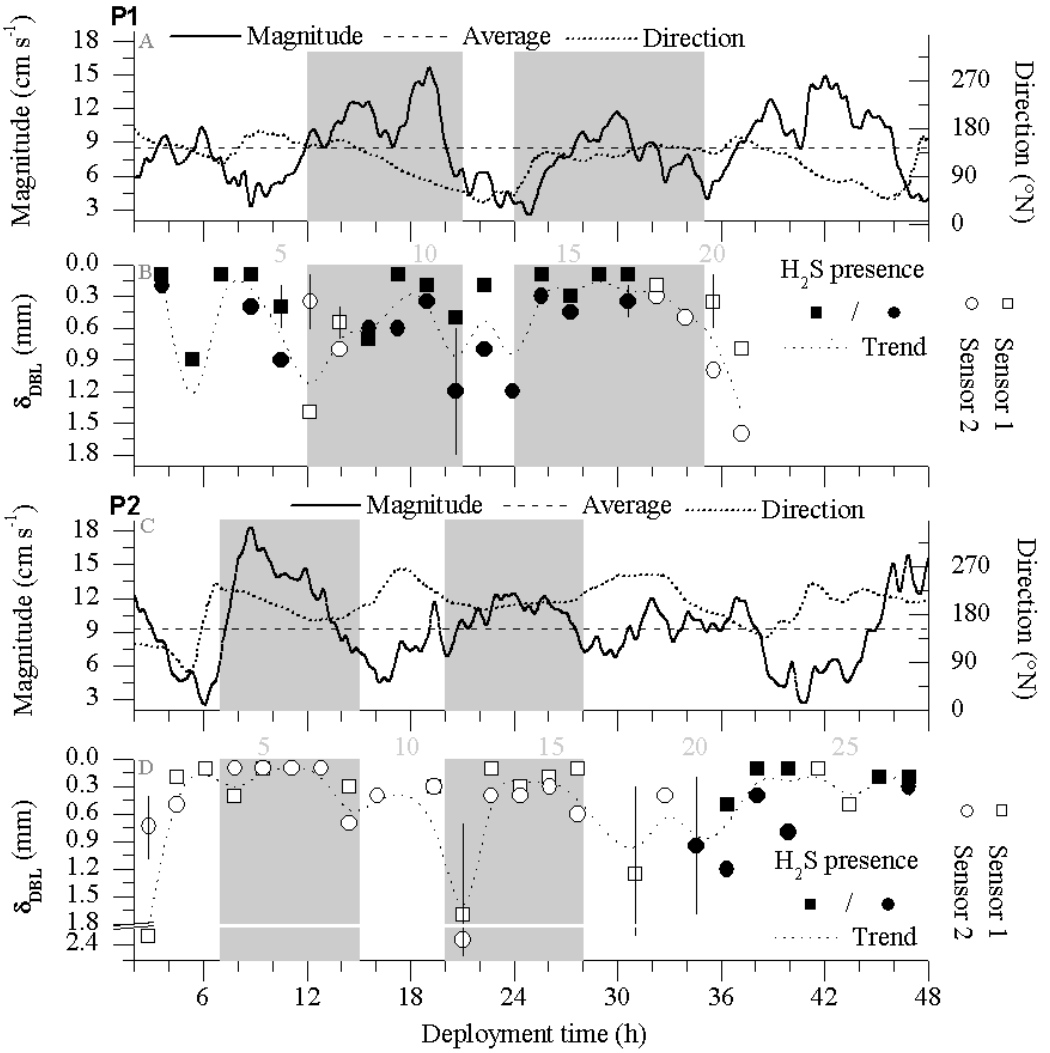

Fig. III.5. Near-bottom current magnitude and δ_{DBL} for P1 (A, B) and P2 (C, D). The vertical lines refer to the range of δ_{DBL} for profiles where δ_{DBL} could not be unequivocally determined for sensor 1 (squares) and sensor 2 (circles), respectively. Solid squares and circles identify profiles where H_2S was detected during P1 and P2 transects, respectively. Numbers indicate profile number. Note that the y-axis on panel (D) was blended between 1.8 – 2 mm to provide better readability. Shaded areas identify the regions where trends between near-bottom current and δ_{DBL} were observed.

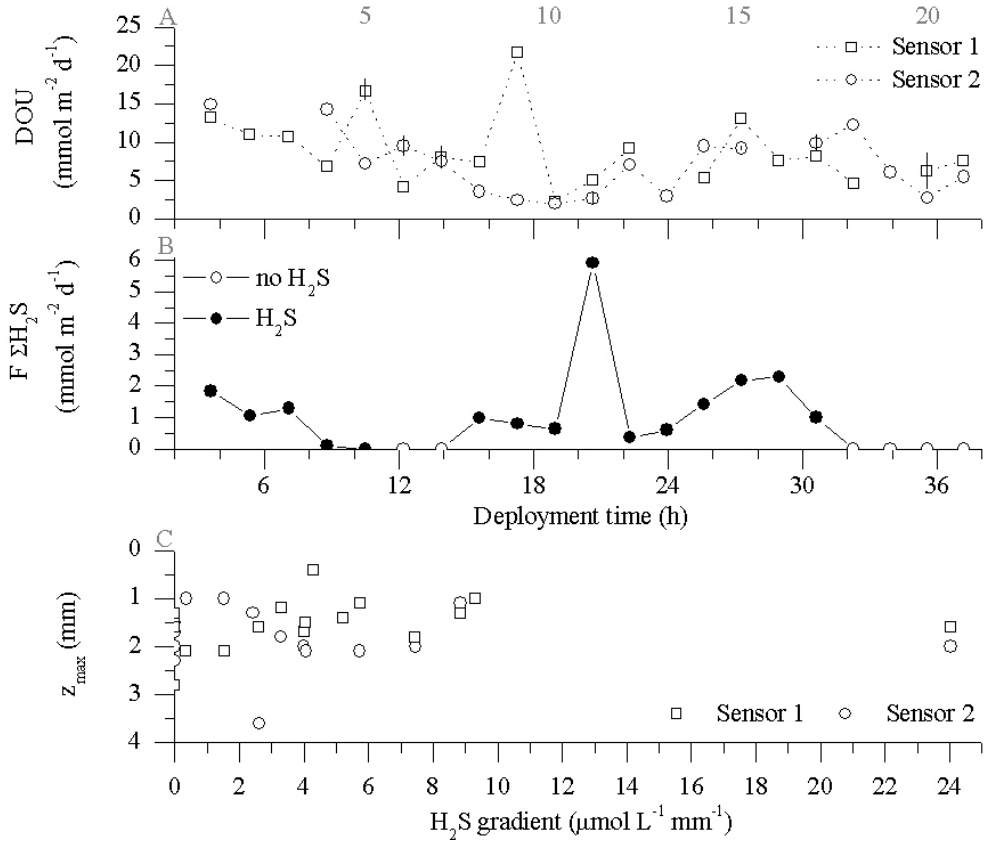

Fig. III.6. Diffusive O_2 uptake (*DOU*) rates (A) and total sulfide (ΣH_2S) fluxes (B) as a function of deployment time, and O_2 penetration depth (z_{max}) as a function of H_2S gradient (C) for the P1 transect. The vertical lines in panel A refer to the *DOU* range for profiles where δ_{DBL} could not be unequivocally determined for sensor 1 (squares) and sensor 2 (circles), respectively. Numbers indicate profile number.

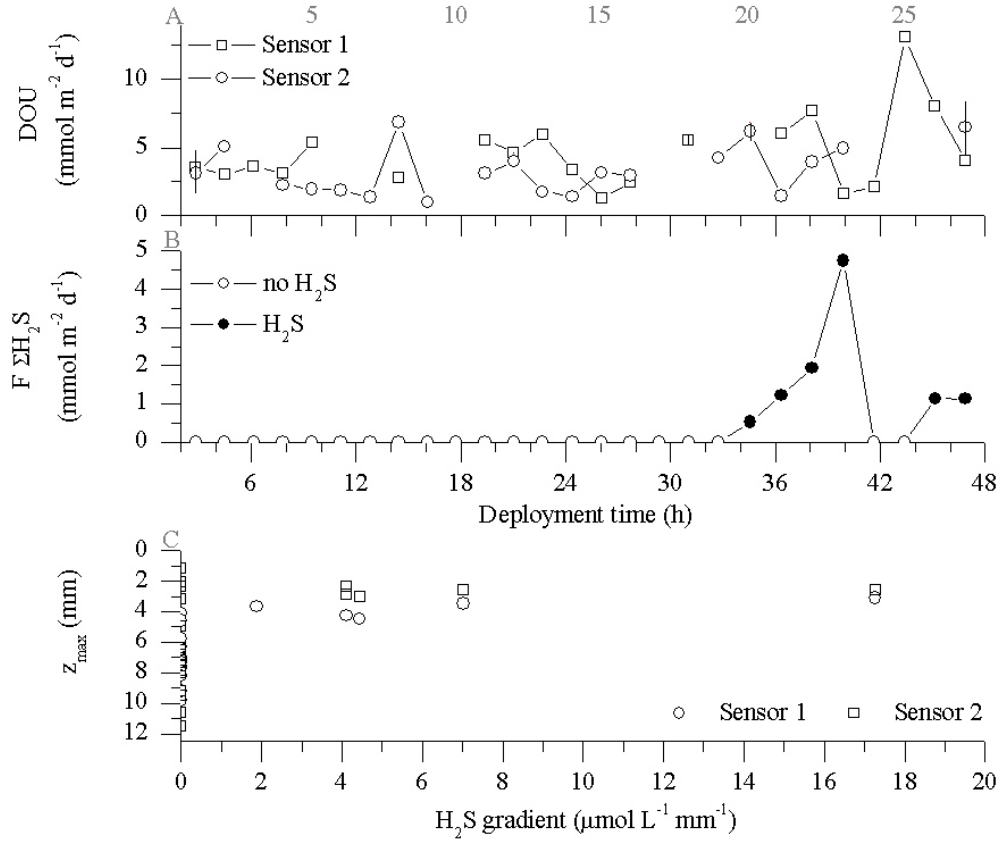

Fig. 7. Diffusive O_2 uptake (*DOU*) rates (A) and total sulfide (ΣH_2S) fluxes (B) as a function of deployment time, and O_2 penetration depth (z_{max}) as a function of H_2S gradient (C) for the P2 transect. The vertical lines in panel A refer to the *DOU* range for profiles where δ_{DBL} could not be unequivocally determined for sensor 1 (squares) and sensor 2 (circles), respectively. Numbers indicate profile number.

Table III.1. Results summary[1]

	Transect on seep habitat P1		Transect on seep habitat P2	
Location	36°28.290' S / 73°40.716' W		36°28.236' S / 73°40.704' W	
Depth (m)	705		700	
Temperature (°C)	4.73 ± 0.07		4.75 ± 0.07	
Salinity	34.3		34.3	
pH	7.45		7.45	
Current velocity (cm s^{-1})	8.5 ± 3.0 [2.5 – 15.7]		9.3 ± 3.3 [2.5 – 18.3]	
Bottom O_2 (μmol L^{-1})	131 ± 3 [122 – 135]		165 ± 5 [152 – 169]	
Analyzed profiles[1]	37/42		40/54	
δ_{DBL} (mm)	0.5 ± 0.4 [0.1 – 1.6]		0.5 ± 0.5 [0.1 – 2.3]	
ΔO_2 (µmol L^{-1})	29 ± 22 [3.5 – 91.5]		16 ± 19 [1.2 – 85.4]	
DOU (mmol m^{-2} d^{-1})	7.9 ± 4.5 [2.0 – 21.6]		4.0 ± 2.3 [1.0 – 13.1]	
O_2 penetration depth (mm)	1.7 ± 0.6 [0.4 – 3.6]		5.8 ± 2.6 [1.2 – 11.5]	
Presence of H_2S	15/21		6/27	
H_2S gradient (µmol L^{-1} mm^{-1})	6 ± 5.8 [0.4 – 24]		6.5 ± 5.5 [1.9 – 17]	
H_2S Flux (mmol m^{-2} d^{-1})	0.4 ± 0.35 [0.3 – 1.5]		0.4 ± 0.3 [0.1 – 1.2]	
ΣH_2S Flux (mmol m^{-2} d^{-1})	1.5 ± 1.4 [0.1 – 5.9]		1.8 ± 1.5 [0.5 – 4.7]	
	H_2S	no H_2S	H_2S	no H_2S
δ_{DBL} (mm)[2]	0.4 ± 0.3 [0.1 – 1.2]	0.6 ± 0.5 [0.1 – 1.6]	0.5 ± 0.4 [0.1 – 1.2]	0.5 ± 0.6 [0.1 – 2.3]
DOU (mmol m^{-2} d^{-2})[2]	8.6 ± 5.0 [2.0 – 21.6]	6.3 ± 2.6 [2.7 – 12.2]	5.1 ± 2.3 [1.4 – 8]	3.7 ± 2.3 [1.0 – 13.1]
O_2 penetration depth (mm)[2]	1.6 ± 0.6 [0.4 – 3.6]	1.9 ± 0.5 [1.3 – 2.8]	3.3 ± 0.7 [2.4 – 4.5]	6.8 ± 2.5 [1.2 – 11.5]

1: Note that five and 14 O_2 profiles, for P1 and P2 respectively, were bad or strongly scattered and were therefore discarded from further analysis. The range of each parameter is given in the square brackets.

2: The averages, standard deviations, and ranges are provided for profiles obtained in regions where H_2S was and was not detected (H_2S was measured during 15 and 6 profiles for P1 and P2, respectively).

III.4. Discussion

Physical forcing on DBL and DOU

Near-bottom current velocity and δ_{DBL} were highly variable during both the deployment on P1 and P2 (Fig. III.5 and Table III.1). While there were similar trends in δ_{DBL} and near-bottom current velocity, the attempt to correlate these parameters was inconclusive for the full dataset (Fig. 8A; open circles). This was largely attributed to disturbances in the flow related to the orientation of the lander. Due to the lander design, lander-related flow disturbance is strongly reduced when current-flow direction is toward the front of the lander, i.e. approaching within a 120° window between the front legs of the lander (Fig. III.1). During the transect on P2, the lander was oriented towards 330° and against the main flow direction. Thus, the majority of profiles were obtained within the 120° window. Conversely, on the P1 transect the profiles were primarily performed outside that window and, as a result, flow into the profiling area may have been altered by the lander frame.

The observed trends scaled only partially with the theoretical DBL distribution under the Law-of-the-Wall assumption (Imberger and Wüest 1995). The strongest deviations from LOW were unexpectedly detected in the mid-range velocity (8 – 11 cm s^{-1}), where both P1 and P2 δ_{DBL} maxima occurred (Fig. III.8A, shaded area). Interestingly, regardless of the observed trends in variability in δ_{DBL} and current velocity, once current velocities increased to 12 cm s^{-1}, the δ_{DBL} appeared to stabilize at approximately 0.2 mm, which suggested that at this point δ_{DBL} was no longer influenced by flow variations. The lack of a stronger correlation was primarily attributed to flow disturbances from the lander and its orientation over the current velocity main axis. With the exception of the above mentioned mid-range velocity conditions, the removal of possible δ_{DBL} artefacts resulting from lander-induced flow disturbances did indeed reveal a better relationship between the measured δ_{DBL} and LOW (Fig. 8A, filled circles).

During most profiles, δ_{DBL} remained relatively thin (0.1 – 0.4 mm) and thereby supported rapid diffusive transport. Throughout both transects, there were only a few occasions during which δ_{DBL} exceeded 1 mm. On P1, the occurrences of increased δ_{DBL} often coincided with periods of reduced flow (Fig. III.8A). As the studied system was not limited by O_2 availability (near-bottom O_2 saturations remained above 40%), transport across the P1 SWI may have become transport-

limited under such situation with high δ_{DBL}. Though the correlation was less evident during periods of lower velocity, *DOU* for the periods of 2 – 6 hours and 24 – 32 hours (Fig. III.5 and Fig. III.6) appeared to scale directly with δ_{DBL} with increased fluxes observed during periods of reduced δ_{DBL}, which would be compatible with a transport-limited system. However, such a correlation was not observed on P2.

This became even more apparent when comparing the *DOU* distribution of P1 and P2 against the δ_{DBL} (Fig. III.8B). The *DOU* maxima determined for P1 were characterized by a hyperbolic trend as would be expected for a strictly physically controlled system, with δ_{DBL} being the main control parameter for Eq. III.1. Given the high number of O_2 profiles, the maximum observed ΔO_2 for P1 and P2 (Table III.1) were inferred to be representative for the overall habitat maximum and thus used to define the maximum *DOU* range possible within a physically controlled system (estimated by Eq. III.1 using a maximum ΔO_2; Fig. III.8B, dashed and dotted lines). The closer the estimated *DOUs* are located to these endpoint-lines the stronger the likelihood that the system can become transport-limited. The fact that several P1 points approached this boundary supports that this mat-dominated transect was often a physically controlled, and thus limited, system. This is well in agreement with results from an ex-situ experiment focused on fluxes across bacterial mats by Jørgensen and Revsbech (1983), which showed that the DBL regulated solute fluxes. In contrast, P2 *DOUs* seemed to be less affected by δ_{DBL} variability (Fig. III.8B). Deviation from a physically controlled system, i.e., the scatter below the curves on Fig. III.8B, can be attributed to several factors including small-scale topography, sediment biogeochemical processes, infauna respiration.

Biogeochemical implications of DBL transport limitations.

We cannot disentangle the different physical and biogeochemical processes leading to the observed scatter in the *DOU*, which is beyond the scope of this study. However, geochemical processes generating the observed *DOU* will be explored with a particular focus on sulfide fluxes whose oxidation might involve O_2 consumption. In both seep habitats P1 and P2, average *DOU* of 7.9 (maximum 21.6) and 4.0 mmol m^{-2} d^{-1} (maximum 13.1), respectively, strongly exceeds the O_2 consumption that would be needed for the degradation of allochthonous organic matter from the sea surface.

Based on the empirical equation of Suess (1980) for carbon export and on a surface water primary production of 0.3 – 0.4 g C m^{-2} d^{-1} (Antoine et al. 1996), a benthic organic carbon supply of 1.2 – 1.7 mmol C m^{-2} d^{-1} was estimated. Assuming Redfield ratio (Redfield 1963) and a burial efficiency of 3% (Dunne et al. 2007), particulate organic matter mineralization was calculated to account for a *DOU* of up to 2.1 mmol m^{-2} d^{-1} and an ammonium (NH_4^+) release of 0.24 mmol m^{-2} d^{-1}. Resultant NH_4^+ oxidation accounted for an additional O_2 flux of 0.5 mmol m^{-2} d^{-1}.

As indicated by previous mass balance calculations for a seep site at Hydrate Ridge, Cascadia convergent margin, it has been shown that 60 to 73 % of *DOU* is typically used for sulfide oxidation (Suess 1999; Sommer et al. 2006). A recent compilation of in-situ fluxes at cold seeps (Boetius and Wenzhöfer 2013) further confirmed that at cold seeps a large proportion of benthic O_2 uptake is explained by microbial oxidation of sulfide.

As reviewed by Jørgensen and Nelson (2004), there are multiple aerobic and anaerobic oxidation pathways for sulfide. Beyond sulfide release during sulfate reduction during anaerobic organic matter degradation, substantial amounts of sulfide are produced in seep environments via the anaerobic oxidation of methane (AOM) which is conducted by a consortium of methanogenic archaea and sulphate-reducing bacteria (Boetius et al. 2000) and represents a major sink for methane in cold seep environments (e.g. Judd and Hovland 2007; Reeburgh 2007 and references therein). In seep habitats (*see* Boetius & Wenzhöfer 2013) as well as in oxygen minimum zone (OMZ) sediments subjected to O_2 depleted bottom water conditions (Gallardo 1977, Schmaljohann et al. 2001; Mosch et al. 2012) and elevated sulfide fluxes to the sediment surface often lead to the formation of dense mats of vacuolated sulfur bacteria belonging to the genera *Beggiatoa sp.* or *Thioploca sp*. These filamentous bacteria can accumulate nitrate/nitrite (NO_3^- /NO_2) inside their vacuoles and, in the absence of O_2, can oxidize sulfide through dissimilatory nitrate reduction to ammonia (DNRA). This results in the release of large amounts of ammonium into the porewater (e.g. Farías et al. 1996; Graco et al. 2001; Bohlen et al. 2011), which will then be oxidized at the sediment surface when O_2 is available.

The presence of a well-defined suboxic zone in all profiles (Fig. III.3) suggests that sulfide oxidation in the studied seep sediments proceeded anaerobically likely via DNRA. During DNRA, the oxidation of 1 mole of sulfide leads to the release of 1 mole of NH_4^+ (Jorgensen and

Nelson 2004). At the sediment surface when O_2 becomes available, the oxidation of NH_4^+ during nitrification requires approximately 1.5 moles of O_2 (VanCappellen and Wang 1996; Bohlen et al. 2011; Dale et al. 2013). Neglecting anaerobic oxidation of NH_4^+ (Anammox), which is susceptible to the presence of sulfide (*see* Jensen et al. 2008), it can be assumed that all NH_4^+ is oxidized at the sediment surface. At P1 and P2, maximum sulfide fluxes would require a maximum *DOU* of 8.9 mmol m^{-2} d^{-1} (average 2.3 mmol m^{-2} d^{-1}) and 7.1 mmol m^{-2} d^{-1} (average 2.7 mmol m^{-2} d^{-1}), respectively. At P2, the O_2 needed to oxidize the maximum sulfide flux in combination with the aerobic C_{org} degradation (2.6 mmol m^{-2} d^{-1}) would be sufficient to match the maximum O_2 flux of 13.1 mmol m^{-2} d^{-1} (*see* Table III.1). This is in contrast to P1 where the maximum O_2 flux is about twice as much as that required to support sulfide oxidation and the C_{org} degradation. One likely explanation for this offset is aerobic methane oxidation (AeOM) at the oxic sediment surface; yet, our data do not allow for quantifying AeOM. However, this process has been shown to occur in various magnitudes in a variety of cold seep habitats (Niemann et al. 2006; Sommer et al. 2006, 2010; Boetius and Wenzhöfer 2013).

Although sulfide oxidation appears to represent a prominent process contributing to O_2 uptake and consumption in both seeps, it needs to be mentioned that sulfide could be anaerobically oxidized without consuming O_2 at all. Similarly to DNRA, sulfide can be oxidized during chemolithotrophic denitrification using NO_3^-/NO_2^-; however, dinitrogen gas N_2 is released instead of NH_4^+ (Cardoso et al. 2006). This process thus circumvents O_2 consumption. Although there are still many open research questions on when and where each of these sulphide-oxidation processes take place, several studies support that DNRA frequently takes place in organically enriched sediments covered with microbial mats such as those assessed in this study (Farias et al 1996; Graco et al. 2001; Bohlen et al. 2011). Conversely, chemolithotrophic denitrification has been only observed at waste-treatment sites (*see* Cardoso et al. 2006) or along the African shelf (*see* Lavik et al. 2009).

Irrespective of the processes causing the high O_2 demand in both seep sediments, maximum O_2 uptake rates were only supported when δ_{DBL} is lower than about 0.4 and 0.5 mm for P1 and P2, respectively, otherwise, both seep habitats become transport limited (Fig. III.8A). According to the LOW, δ_{DBL} of 0.4 and 0.5 mm are achieved at flow conditions of 9 and 8 cm s^{-1} or above. These conditions prevailed for about 44 % of the P1 and 64% of the P2 48-hour-long

deployment. During the remaining time, the maximum *DOU* in both seeps habitats was not maintained despite the fact that geochemical conditions and corresponding consumption processes within the sediment facilitated a relatively constant and high demand for O_2. Thus, it is evident that the maximum and average *DOU* are dependent on hydrodynamics as well as on the patchiness of material turnover in the sediment (Glud et al. 2005; Jørgensen et al. 2005; Glud et al 2009) which, as indicated by this study, can be very high in seep sediments. It is thus critical to fully characterize this variability when assessing *DOU* and geochemical benthic fluxes.

Outlook

The scale at which the microprofiling technique operates (within a range of a few cm on the horizontal scale and few hundred mm on the vertical) makes it a viable tool for sampling the established heterogeneity of cold-seep habitats (e.g., de Beer et al. 2006). However, the representativeness of *DOU* can be strongly influenced by the number of profiles and on the related spatial resolution. This is particularly important when the occurrence of a relatively thin DBL, which minimizes physical transport limitations at the SWI, occurs in a biogeochemically active region of sediment. As shown in Table 1, this study included an unusually large amount of profile data that includes simultaneous O_2 and H_2S profile data. However, the large standard deviation on P2 suggests that the habitat was still slightly undersampled. This is a critical issue and raises further questions about the representativeness of *DOU* studies, which rely on only a few O_2 profiles. Despite inherent statistical uncertainties, this study provides evidence that these seeps systems are highly transient and, in contrast to what it is generally assumed for deep-sea sediments, can become transport-limited. This is well in agreement with the results of previous studies, made ex-situ (Jorgensen and Revsbech 1983) or in lacustrine systems (Bryant et al. 2010a), and highlights the fact that, with increasing geochemical activity, benthic turnover becomes increasingly limited. Transport limitation not only affects benthic material turnover in cold-seep environments but may also have significant influence at organically enriched shelf and upper continental slope environments where oxygen consumption rates via *DOU* are even higher (>10 mmol m^{-2} d^{-1}) than those evaluated by the current study (*see* Wenzhöfer and Glud 2002; Glud 2008).

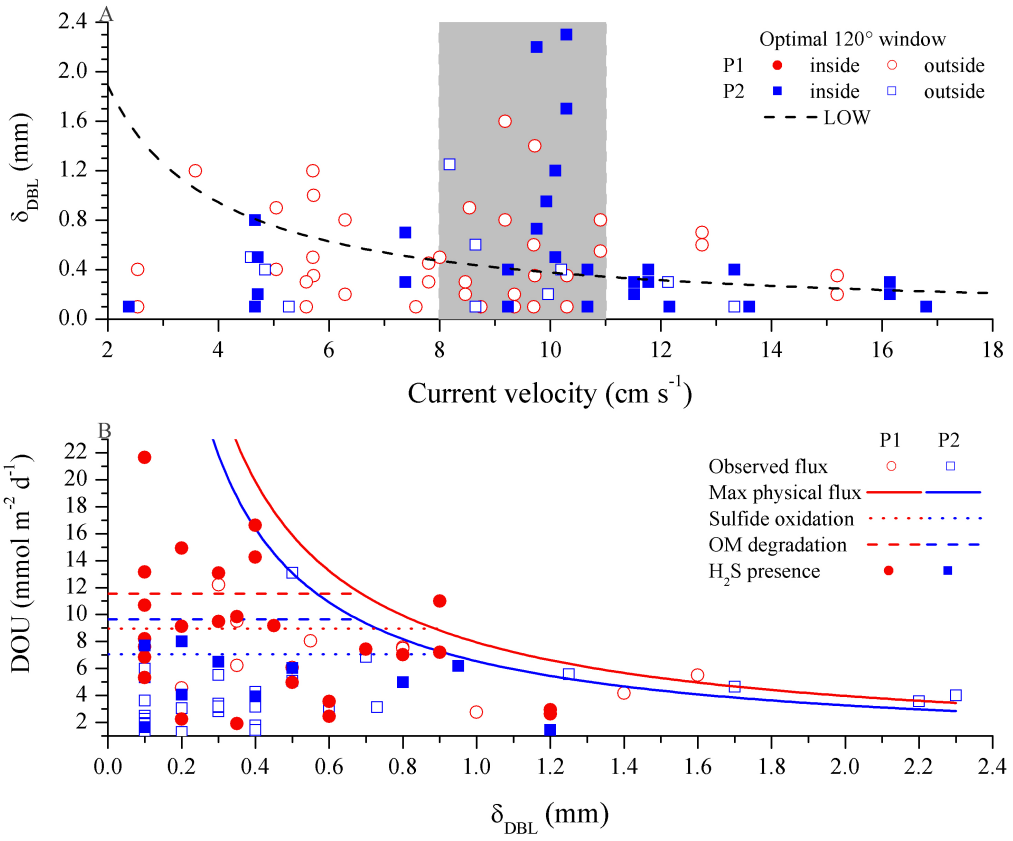

Fig. 8. Correlation plots. (A) δ_{DBL} as a function of near-bottom current for all profiles. The dashed line represents the estimated theoretical δ_{DBL} distribution assuming Law-of-the-Wall (LOW). The shaded area represents the region of mid-range velocity, where the strongest deviation from LOW was observed. (B) O_2 fluxes as a function of measured δ_{DBL}. The solid lines represent the maximum *DOU* distribution assuming a strictly physical system with constant ΔO_2 and δ_{DBL} as sole variable (i.e., maximum ΔO_2 for P1 and P2, respectively). Dotted and dashed lines represent the amount of *DOU* attributed to sulfide oxidation and OM degradation, respectively. Filled circles and squares indicate *DOUs* obtained in the presence of H_2S.

III.5. Acknowledgments

We are thankful to the captain and crewmembers of the R/V Sonne for their outstanding collaboration and support during the survey. We are grateful to Sergiy Cherednichenko and Ralf Schwarz for the technical development and support in deployment of the transecting profiler; further thanks go to the GEOMAR's Technical and Logistics Center for their building the transecting profiler system. Financial support was provided by the Sonderforschungsbereich 754 "Climate – Biogeochemisty in the tropical Ocean" (LR) and by the Cluster of Excellence 80/1 "The Future Ocean" (project 2009/1 CP 0915, LR), both supported by the Deutsche Forschungsgemeinschaft (DFG). The R/V *Sonne* 210 cruise occured within the framework of the Sonderforschungsbereich 574 "Volatiles and Fluids in Subduction Zones".

III.6. References

Antoine, D., J. André, and A. Morel. 1996. Oceanic primary production 2. Estimation at global scale from satellite (coastal zone color scanner) chlorophyll. *Global Biogeochem. Cycles* **10**: 57–69, doi:10.1029/95GB02832

Berg, P., S. Rysgaard, and B. Thamdrup. 2003. Dynamic modeling of early diagenesis and nutrient cycling. A case study in an artic marine sediment. *Am. J. Sci.* **303**: 905–955, doi:10.2475/ ajs.303.10.905

Boetius, A., and F. Wenzhöfer. 2013. Seafloor oxygen consumption fuelled by methane from cold seeps. *Nat. Geosci.* **6**: 725–734, doi:10.1038/NGEO1926

Boetius, A., K. Ravenschlag, C. Schubert, D. Rickert, F. Widdel, A. Gieseke, R. Amann, B. B. Jørgensen, U. Witte, O. Pfannkuche. 2000. A marine microbial consortium apparently mediating anaerobic oxidation of methane. *Nature* **407**: 623–626, doi:10.1038/35036572

Bohlen, L., A. W. Dale, S. Sommer, T. Mosch, C. Hensen, A. Noffke, F. Scholz, and K. Wallmann. 2011. Benthic nitrogen cycling traversing the Peruvian oxygen minimum zone. *Geochim. Cosmochim. Acta* **75**: 6094–6111, doi:10.1016/ j.gca.2011.08.010

Boudreau, B.P. 1997. Diagenetic Models and Their Implementation. Springer, Berlin, 414 p.

Brand, A., C. Dinkel, and B. Wehrli. 2009. Influence of the diffusive boundary layer on solute dynamics in the sediments of a seiche-driven lake: A model study. *J. Geophys. Res.*, [Biogeosci.] **114**: G01010, doi:10.1029/2008JG000755

Broecker, J., and T. H. Peng. 1974. Gas Exchange Rates Between Air and Sea. Tellus 26: 21–35, doi:10.1111/j.2153-3490.1974.tb01948.x

Bryant, L.D., C. Lorrai, D. F. McGinnis, A. Brand, A. Wüest, and J. C. Little. 2010a. Variable sediment oxygen uptake in response to dynamic forcing. *Limnol. Oceanogr.* **55**: 950–964, doi:10.4319/lo.2010.55.2.0950

Bryant, L.D., D. F. McGinnis, C. Lorrai, A. Brand, J. C. Little, and A. Wüest. 2010b. Evaluating oxygen fluxes using microprofiles from both sides of the sediment-water interface. *Limnol. Oceanogr.: Methods* **8**: 610–627, doi:10.4319/lom.2010.8.0610

Canfield, D. E., B. Thamdrup, J. W. Hansen. 1993. The anaerobic degradation of organic matter in Danish coastal sediments: Iron reduction, manganese reduction, and sulfate reduction. *Geochim. Cosmochim. Acta* **57**: 3867–3883, doi: 10.1016/0016-7037(93)90340-3

Cardoso, R. B., R. Sierra-Alvarez, P. Rowlette, E. R. Flores, J. Gómez, and J. A. Field. 2006. Sulfide oxidation under chemolithoautotrophic denitrifying conditions. *Biotechnol. Bioeng.* **95**: 1148–57, doi:10.1002/bit.21084

Dale, A. W., V. J. Bertics, T. Treude, S. Sommer and K. Wallmann. 2013. Modeling benthic–pelagic nutrient exchange processes and porewater distributions in seasonally hypoxic sediment: evidence for massive phosphate release by Beggiatoa? *Biogeosciences* **10**: 629–651, doi:10.5194/bg-10-629-2013

de Beer, D., E. J. Sauter, H. Niemann, N. Kaul, J.-P.Foucher, U. Witte, M. Schlüter, and A. Boetius (2006). In situ fluxes and zonation of microbial activity in surface sediments of the Håkon Mosby Mud Volcano. *Limnol. Oceanogr.* **51**: 1315–1331, doi:10.4319/ lo.2006.51.3.1315

Dunne, J. P., J. L. Sarmiento, and A. Gnanadesikan. 2007. A synthesis of global particle export from the surface ocean and cycling through the ocean interior and on seafloor. *Global Biogeochem. Cycles* **21**: GB4006, doi: 10.1029/2006GB002907.

Emerson, S., and J. I. Hedges. 2004 Sediment Diagenesis and Benthic Flux. p. 293–320. In: K. K. Turekian and H. D. Holland [eds.]. Treatise on Geochemistry, Vol. 6, Elsevier, Amsterdam.

Farías, L., L. A. Cuechas, and M. A. Salamanca. 1996. Effect of coastal upwelling on nitrogen regeneration and ammonium supply to the water column in Concepcion Bay, Chile. *Est. Coast. Shelf Sci.* **43**: 137–155, doi:10.1006/ ecss.1996.0062

Gallardo, V. A., 1977. Large benthic microbial communities in sulphide biota under Peru-Chile Subsurface Countercurrent. *Nature* **268**: 331–332, doi:10.1038/268331a0

Glud, R. N., H. Stahl, P. Berg, F. Wenzhöfer, K. Oguri, and H. Kitazato. 2009. In situ microscale variation in distribution and consumption of O_2: A case study from a deep ocean margin sediment (Sagami Bay, Japan). *Limnol. Oceanogr.* **54**: 1–12, doi: 10.4319/ lo.2009.54.1.0001

Glud, R. N. 2008. Oxygen dynamics of marine sediments. *Mar. Biol. Res.* **4**: 243–289, doi:10.1080/17451000801888726

Glud, R. N., P. Berg, H. Fossing, B. B. Jørgensen. 2007. Effect of the diffusive boundary layer (DBL) on the benthic mineralization and O_2 distribution: a theoretical modelling exercise. *Limnol. Oceanogr.* **52**: 547–557, doi:10.4319/lo.2007.52.2.0547

Glud, R. N., J. K. Gundersen, H. Røy and B. B. Jørgensen. 2003 Seasonal dynamics of benthic O2 uptake in a semienclosed bay: Importance of diffusion and faunal activity. *Limnol. Oceanogr.* **48**: 1265–1276

Glud, R. N., F. Wenzhöfer, A. Tengberg, M. Middelboe, K. Oguri, and H. Kitasato. 2005. Distribution of oxygen in surface sediments from central Sagami Bay, Japan: in situ measurements by microelectrodes and planar optodes. *Deep-Sea Res.*, Part I **52**: 1974–1987, doi:10.1016/j.dsr.2005.05.004

Graco, M., L. Farías, V. Molina, D. Gutiérrez, and L. P. Nielsen. 2001. Massive developments of microbial mats following phytoplankton blooms in a naturally eutrophic bay: Implications for nitrogen cycling. *Limnol. Oceanogr.* **46**: 821–832, doi:10.4319/ lo.2001.46.4.0821

Gundersen, J. K., and B. B. Jørgensen. 1990. Microstructure of diffusive boundary layers and the oxygen uptake of the sea floor. *Nature* **345**: 604–607, doi:10.1038/345604a0

Haeckel, M., I König, V. Riech, M . E. Weber, and E. Suess. 2001. Pore water profiles and numerical modelling of biogeochemical processes in Peru Basin deep-sea sediments. *Deep-Sea Res.* **48**: 3713–3736, doi:10.1016/S0967-0645(01)00064-9

Higashino, M., H. G. Stefan, and C. J. Gantzer. 2003. Periodic diffusional mass transfer near sediment/water interface: Theory. *J. Environ Eng.* **129**: 447–455, doi:10.1061/(Asce)0733-9372(2003)129:5(447)

Imboden, D. M., and A. Wüest. 1995. Mixing mechanisms in lakes. p. 83–138. In: A. Lerman, D. M. Imboden and J. R. Gat [eds.]. Physics and Chemistry of Lakes. Springer-Verlag, Berlin.

Jensen, M. M., M. M. M. Kuypers, G. Lavik, and B. Thamdrup. 2008. Rates and regulation of anaerobic ammonium oxidation and denitrification in the Black Sea. *Limnol. Oceanogr.* **53**: 23-36, doi:10.4319/lo.2008.53.1.0023

Jeroschewski, P., C. Steuckart, and M. Kühl. 1996. An amperometric microsensor for the determination of H_2S in aquatic environments. *Analyt. Chem.* **68**: 4351–4357, doi:10.1021/ac960091b

Jørgensen B. B., R. N. Glud, and O. Holby. 2005. Oxygen distribution and bioirrigation in Arctic fjord sediments (Svalbard, Barents Sea). *Mar. Ecol.: Prog. Ser.* **292**: 85–95, doi:10.3354/meps292085

Jørgensen, B. B., and D. C. Nelson. 2004. Sulfide oxidation in marine sediments: Geochemistry meets microbiology. *Spec. Pap. - Geol. Soc. Am.* **379**: 63–81, doi: 10.1130/0-8137-2379-5.63

Jørgensen, B. B., and D. Des Marais. 1990. The diffusive boundary layer of sediments: oxygen microgradients over a microbial mat. *Limnol. Oceanogr.* **35**: 1343–1355, doi:10.2307/2837444

Jørgensen, B. B., and N. P. Revsbech. 1985. Diffusive boundary layers and the oxygen uptake of sediments and detritus. *Limnol. Oceanogr.* **30**: 111–122, doi:10.4319/lo.1985.30.1.0111

Jørgensen, B. B., and N. P. Revsbech. 1983. Colorless sulfur bacteria, Beggiatoa spp and Thiovulum spp in O_2 and H_2S microgradients. *Appl. Environ. Microbiol.* **45**: 1261–1270.

Judd, A., and M. Hovland. 2007. Seabed fluid flow. The impact on Geology, Biology and the Marine Environment. Cambridge University Press, Cambridge, p. 475

Kelly-Gerreyn, B. A., D. J. Hydes, and J. J. Waniek. 2005. Control of the diffusive boundary layer on benthic fluxes: a model study. *Mar. Ecol.: Prog. Ser.* **292**: 61–74, doi:10.3354/meps292061

Klaucke, I., R. W. Weinrebe, P. Linke, D. Klaeschen, and J. Bialas. 2012. Sidescan sonar imagery of widespread fossil and active cold seeps along the central Chilean continental margin. *Geo-Mar. Lett.* **32**: 489–499, doi:10.1007/s00367-012-0283-1

Lavik, G., T. Stührmann, V.Brüchert, A. Van der Plas, V. Mohrholz, P. Lam, M. Mußmann, B. M. Fuchs, R. Amann, U. Lass, and M. M. M. Kuypers. 2009. Detoxification of sulphidic African shelf waters by blooming chemolithotrophs. *Nature* **457**: 581-584, doi:10.1038/nature07588

Li, Y. H., and S. Gregory. 1974. Diffusion of ions in sea water and in deep-sea sediments. *Geochim. Cosmochim. Acta* **38**: 703–714, doi:10.1016/0016-7037(74)90145-8

Linke, P., [ed.] 2011. Cruise Report SO210 ChiFlux: Identification and investigation of fluid flux, mass wasting and sediments in the forearc of the central Chilean subduction zone, Valparaiso - Valparaiso, 23.09.-01.11.2010 IFM-GEOMAR Report, 44. IFM-GEOMAR, Kiel, 103 p., doi:10.3289/IFM-GEOMAR_Rep_44_2011

Lorke, A., B. Müller, M. Maeki, and A. Wüest. 2003. Breathing sediments: The control of diffusive transport across the sediment–water interface by periodic boundary-layer turbulence. *Limnol. Oceanogr.* **48**: 2077–2085, doi:10.4319/lo.2003.48.6.2077

Millero, F. J., T. Plese, and M. Fernandez. 1988. The dissociation of hydrogen sulfide in seawater. *Limnol. Oceanogr.* **33**: 269–274, doi:10.4319/lo.1988.33.2.0269

Mosch, T., S. Sommer, M. Dengler, A. Noffke, L. Bohlen, O. Pfannkuche, V. Liebetrau, K. Wallmann. 2012. Factors influencing the distribution of epibenthic megafauna across the Peruvian oxygen minimum zone. *Deep-Sea Res.* **68**: 123–135, doi:10.1016/ j.dsr.2012.04.014

Niemann, H., T. Lösekann, D. de Beer, M. Elvert, T. Nadalig, K. Knittel, R. Amann, E. J. Sauter, M. Schlüter, K. Klages, J. P. Foucher, and A. Boetius. 2006. Novel microbial communities of the Haakon Mosby mud volcano and their role as a methane sink. *Nature* **443**: 855–858, doi:10.1038/Nature05227

Pfannkuche, O., and P. Linke. 2003. GEOMAR landers as long-term deep-sea observatories. Sea Technol. 44: 50–55.

Redfield A. C., B. H. Ketchum, and F. A. Richards. 1963. The influence of organisms on the composition of sea water. p. 26–77. *In*: M. N. Hill [ed.]. The sea. Vol II. Interscience Publishers, New York.

Reeburgh, W. S. 2007. Oceanic Methane Biogeochemistry. *Chem. Rev.* **107**: 486–513, doi:10.1021/cr050362v

Revsbech, N. P. 1989. An oxygen microelectrode with a guard cathode. *Limnol. Oceanogr.* **34**: 474–478, doi:10.4319/lo.1989.34.2.0474

Schmaljohann, R., M. Drews, S. Walter, P. Linke, U. von Rad, and J. F. Imhoff. 2001. Oxygen–minimum zone sediments in the northeastern Arabian Sea off Pakistan: a habitat for the bacterium Thioploca, *Mar. Ecol.: Prog. Ser.* **211**: 27–42.

Sommer S., O. Pfannkuche, P. Linke, R. Luff, J. Greinert, M. Drews, S. Gubsch, M. Pieper, M. Poser, and T. Viergutz. 2006. Efficiency of the benthic filter: Biological control of the emission of dissolved methane from sediments containing shallow gas hydrates at Hydrate Ridge. *Global Biogeochemical Cycles* **20**: GB2019, doi:10.1029/2004GB002389

Sommer, S., P. Linke, O. Pfannkuche, H. Niemann, and T. Treude. 2010. Benthic respiration in a seep habitat dominated by dense beds of ampharetid polychaetes at the Hikurangi Margin (New Zealand). *Mar. Geol.* **272**: 223–232, doi:10.1016/j.margeo.2009.06.003

Steinberger, N., and M. Hondzo. 1999. Diffusional mass transfer at sediment–water interface. *J. Environ. Eng.* **125**: 192–200, doi:10.1061/(ASCE)0733-9372(1999)125:2(192))

Suess, E. 1980. Particulate organic carbon flux in the oceans: Surface productivity and oxygen utilization. *Nature* **288**: 260–263, doi:10.1038/288260a0

Suess, E., M. E. Torres, G. Bohrmann, R. W. Collier, J. Greinert, P. Linke, G. Rehder, A. Trehu, K. Wallmann, G. Winckler, and E. Zuleger. 2001. Gas hydrate destabilization: enhanced dewatering, benthic material turnover and large methane plumes at the Cascadia convergent margin. *Earth Planet Sci. Lett.* **170**: 1–15, doi:10.1016/S0012-821X(99)00092-8

Van Cappellen, P., and Y. Wang. 1996. Cycling of iron and manganese in surface sediments: A general theory for the coupled transport and reaction of carbon, oxygen, nitrogen, sulfur, iron, and manganese. *Am. J. Sci.* **296**: 197–243, doi:10.2475/ajs.296.3.197

Wang, J., H. Wei, Y. Lu, and L. Zhao. 2013. Diffusive boundary layer influenced by bottom boundary hydrodynamics in tidal flows. *J. Geophys. Res.* **118**: 1-12, doi:10.1002/2013JC008900

Wenzhöfer, F., and R. N. Glud. 2002. Benthic carbon mineralization in the Atlantic: a synthesis based on in situ data from the last decade. *Deep-Sea Res.* **49**: 1255–1279

IV. Chapter

Fine-structure oxygen measurements on microstructure CTD profilers: first field results from the Chilean margin

Lorenzo Rovelli, [a] Daniel F. McGinnis, [a] Marcus Dengler, [a] and Peter Linke [a]

[a] Helmholtz Centre for Ocean Research Kiel, GEOMAR, Kiel, Germany
[b] University of Southern Denmark, Institute of Biology, Nordic Center for Earth Evolution (NordCEE), 5320 Odense M, Denmark

To be submitted to the *Journal of Atmospheric and Oceanic Technology*

Abstract

A fast-response, pressure compensated Clark type aperometric oxygen (O_2) microsensor system was custom designed and mounted on a microstructure profiler to enable undisturbed O_2 fine-structure measurements in the water column. While other commercially available systems have a similar response time (0.5 s or faster), this system has a much higher depth rating and it is thus more suitable for oceanic applications. The system was tested at a 700 m depth study site at the Chilean continental margin, where 6 profiles up to 480 m depth were collected. Above the O_2 minimum, O_2 gradients of ~5 μmol kg^{-1} m^{-1} were measured, which were two times higher than those reported by standard sensors for the same oxycline. Most striking was the detection of O_2 step-like structures in the deeper water column, between 360 m and 420 m depth, where double diffusion (finger regime) was found to occur. The sensor thus proved to be fast and accurate enough to detect double diffusion driven O_2 structures that would have been missed by other O_2 sensors. The sensor appears robust, with over 180 profiles (from this and other studies) obtained with a single sensor. The depth rating and measurement performance clearly show that such a system has several potential applications, especially in O_2 minimum zones and will lead better understanding of O_2 dynamics and budgets in the water column.

IV. 1. Introduction

Oxygen (O_2) measurements with Clark type aperometric microsensors are established oceanographic tools (Taillefert et al. 2000; Prien 2007). These microsensors, based on the design of Baumgärtl and Lübbers (1973) with a guard cathode (Revsbech 1989) are routinely used in benthic studies to assess O_2 concentrations in porewater or O_2 fluxes at the sediment water-interface via benthic chambers (Glud et al. 1999), microprofiles into the sediment (Grundersen and Jorgensen 1990, Jorgensen and Des Marais 1990) or recently, with the eddy correlation technique (EC; Berg et al. 2003, McGinnis et al. 2008, Lorrai et al. 2010).

O_2 microsensor applications for water column measurements, however, are scarce. The first attempts were carried out by Atkinson (1988) on an estuary using a free-falling conductivity-temperature-depth (CTD) device. Still, the first water column profiles with Clark type O_2 microsensors following the Revsbech (1989) design were provided by Oldham (1994). In order to fit on their microstructure CTD, the sensors and electronics had to be slightly modified. The system was then used to study O_2 patchiness in lakes (Oldham and Imberger 1995). Both studies, however, focused only on shallow sites (up to ~16 m depth) and mainly on fresh waters. To the author's knowledge, no further studies utilizing fast membrane Clark type O_2 microsensors for high-resolution water column profiling have been published.

Among the reasons for the limited amount of studies are the strong pressure and temperature dependencies, slow response times, difficult field calibration, sensor drift (Carlson 2002) as well handling issues due to the sensors fragility. As the presence of a membrane was found to be the main contributor to pressure effects, to O_2 hysteresis (i.e., substantial disagreements between downcast and upcast readings) and to slow response time, sensor development was focused on membrane-free microelectrodes (Sosna et al. 2007; Sosna et al. 2008). Those sensors did provide very encouraging results even at the notable depth of ~3500 m (Sosna et al. 2008), but they are currently much more voluminous that the Clark type microsensors system used for EC (*see* Lorrai et al. 2010), and thus not suitable for microstructure profilers.

While the sturdiness of the glass body construction of the Clark type microsensors might still be an unresolved issue for more demanding applications, improvements in the sensor assembly has

made them very fast (90% response time up to 0.2 s) and more stable in terms of signal drift. Furthermore, in contrast to other commercially available fast O_2 sensors such as the shallow water AMT galvanic sensor (up to a 100 m; AMT Analysenmeßtechnik, Rostock, Germany), pressure compensated Clark type microsensors were successfully used in deep-sea deployments (Berg et al. 2009).

To fill this equipment gap for O_2 fine scale oceanographic measurements, we develop a fast pressure compensated Clark type O_2 microsensor system to be installed on a MSS microstructure profilers (Sea & Sun Technology, Trappenkamp, Germany), the idea of which is to both 1) resolve the fine scale oxygen structure while 2) simultaneously resolving turbulence, density and hence, diffusivity. Below, we describe the prototype field tests at the Chilean continental margin with the goal of assessing its ability to well-resolved oxygen gradients and O_2 fine-structures at the cm scale.

IV. 2. Methods

Study site

The fast O_2 microsensor system performance was evaluated during the R/V *Sonne* 210 cruise at the central Chilean seduction zone (23 September to 1 November 2010). The Chilean location (36°28.2 S, 73°44.7 W) offered an optimal testing site for our fast O_2 system due to the presence of large oxyclines below and above the O_2 minimum and relatively deep waters (up to 700 m).

Instrumental setup

Background measurements: Water column background data were collected with a ship-based conductivity-temperature-depth (CTD) system (SBE9plus CTD, Seabird, Washington, United States) equipped with a 24-bottle rosette. The CTD was deployed right before or after the MSS casts, and discrete water samples from the Niskin bottles were collected at specific depths and used to calibrate the O_2 sensor measurements via Winkler titrations.

Microstructure profiler: For this study we used a loosely-tethered MSS90-L multi-parameter profiler sampling at 1024 Hz over 16 channels. The profiler was equipped with 2x shear probes,

1x FP07 temperature sensor, 1x accelerometer, standard CTD sensors and an Oxyguard membrane O_2 sensor. One channel and a sensor slot were left unused to mount the custom designed fast O_2 system. The MSS is designed as a free-falling profiler to decouple the instrument from surface (wave) and ship motions. The profiler decends at 0.5 – 0.6 m/s, and besides high resolution CTD, also resolves water column turbulence (*see* Lueck et al. 2002).

Fast O_2 microsensor system

The O_2 microelectrode system (Fig. IV.1) consists of a pressure compensated in-situ connector system, a custom made stainless steel amplifier housing compatible with the MSS mounting ring, a custom-made amplifier and O_2 microsensor (0.3–0.5 s response time). The in-situ connector system is manufactured by Unisense (Unisense A/S, Aarhus, Denmark) and consists of a stainless steel sleeve and bulkhead, both rated for 6000 m depth.

The customized amplifier housing was built at GEOMAR's technical facility to fit into the MSS sensor-mounting ring and interface with the internal electronics (Fig. IV.1); the housing length was kept short to provide both enough space for the amplifier board and limit the system overall length. Without the sensor, the system is 17.5 cm long and thus standard size O_2 microsensors, which are typically 15–18 cm in length, would result in the overall length substantially exceeding that of shear sensors, thus risking contamination of their readings. To avoid that, A. Glud (University of Southern Denmark, Odense, Denmark) provided custom-built 6–7 cm long O_2 microsensors. Those sensors have the same performance as the longer versions but are slightly more robust, i.e. they have a bulkier rather than elongated design while still having the same response time.

The amplifier embeds a trimmer potentiometer to adjust the voltage output range of each sensor (from -2.5V to theoretically +5V) to the ±3V input channel range requirements of the MSS profiler. Furthermore, when the profiler is powered up, the amplifier provides the required polarization current (-0.78 V; Revsbech 1989) to keep the sensor operational. For this reason, however, the profiler has to be powered all the time to avoid gaps in the polarization and signal quality loss.

Fig. IV.1. The fast O_2 microsensor system. (A) The main system components: the amplifier housing (top), the in-situ connector system with pressure compensation and the O_2 Clark type microsensor (bottom). (B) Close-up of the MSS system microstructure profiler with mounted the fast O_2 microsensor system and other sensors (described below) prior to deployment.

Fast O_2 microsensors data processing

Once the sensor is mounted to the in-situ connector, the fast O_2 system is essentially "plug-and-play" and only requires a free MSS channel to be operational; the data processing, however, requires several steps. The data processing mainly relies on the Microstructure Toolbox (MSTB, ISW Wassermesstechnik, Fünfseen, Germany) for the initial pressure sensor despiking and filtering (0.5 second running average) that removes pressure spikes to the overall signal disturbances for each MSS channel. The rest of the data processing is carried out by a self-written Matlab routine.

In the Matlab routine the raw O_2 data, which were converted from voltage to counts by the MSS 16-bit analog-to-digital conversion, are firstly despiked using the Despiking Toolbox of Mori et al. (2007). The Toolbox uses a modified 3D phase space method (Goring and Nikora 2002), which is based on a 3D Poincaré map in which the data variable, its first and second derivatives are plotted against each other. The data located outside of the ellipsoid in the Poincaré map are flagged as spikes; the process is repeated until no additional spikes are detected (Mori et al. 2007). The flagged data are successively replaced using a linear interpolation. Although it was mainly designed to despike acoustic Doppler velociments (ADV), it was found to be effective for our O_2 datasets as well.

The despiked data are then converted to O_2 concentration in % saturation based on Winkler corrected MSS-mounted Oxyguard data or ship CTD oxygen measurements (if applicable) assuming a linear relationship. As the Oxyguard sensor is mounted lower than our fast O_2 system (Fig. IV.1) and has a much slower response time (~10 seconds depending on the temperature), the Oxyguard readings are aligned to the fast O_2 sensor taking both response time and sensor placement driven time lag into account. Furthermore, given the 0.5 – 0.6 m s^{-1} falling speed of the MSS profiler and the Oxyguard response time, only sections with relatively constant O_2 concentrations over several meters (such as SBL, O_2 minima and BBL) were considered for calibration values. The final step of the routine calculates the O_2 saturation concentrations (in μmol kg^{-1}) at each depth from the calibrated fast temperature and salinity based on the Garcia and Gordon (1992) equations and the absolute O_2 concentrations. Based on the dataset, a running average over a 0.25–0.5 s window size (256–512 samples at the standard MSS sampling rate) or a Butterworth low-pass filter may be required to reduce the signal noise while still keeping the sensor resolution intact.

Data quality control

A quality control on the O_2 concentration profiles was also performed. This includes a preliminary response time test, spectral analysis to verify the actual sensor and amplifier cutoff frequency and response time as well as point-to-point noise analysis. The preliminary response time test is performed by considering the time the microsensor need to adjust the reading from air to water, when immerging the sensor into anoxic (nitrogen bubbled) water. The spectral

analysis relies on the power spectral density of the O_2 concentration profiles at their full resolution (1024 Hz). The point-to-point noise analysis relies on the frequency count of the concentration difference between consecutive data points of the high resolution O_2 profile that then displayed graphical via a histogram plot; for practical reason the plot is normalized dividing the frequency count by its maximum value. Such a plot is expected to display a Gaussian distribution. Deviations from that distribution are usually the result of noise caused by electrical interference, which is more evident when using Clark type microsensors in the lab.

IV. 3. Results

A total of 6 profiles were taken over two days 6th October (cast 1–2) 2010, 7th October (cast 3–6) during the R/V Sonne cruise in 2010. Emphasis was given to the depth rating assessment and capability to resolve O_2 fine structure at the cm scales. As the MSS winch contained only around 600 m cable, the maximum deployment depth was ~480 m (due to ship drift); the average depth of the study site was ~700 m.

The MSS profiler was powered most of the time to keep the O_2 microsensor polarized; the only power gaps were due to the MSS profiler being moved from the lab to the work deck a couple of hours before its deployment. As a result, no polarization driven sensor drift was detected. As one of the main aims of the field test was to resolve the O_2 minimum region, the amplification range was at first (casts 1–2) tuned to the lower concentration range and thus the upper 70 m of the water column were out of the MSS channel range (65536 counts, i.e., raw voltage above 3 V); the amplification range was subsequently increased and for the remaining casts and only the first 20 m were out of range

Fig. IV.2 shows an overview of the O_2 measurements for each cast, together with temperature from the calibrated fast temperature sensor and salinity. Most apparent is the large hypoxic region located between ~150–250 m depth. The O_2 concentration within that region was ~20 μmol kg^{-1}, which corresponded to a saturation level of ~7 %. Sharp oxyclines were detected above that region, at 120 – 140 m depth depending on the profile. In addition, all profiles indicated that the fast O_2 sensor was able to resolve fine structures.

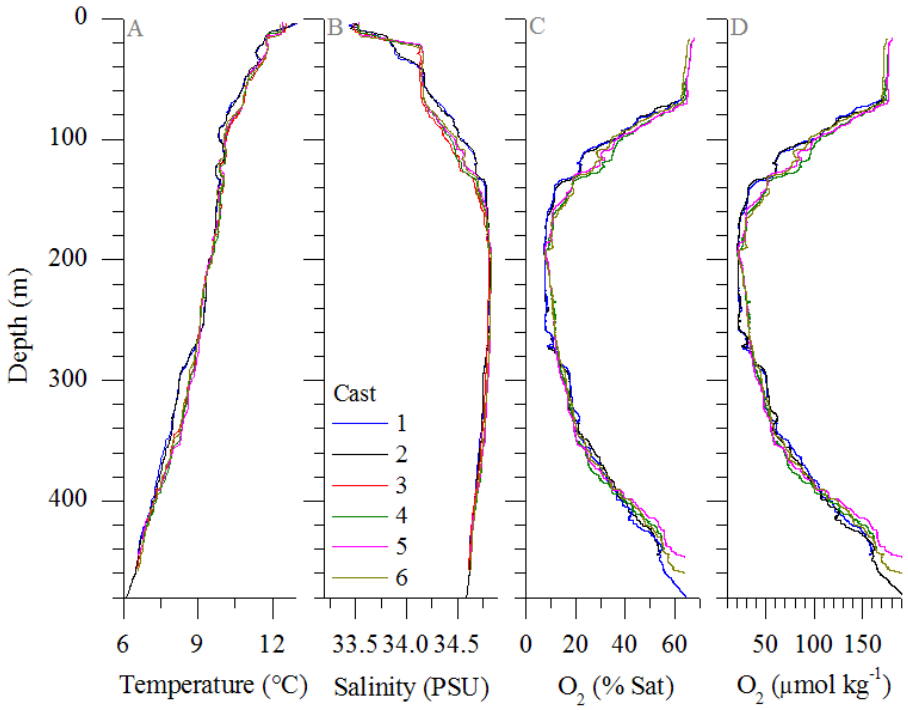

Fig. IV.2. Water column profiles. (A) High resolution temperature profiles. (B) Salinity. (C) O_2 in % saturation and Winkler corrected absolute concentration (D). Note that O_2 readings that were out of the MSS range (signal >3 V) are not shown.

To provide more insight into the O_2 sensor capability and to rule out artifacts in the sensor reading, such as electric noise, cast 5 was selected for a closer look at the O_2 depleted region and the fine structure detected in the deeper parts of the water column (Fig. IV.3). The O_2 profile from the Oxyguard O_2 sensor, which is of course much slower but nevertheless robust and less subject to short term drift (hours to few days) and temperature effects, was also considered to better highlight the advantages of the fast system. To account for the different response times, the Oxyguard readings were shifted ~4 m in order to align with those of the fast O_2 sensor. The fast O_2 sensor shows a much sharper oxycline with gradients of up to 5.1 µmol kg^{-1} m^{-1}, which are a two times higher than those of the Oxyguard sensor (2.4 µmol kg^{-1} m^{-1}). Furthermore, below the O_2 depleted region, the O_2 data showed evidence of several fine structures, most prominent between 350 – 420 m depth. As Fig. IV.3 shows, these structures are step-like and resemble those seen in temperature and salinity profiles in double diffusive systems. In this regard, Fig. IV.2 does show that deeper regions of the water column were characterized by both decreasing temperature and decreasing salinity suggesting a temperature stabilized and salinity destabilized system, which could support double diffusion (finger regime; *see* Turner 1967).

Indeed, step-like structures were clearly identified in both temperature and salinity profiles, especially between 350 – 420 m depth (Fig. IV.3B); furthermore, the temperature and salinity changes reported within that depth zone fall in the double diffusive range (data not shown). As the depths of the 1 – 2 m thick O_2 concentration steps were found to coincide with those of the temperature and salinity profiles, there is enough evidence to suggest that the O_2 sensors report the same double diffusive signal. Temperature dependencies of the O_2 microsensor, which can account for ~2–3% of the microsensor signal per °C (Gundersen et al. 1998) were found to be of marginal relevance given the reduced temperature difference (~0.1 °C) and large O_2 concentration changes (~10 µmol kg^{-1}) between the steps.

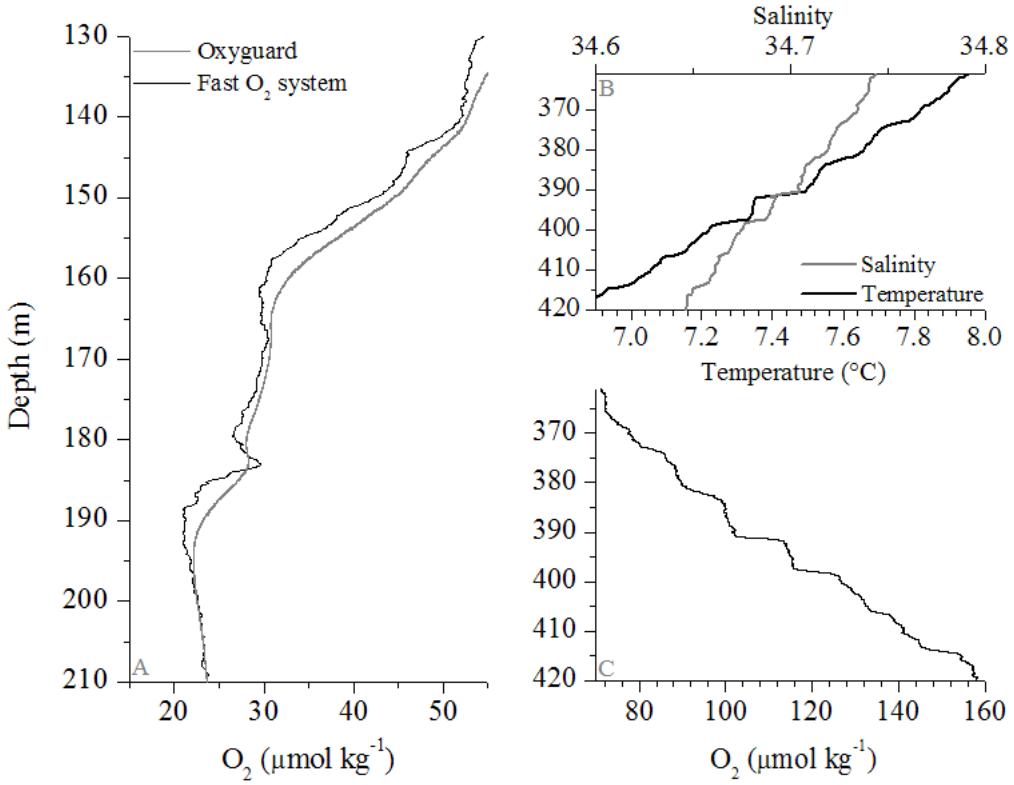

Fig. IV.3. Selected regions of the O_2 profile from cast 5. (A) Profile region near the O_2 minimum depth range with under-layered Oxyguard readings. Note that the Oxyguard data were aligned to the fast O_2 readings shifting the dataset by 4 m. (B, C) Close-up of the step-like structures on detected below the O_2 minimum region and attributed to double diffusion (finger regime).

The detection of water column O_2 fine structure is obviously linked to the response time of the microsensor system as well as from its noise level. At the MSS profiling speed and sampling rate (0.5 – 0.6 m s^{-1} and 1024 Hz, respectively) and a 0.2 second response time Clark microsensor

should be able to provide a ~10 cm resolution. The preliminary response time test performed on deck prior to the deployment suggested a 90% response time of ~0.4 seconds. As the system electronics does not contain a filter, the signal cutoff frequency is given by the response time of the amplifier, which was estimated from the power spectral density analysis to be ~5 × 10^{-3} seconds (Fig IV.4A). The spectra revealed that most of the signal strength was below 2 Hz, thus suggesting that the actual system response time (amplifier + microsensor) was ~0.5 seconds allowing a resolution of ~25 cm. With regard to noise level, the system benefits from the MSS grounding and fast sampling rate. The normalized frequency counts histogram (Fig IV.4B) showed no evidence of electrical interference and point-to-point noise was strongly reduced (± 0.04 µmol kg^{-1}).

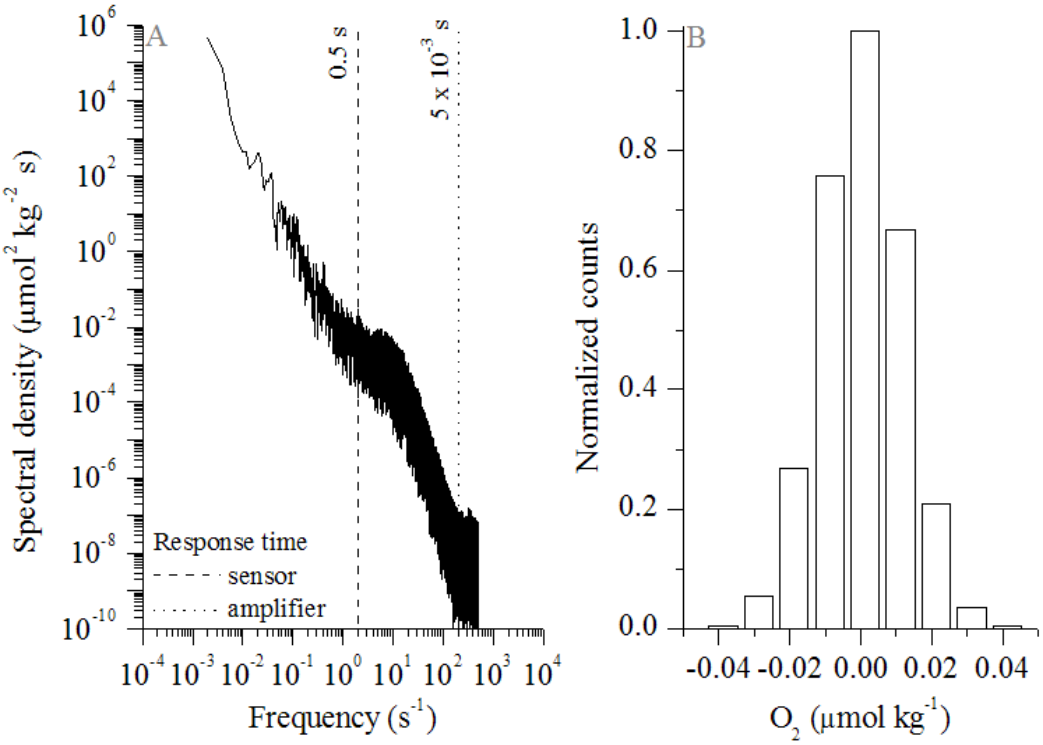

Fig. IV.4. O_2 spectra and noise analysis for cast 5. (A) Power spectral density of the high resolution O_2 profile. (B) Point-to-point noise histogram based on the normalized frequency count of concentration changes between consecutive data points of the O_2 profiles.

IV.4. Discussion

The fast O_2 system performed well within the almost 500 m depth range of this study and showed very encouraging results. Besides the evident advantage of being able to provide better-resolved O_2 gradients for further O_2 flux estimations, the system also provides a better insight into the O_2 dynamics revealing O_2 fine structures that cannot be detected by standard O_2 measurements. With this regard, to detection of previously overlooked step-like O_2 changes in the O_2 concentration associated with a double diffusive regime clearly highlight the system scientific potential. As double diffusion can, depending on the study site characteristics, become a significant source of vertical mixing, the system might become a valid tool to better understand O_2 transport in such particular environments as well.

In addition, due to its reduced size, fast readings and depth rating, the system can be implemented in larger measurements devices such as CTDs or benthic landers. The amplifier used in this study is also suitable for hydrogen sulphide (H_2S) microsensors, which are based on a similar measuring principle but require a different polarization (+0.08 V; Kuhl et al. 1998); only minor adjustments to the amplifier board would be required. The H_2S microsensors, however, would have to be manufactured in a length suitable for the profiler (~7 cm).

With the improvements to the Clark type microsensors manufacturing both in terms of robustness and with regard to pressure compensation, the microsensors are not necessarily more fragile than other microstructure sensors such as the FP07 temperature sensor or the AMT O_2 sensor; with 180 profiles performed (from this and other studies) with the same microsensor. Together with other microstructure sensor such as the one listed above, the fast O_2 system shares, however, the same issues with regard to long-term stability and absolute accuracy. While during the rather short measuring time of this study, no evidence of significant signal drift was detected on the fast O_2 system, the stability of the sensor on longer time frames and the consequent absolute accuracy might become an issue and should be therefore addressed with specific experimental setups in future studies. However, the main purpose of our O_2 system is resolving local concentration gradients as well as the fine structure. With this regard the system proposed here is not a replacement for standard CTD O_2 measurements or Winkler titrations on discrete

water samples, but a valuable addition. For instance, in several aquatic environment, such as seasonally stratified shelf shear, the extent of the oxyclines is limited to few meters which cannot generally be properly sampled, either with standard ship operated CTD system and discrete sampling, or with standard O_2 system on a microstructure profiler. Thus, until other systems such as the fast micro-optodes currently under development (Chipman et al. 2012; Klimant et al. 1999) will evolved enough to be customarily deployed on a microstructure profiler, Clark type microsensors based system still represent the most valid alternative for water column high resolution O_2 profiling, with the potential of making O_2 fine scale measurements a routine procedure.

IV.5. Acknowledgments

We are thankful to the captain and crew members of the R/V Sonne for their outstanding collaboration and support during the survey. We are grateful to Sergiy Cherednichenko for the technical development and support in deployment of the fast O_2 system; further thanks go to the GEOMAR's Technical and Logistics Center for their building the amplifier housings. Financial support was provided by the Sonderforschungsbereich 754 "Climate - Biogeochemisty in the tropical Ocean" (LR) and by the Cluster of Excellence 80/1 "The Future Ocean" (project 2009/1 CP 0915, LR), both supported by the Deutsche Forschungsgemeinschaft (DFG). The R/V *Sonne* 210 cruise occured within the framework of the Sonderforschungsbereich 574 "Volatiles and Fluids in Subduction Zones".

IV.6. References

Atkinson, M. J. 1988. Fast-response oxygen sensor for a free-fall CTD. *Limnol. Oceanogr.* **33:** 141–145.

Baumgärtl, H., and D. W. Lübbers. 1973. Platimun needle electrodes for polarographic measurements of oxygen and hydrogen, p.130–136. *In*: M. Kessler [ed.], Oxygen supply. Urban and Schwarzenberg.

Berg, P., H. Roy, F. Janssen, V. Meyer, B. B. Jorgensen, M. Huettel and D. de Beer. 2003. Oxygen uptake by aquatic sediments measured with a novel non-invasive eddy-correlation technique. *Mar. Ecol.: Prog. Ser.* **261**: 75–83, doi:10.3354/meps261075.

Berg, P., R. N. Glud, A. Hume, H. Stahl, K. Oguri, V. Meyer and H. Kitazato. 2009. Eddy correlation measurements of oxygen uptake in deep ocean sediments. *Limnol. Oceanogr.: Methods* **7**: 576–584, doi:10.4319/lom.2009.7.576

Carlson, J. 2002. Development of an optimized dissolved oxygen sensor for oceanographic profiling. *Int. Ocean Syst.* **6**: 20–21.

Chipman, L., M. Huettel, P. Berg, V. Meyer, I. Klimant, R. Glud, and F. Wenzhoefer. 2012. Oxygen optodes as fast sensors for eddy correlation measurements in aquatic systems. *Limnol. Oceanogr.: Methods* **10**: 304–316, doi:10.4319/lom.2012.10.304

Garcìa, H. E. and L. I. Gordon. 1992. Oxygen solubility in seawater: Better fitting equations. *Limnol. Oceanogr*. **37**: 1307–1312, doi:10.4319/lo.1992.37.6.1307

Glud, R. N, J. K. Gundersen, and O. Holby. 1999. Benthic in situ respiration in the upwelling area off central Chile. *Mar Ecol Prog Ser.* **186**: 9–18, doi: 10.3354/meps186009

Goring, D. G., and V. I. Nikora. 2002. Despiking Acoustic Doppler Velocimeter Data. *J. Hydraul. Eng.* **128**: 117–126, doi:10.1061/(ASCE)0733-9429(2002)128:1(117)

Gundersen, J. K., and B. B. Jorgensen. 1990. Microstructure of diffusive boundary-layers and the oxygen-uptake of the sea-floor. *Nature* **345**: 604-607, doi:10.1038/345604a0

Gundersen, J. K., N. B. Ramsing, and R. N. Glud. 1998. Predicting the signal of O_2 microsensors from physical dimensions, temperature, salinity, and O_2 concentration. *Limnol. Oceanogr.* **43**: 1932–1937.

Jørgensen, B. B., and D. Des Marais. 1990. The diffusive boundary layer of sediments: oxygen microgradients over a microbial mat. *Limnol. Oceanogr.* **35**: 1343–1355, doi:10.2307/2837444

Klimant, I., F. Ruckruh, G. Liebsch, A. Stangelmayer, and O. S. Wolfbeis. 1999. Fast Response Oxygen Micro-Optodes Based on Novel Soluble Ormosil Glasses. *Mikrochim. Acta* **131**: 35–46, doi:10.1007/s006040050007

Kuhl, M., C. Steuckart, G. Eickert, and P. Jeroschewski. 1998. A H2S microsensor for profiling biofilms and sediments: application in an acidic lake sediment. *Aquat. Microb. Ecol.* **15**: 201-209, doi:10.3354/ame015201

Lorrai, C., D. F. McGinnis, P. Berg, A. Brand and A. Wuest. 2010. Application of Oxygen Eddy Correlation in Aquatic Systems. *J. Atmos. Oceanic Technol.* **27**: 1533–1546, doi: 10.1175/2010JTECHO723.1.

Lueck, R. G., F. Wolk, and H. Yamazaki. 2002. Oceanic velocity microstructure measurements in the 20th century. *J. Oceanogr.* **58**: 153–174, doi:10.1023/A:1015837020019

McGinnis, D. F., P. Berg, A. Brand, C. Lorrai, T. J. Edmonds, and A. Wüest. 2008. Measurements of eddy correlation oxygen fluxes in shallow freshwaters: Towards routine applications and analysis. *Geophys. Res. Lett.* **35**: L04403, doi:10.1029/ 2007GL032747

Mori, N., T. Suzuki and S. Kakuno. 2007. Noise of acoustic Doppler velocimeter data in bubbly flow. *J. Eng. Mech.* **133**: 122–125, doi:10.1061/(ASCE)0733-9399(2007)133:1(122)

Oldham, C. 1994. A fast-response oxygen sensor for use on fine-scale and microstructure CTD profilers. *Limnol. Oceanogr.* **39**: 1959–1966, doi:10.4319/lo.1994.39.8.1959

Oldham, C. and J. Imberger. 1995. Oxygen patchiness in a lake. *Aquat. Sci.* **57**: 325–337, doi:10.1007/Bf00878396

Prien, R. D. 2007. The future of chemical in situ sensors. *Mar. Chem.* **107**: 422–432, doi:10.1016/j.marchem.2007.01.014

Revsbech, N. P. 1989. An oxygen microsensor with a guard cathode. *Limnol. Oceanogr.* **34**: 474–478.

Sosna, M., G. Denuault, R. W. Pascal, R. D. Prien and M. Mowlem. 2007. Development of a reliable microelectrode dissolved oxygen sensor. *Sens. Actuators, B.* **123:** 344–351, doi:10.1016/j.snb.2006.08.033

Sosna, M., G. Denuault, R. W. Pascal, R. D. Prien and M. Mowlem. 2008. Field assessment of a new membrane-free microelectrode dissolved oxygen sensor for water column profiling. *Limnol. Oceanogr.: Methods* **6**: 180–189, doi: 10.4319/lom.2008.6.180

Taillefert, M., G. W. Luther and D. B. Nuzzio. 2000. The application of electrochemical tools for in situ measurements in aquatic systems. *Electroanalysis* **12**: 401–412, doi: 10.1002/(SICI)1521-4109(20000401)12:6<401::AID-ELAN401>3.0.CO;2-L

Turner, J. S. 1967. Salt fingers across a density interface. *Deep Sea Res.* **14**: 599–611, doi:10.1016/0011-7471(67)90066-6.

V. Chapter

Summary and Outlook

V.I. Summary

This work presents, based on a continental margin and a shelf sea study site, an interdisciplinary approach on investigating O_2 dynamics. These studies considered both physical and biogechemical processes directly or indirectly related with O_2 transport in the water column, the benthic regions and across the SWI.

The O_2 dynamics in the thermocline and BBL of seasonally stratified seas during the summer stratification were investigated in the central North Sea (Tomeliten site) using high resolution current measurements and turbulence microstructure profiling with concurrent O_2 fine-scale measurements. The results showed the occurrence of a second mode near-inertial wave that was superposed to the dominant semi-diurnal tide, as well as two 2 – 3 m thick regions of elevated near-inertial vertical shear and strong stratification at the upper and lower limit of the interior boundary, respectively. The turbulent dissipation rate in those regions was a factor ten higher than in the central interior (10^{-9} W kg^{-1}). A shear spike mechanism (*see* Burchard and Rippeth 2009) was identified as possible process driving the observed increased turbulence at those limits. In contrast to previous North Sea studies, which reported a two-layer system, the water column during the observational period clearly showed a four-layer system. Such a system thus would require a slightly different approach than reported by those studies. In addition, the fast galvanic O_2 sensor revealed a very sharp oxycline in the lower thermocline (up to 34 µmol kg^{-1} m^{-1}) from which a significant source of O_2 replenishing the BBL water was identified; the O_2 fluxes toward the BBL were on average 54 mmol m^{-2} d^{-1} ranging from 9 to 134 mmol m^{-2} d^{-1}. This substantial additional source of O_2 to the BBL has previously been overlooked and not accounted for when estimating the bottom water carbon remeneralisation, which is routinely inferred assuming a 1:1 ratio with the apparent BBL O_2 concentrating loss. It was thus hypothesitzed that the carbon turnover is actually larger that previously accounted.

Despite the excellent results provided by the galvanic O_2 sensor on the Tommeliten study, the deep rating is limitating (100m). These shallow water sensors are therefore not useful for oceanic applications where profiling over several 100s of meters is required. To fill that instrumentation gap, a deep-sea rated fast Clark type O_2 microsensor system (0.5 s response time) was developed

to be mounted on microstructure profilers. The first field measurements at the Chilean continental margin, where the system was tested up to 480 m depth, were very encouraging. The system resolved oxyclines, whose O_2 gradients (~5 mmol kg^{-1} m^{-1}) were found to be around a factor 2 higher than reported by standard O_2 sensors. Furthermore the system revealed step-like O_2 fine-structures occurring at depths between 360 to 420 m. These few meters thick steps were concurrent with those in the temperature and salinity profiles that were attributed to double diffusion (finger regime). As the temperature difference at the steps interfaces was limited to 0.1 °C, temperature dependencies of the microsensor were negligible thus suggesting that the fast O_2 system was fast and accurate enough to detect step-like O_2 changes associated with double diffusive regimes at the Chilean continental margin.

The Chilean continental margin was also investigated in terms of the interplay between sediment activity and hydrodynamic forcing on the benthic O_2 dynamics and on O_2 flux specifically. O_2 and H_2S fluxes were collected in habitats of the Concepción Methane Seep Area (CMSA) via microprofiling using the GEOMAR designed in-situ transecting profiler. The aim of the study was to disentangle the O_2 flux contributions of hydrodynamics, i.e., DBL variability, from sediment processes, i.e., organic matter degradation and reoxidation of reduced compounds. For that, ~40-cm-long transects were performed in a sulfidic sediment with frequent bacterial mat occurrence and on a less sulfidic sediment where bacterial mat coverage was reduced and limited to the last section of the transect. The habitats were characterized by comparable physical settings and similar near-bottom current flow (2.5 – 18.3 cm s^{-1}). *DOUs* were on average about a factor two higher (7.9 mmol m^{-2} d^{-1}) in the more sulfidic habitat than in the less sulfidic one, although H_2S fluxes were of equal magnitude (~0.4 mmol m^{-2} d^{-1}). At the more sulfidic habitat, sulfide oxidation and organic matter degradation were estimated to account for 65% of the *DOU* whereas aerobic methane oxidation, reoxidation of other reduced compounds, infauna respiration and small-scale topography were inferered to cover the remaining O_2 uptake. The O_2 transport across the SWI in the more sulfidic habitat was found to be more prone to become DBL limited. These findings provided supporting evidence of transport limitation in the studied seeps habitats and, by extention, the probable occurrence of transport limited conditions in other highly active benthic system such as those along organically enriched continental margins and shelf.

While the result presented within the framework of this thesis offer both new tools and different approaches to aquatic system characterization in regard to O_2 dynamics, much still needs to done. In particular, the integration and interplay of benthic and water column studies, which was often overlooked in the past, need to be more emphasized on future investigations.

V.II. Outlook

With the importance of O_2 dynamics for the ecosystem functioning (e.g., Glud 2008) and water quality, concerns about the spreading of hypoxia (Diaz 2001) and evidence of expanding oceanic O_2 minimum zones (Stramma et al. 2008), as well as the results presented within the framework of this thesis clearly highlight the need for more extensive interdisciplinary studies which include 1) high-resolution, fine-structure, constituent measurements, 2) comprehensive investigation of the physical processes modulating the constituent distribution as well as 3) biogeochemical process assessment with regard to constituent source and sinks.

In this regard the results of the interdisciplinary study presented on Chapter II, the suggested enhanced BBL O_2 replenishment has strong implication for the carbon turnover, and thus having the potential to advance the understanding of the North Sea system. However, much still needs to be done to verify how often the reported enhanced BBL O_2 replenishment is actually occurring during stratification, and thus to quantify its relevance for the O_2 and carbon budget at the seasonal time scale. For this, however, beside frequent measurement campaigns, monitoring studies relying on moored instruments will be required. In particular, emphasis should be given to the seasonal variability of the processes modulating the reported enhanced O_2 fluxes, in particular the occurrence of near-inertial waves and shear spikes production which would also imply adapting the model of Burchard and Rippeth (2009) to a three-layer of even four-layer system. Given the implication of nutrients transport to the DCM region for the sustainment of the thermocline O_2 maxima, future emphasis should also be given in refining the resolution of nitrate and phosphate measurements as the associated concentration gradients can be limited to few meters and thus difficult to resolve or to estimate, as deviation from the Redfield ratio are often reported (e.g., Geider and La Roche 2002). The study also revealed the importance of using high-resolution O_2 measurements to resolve the oxycline as standard sensors were found to be inadequate for flux estimations. Fast O_2 sensors, coupled with turbulence profilers, are very valuable tool, which have obviously a wide range of possible scientific application in both shelf seas and coastal regions. With the actual shallow waters depth rating of the commercially available fast O_2, however, ocean application is strongly limited. For this reason, the deep-sea rated fast O_2 system proposed on Chapter IV, has the potential to fill the research gap on oceanic

O_2 fine structure measurements and flux estimations. In particular, this tool can lead to a better understanding of the dynamics at within the O_2 minimum zones by providing well-resolved oxyclines for both O_2 flux estimations and budgets.

In regard to benthic measurements, the results presented on chapter III provide real-world data to support the results of modeling approaches aiming to quantify the role of the hydrodynamics in controlling marine benthic O_2 dynamics. The results of this study support the relatively undocumented occurrence of transport limitation in highly active seeps habitats. Cold seeps habitats are well distributed along both active and passive continental margins and are characterized by strongly established habitat heterogeneity (*see* Sibuet and Olu 1998). In the presented study, sulfide oxidation based on H_2S measurements were found to be a key process in O_2 uptake; however, several additional key constituents directly or indirectly consuming O_2 were not quantified or quantifiable. Among these constituents, CH_4 was found to play a principal role in benthic O_2 dynamics at seeps habitats (Boetius and Wenzhöfer 2013) and thus future investigations should also quantify CH_4 fluxes and the associated oxidation rates. Obviously, beside CH_4, more constituent have to be concurrently measured to ensure comparable resolutions of the involved chemically and biologically mediated processes. Very promising results in this direction were reported on solid-state gold/mercury (Au/Hg) voltametric microeletrodes (Luther et al. 1998); those microelectrodes have the advantage to enable the simultaneous acquisition of O_2, manganese, iron, sulfide and iodine concentration profiles. In addition, robust nitrate microsensors have also been recently developed (Revsbech and Glud 2009); data from these microsensors will provide valuble information to identify the key processes occurring within the sediment suboxic zone and to better frame the coupling (or decoupling) between O_2 and nitrogen cycles. The validation of these measurements and inferred interactions may, however, still require the coupling of in-situ data acquisition with dynamic diagenetic models (*see* Berg et al. 2003; Glud et al. 2007).

The combination of high-resolution water column current and turbulence measurements with high-resolution constituent measurements, as well as adequate monitoring might thus be the best way to proceed to further advance the knowledge on the O_2 dynamics. On the long run, also profiting from the progress in the water column constituent measurements (e.g., Chapter IV) and constituents flux estimations in the BBL (e.g., flux-ratio method; Holtappels et al. 2011) and at

the SWI (e.g., eddy correlation technique) as well as from diagenetic models, the overarching goal of future studies is that of combining benthic and water column measurements to gain a better insight on the constituent flux pathways and their dynamics from the sediment to the atmosphere.

V.III. References

Berg, P., S. Rysgaard, and B. Thamdrup. 2003. Dynamic modeling of early diagenesis and nutrient cycling. A case study in an artic marine sediment. *Am. J. Sci.* **303**: 905–955, doi:10.2475/ ajs.303.10.905

Boetius, A., and F. Wenzhoefer. 2013. Seafloor oxygen consumption fuelled by methane from cold seeps. *Nat. Geosci.* **6**: 725–734, doi:10.1038/NGEO1926

Burchard, H., and T .P. Rippeth. 2009. Generation of bulk shear spikes in shallow stratified tidal seas. *J. Phys. Oceanogr.* **39**: 969–985, doi:10.1175/2008JPO4074.1

Diaz, R. J. 2001. Overview of hypoxia around the world. *J. Environ. Qual.* **30**: 275–281, doi:10.2134/jeq2001.302275x

Geider, R., and J. La Roche. 2002. Redfield revisited: variability of C:N:P in marine microalgae and its biochemical basis. *Eur. J. Phycol.* **37**: 1–17, doi:10.1017/S0967026201003456

Glud, R. N., P. Berg, H. Fossing, B. B. Jørgensen. 2007. Effect of the diffusive boundary layer (DBL) on the benthic mineralization and O_2 distribution: a theoretical modelling exercise. *Limnol. Oceanogr.* **52**: 547–557, doi:10.4319/lo.2007.52.2.0547

Holtappels, M., M. Kuypers, M. Schlueter, and V. Bruechert. 2011. Measurement and interpretation of solute concentration gradients in the benthic boundary layer. *Limnol. Oceanogr.: Methods* **9**: 1–13, doi:10:4319/lom.2011.9.1

Luther, G. W., P. J. Brendel, B. L. Lewis, B. Sundby, L. Lefrançois, N. Silverberg, and D. B. Nuzzio. 1998. Simultaneous measurement of O_2, Mn, Fe, I^- and $S(^{-II})$ in marine porewaters with a solid-state voltammetric micro-electrode. *Limnol. Oceanogr.* **43**: 325–333, doi:10.4319/lo.1998.43.2.0325

Revsbech, N. P., and R. N. Glud. 2009. Biosensor for laboratory and lander-based analysis of benthic nitrate plus nitrite distribution in marine environments. *Limnol. Oceanogr.: Methods* **7** : 761–770, doi : 10.4319/lom.2009.7.761

Sibuet, M., and K. Olu. 1998. Biogeography, biodiversity and fluid dependence of deep-sea cold-seep communities at active and passive margins. *Deep Sea Res.* **45**: 517–567, doi:10.1016/S0967-0645(97)00074-X

Stramma, L., G. C. Johnson, J. Sprintall, and V. Mohrholz. 2008. Expanding oxygen-minimum zones in the tropical oceans. *Science* **320**: 655–658, doi:10.1126/science.1153847

Appendix

Lorenzo Rovelli
dipl. sc. nat. biol. ETH

Via Arbostora 2
CH-6913 Carabbia
Switzerland

Home Phone +41 (0)919942474
Office Phone: +44 (0)7452271333
DE Mobile: +49 (0)15125330942
E-mail : lorenzo.rovelli@mac.com

Personal Information

Date of Birth	14 July 1982
Place of Birth	Lugano (Switzerland)
Origin:	Capriasca (Switzerland)
Nationality	Swiss
Marital status	Single

Education

March 2013 – present — SAMS (Scottish Association for Marine Science)

October 2008 – February 2013 — **PhD Student Fellowship**
Topic: "Physical and geochemical controls on solute fluxes at continental margins and shelf seas"
GEOMAR (Helmholtz Centre for Ocean Research Kiel)
[former Leibniz-Institut für Meereswissenschaften]

November 2006 – April 2007 — **Diploma Thesis**
„*Erfolgskontrolle bei Fliessgewässerrevitalisierungen Räumliche Anwendung ausgewählter Indikatoren zur Überprüfung ihrer Aussagekraft und Praxistauglichkeit*"
[*Testing of selected indicators in success control on river restorations*]
Swiss Federal Institute of Aquatic Science and Technology (EAWAG)

October 2002 – September 2007 — **Degree in Biology** (certified equivalence to M.Sc. degree)
Fields of Specialisation: Aquatic and applied Applied Ecology, Biosystematics and Evolution
Swiss Federal Institute of Technology (ETH) Zurich

Professional Experience

May 2007 – March 2008 — **Scientific assistant, 40%**
Aquatic Physics group
Swiss Federal Institute of Aquatic Science and Technology (EAWAG)

June – August of 2000 – 2005 — **Assistant manufacturer,** up to 100%
Rovelli SA, Grancia

Scientific Cruises

8-30. October 2008	*RV Alkor* North Sea: Kiel – Kiel (Germany) Duties: CTD, methane and polyaromatic hydrocarbons sampling, acoustic (ADCP) survey, sidescan sonar helper
4-13. August 2009	*RV Celtic Explorer* North Sea: Cuxhaven - Bremerhaven (Germany) Duties: Microstructure CTD; CTD methane and polyarmatic hydrocarbons sampling, acoustic (ADCP) survey, Eddy Correlation helper
15-26. June 2010	*RV Aegaeo* West Nile Delta: Heraklion (Greece) Duties: Microstructure CTD; CTD helper
23. September – 13 October 2010	*RV Sonne* Chilean margin: Valparaiso – Valparaiso (Chile) Duties: Microstructure CTD, CTD, methane sampling, ADCP, Eddy Correlation
10. March – 12. April 2011	*RV Merian* Atlantic OMZ: Dakar (Senegal), Las Palmas (Spain) Duties: Microstructure CTD, ADCP, Eddy Correlation
22. February – 17. March 2012	*RV Meteor* Gulf of Cadiz : Palma de Maiorca (Spain), Lisbon (Portugal) Duties : CTD ; Multicorer helper

Other

Mother Tongue	**Italian**
Languages	**German**: **fluent** **English: fluent** **French: good**
Computer Skills	Windows, Unix/Linux, MacOS MS Office, OriginPro, Surfer, OceanDataView, ArcGIS, Illustrator, Photoshop, SPSS, Matlab, GMT, CE_Qual_W2
Scientific equipment Skills	Nortek Acoustic Doppler Velocimeter, Nortek and RDI Acoustic Doppler Current Profilers Oxygen and Temperature fast-response Microsensors Contros HydroC/CH4 and HydroC/PAH sensors Seabird CTD devices Temperature loggers Differential GPS Mooring and lander deployments from boats
Laboratory skills	Skills on chemical and biological subjects as well as in testing and improvement of scientific equipment

Publications

peer-reviewed

- McGinnis D. F., S. Cherednichenko, S. Sommer, P. Berg, **L. Rovelli**, R. Schwarz, R. N. Glud, and P. Linke (2011). Simple, robust eddy correlation amplifier for aquatic dissolved oxygen and hydrogen sulfide flux measurements. Limnology and Oceangraphy: Methods 9, 340-347, doi:10.4319/lom.2011.9.340
- McGinnis, D. F., M. Schmidt, T. DelSontro, S. Theman, **L. Rovelli**, A. Reitz, and P.Linke (2011). Discovery of a natural CO2 seep in the German North Sea: Implication for shallow dissolved gas and seep detection. Journal of Geophysical research. doi:10.1029/2010JC006557
- Linke, P., S. Sommer, **L. Rovelli** and D.F. McGinnis (2009). Physical limitations of dissolved methane fluxes:The role of bottom-boundary layer processes. Marine Geology. doi:10.1016/j.margeo.2009.03.020.

Conferences

talks

- **Rovelli, L.**, S. Sommer, P. Linke, R. N. Glud, and D. F. McGinnis. (2012). Development and application of the Eddy Correlation technique: benthic heat, sulfide and oxygen flux estimations from the Baltic Sea. IOW Physics Seminar. Leibniz-Institut für Ostseeforschung Warnemünde IOW. Warnemünde.Germany. 3.01.2012
- Schmid, M., **L. Rovelli**, and A. Wüest. (2011). Mass balance of explosives in Lakes Lucerne, Brienz and Thun, International Conference on Chemistry and the Environment, Zürich. Switzerland. 14.09.2011
- **Rovelli, L.**, M. Dengler, M. Schmidt, S. Sommer, P. Linke, and D. F. McGinnis (2011). Turbulent mixing in the Central North Sea: sources and implications for vertical transport of dissolved gases during the summertime. Warnemünde Turbulence Days, Vilm, Germany. 05.-08.09.2011
- **Rovelli, L.**, M. Dengler, J. Schafstall, M. Schmidt, S. Sommer, P.Linke, and D. F. McGinnis (2010). Physical characterisation of oxygen fluxes across the water column in the central North Sea. 14th International Workshop on Physical Processes in Natural Waters. Reykjavik, Iceland. 28.06.-1.07.2010
- McGinnis, D. F., S. Sommer, **L. Rovelli** and P. Linke (2009). Ephemeral benthic methane peaks: understanding the physis of cold seep emissions. 13th International Workshop on Physical Processes in Natural Waters. Palermo. Italy. 1.-4.09.2009
- Linke, P., S. Sommer, **L. Rovelli** and D.F. McGinnis (2009). Physical controls of cold seep methane emissions. OCEANS '09 IEEE, Balancing Technology with Future Needs. Bremen. Germany. 11.-14.05.2009

posters

- **Rovelli, L.**, M. Dengler, S. Cherednichenko. R. Schwarz, P. Linke, and D.F. McGinnis (2010), Investigation of seafloor warming on oxygen and heat fluxes. Annual Retreat Cluster of Excellence "The Future Ocean". Schleswig. Germany.